Fall 2013

Transport in correlated and uncorrelated random media, with applications to molecularly doped polymers

Nilanka Praveena Gurusinghe

Department: Physics

TRANSPORT IN CORRELATED AND UNCORRELATED RANDOM MEDIA, WITH APPLICATIONS TO MOLECULARLY DOPED POLYMERS

by

NILANKA PRAVEENA GURUSINGHE

A DISSERTATION

Presented to the Faculty of the Graduate School of the

MISSOURI UNIVERSITY OF SCIENCE AND TECHNOLOGY

in Partial Fulfillment of the Requirements for the Degree

DOCTOR OF PHILOSOPHY

in

PHYSICS

2013

Dr. Paul E. Parris, Advisor
Dr. Jerry L.Peacher
Dr. Thomas Vojta
Dr.Alexey Yamilov
Dr.David H. Dunlap

ABSTRACT

The commonly observed Poole-Frenkel field dependence, $\mu \sim \exp\sqrt{\beta_0 E}$, of the mobility of photo-injected charges in molecularly-doped polymers has been shown to arise from the spatially-correlated, Gaussian energy distribution of transport sites encountered by charges moving through the material. Experimental current-time transients obtained for molecularly-doped polymers exhibit universality with respect to electric field and a metal-insulator-like transition from non-dispersive to dispersive transport, features usually identified with multiple trapping models that assume an uncorrelated exponential distribution of trap energies. For materials that exhibit both sets of features the possibility arises that both kinds of disorder coexist. We study here, analytically and numerically, transport in a random medium containing two kinds of energetic disorder, i.e., a spatially correlated Gaussian component and a spatially uncorrelated exponential component associated with traps. The essential question addressed is the degree to which the uncorrelated component of disorder alters or destroys the Poole-Frenkel field dependence associated with the correlated component. In our hybrid model, the bulk mobility theoretically drops to zero when the typical trap depth exceeds the thermal energy, causing a metal-insulator-like transition. In a finite sample this corresponds to a transition to the dispersive transport regime, in which carriers can never equilibrate. For a finite 3D computational sample, the behavior above and below the transition point shows different finite size scaling with the number of sites in the lattice. In agreement with experimental observations, the Poole-Frenkel field dependence of the charge carrier mobility, and the associated temperature dependence observed in a trap-free sample, is unaffected as the transition to dispersive transport is approached from the conducting side.

ACKNOWLEDGEMENTS

Behind the success of my entire life, there are many who deserve my whole-hearted gratitude.

First and foremost, I am greatly indebted to my advisor, Dr. Paul Parris, for his guidance, support, kind advice, and encouragement throughout the project. Besides being a great researcher, he is a uniquely gifted physics teacher who gave me a passion for teaching in the field.

I owe a debt of gratitude to my committee members-Dr. Jerry Peacher, Dr. Thomas Vojta, Dr. Alexey Yamilov, and Dr. David Dunlap-for their extended cooperation and allocation of their valuable time for my benefit.

I would be remiss if I did not also acknowledge Dr. George Waddill and Dr. Jerry Peacher for their enormous support to overcome hard times during my graduate studies and thinking from students' points of view when making important decisions.

There is no way to properly estimate the appreciation I owe to my father, Premadasa, and my mother, Padmalatha, for dedicating their whole lives for the benefit of my success from day one of my presence. Their hard work has finally begun to pay dividends. You two will always be close to my heart even though we are often physically separated by great distances.

I owe a debt of gratitude to my loving, encouraging, and patient wife, Sumudu, who is also working on a physics Ph.D. but amazingly making our family life enjoyable.

Lastly, there is an important person in my life who always teaches me that there is a life beyond physicsmy darling son, Savain.

TABLE OF CONTENTS

LIST OF ILLUSTRATIONS

1. INTRODUCTION

There have been extensive experimental [6–14] and theoretical investigations [15–17] of the transport properties of charge carriers photo-injected into the technologically important class of materials referred to as *molecularly-doped polymers* (MDPs) [18–22]. The technological importance of MDP films arises from their use as charge transport layers in many organic optoelectronic and electrophotographic applications. They are most extensively used as photoreceptors [23–29] in copier machines and laser printers [30], but they have played an increasingly important role in the development of organic photovoltaics [31–33], light emitting diodes [34], and other organic electronic devices [35–45].

Molecularly doped polymers themselves are two component materials formed by doping organic transport molecules into an otherwise insulating polymer matrix [30, 46]. The polymers most commonly used in MDP applications include polycarbonate (PC) and polystyrene (PS), whose polymeric units comprise long molecular chains formed from a large number of smaller molecular repeat units referred to as *monomers* (a sequence of n repeat units forms an n-mer, which for small n includes dimers, trimers, etc.). Materials formed from polymer chains of the same molecular weight (i.e., chain length) can be grown into crystals but evaporated films grown from solution more typically form an amorphous structurally-disordered material, comprised of many entangled polymer chains having a distribution of different chain lengths. A given molecularly-doped polymer is characterized, then, by a specified polymer host, and by the concentration (usually specified as a weight per cent) of organic transport molecules that have been doped into it. For example, one of the most widely studied MDP materials is formed by doping diphenyl hydrazone (DEH) molecules at 30 wt. % into polycarbonate, forming a hole-transporting material

denoted as 30% DEH:PC. The chemical structure of the DEH transport molecules and the polymer repeat unit for this material are presented in Fig. 1.1.

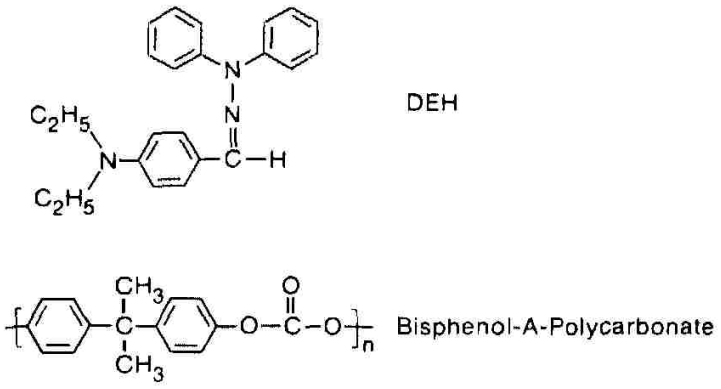

Figure 1.1. The structure of the DEH molecule and polycarbonate. [1]

Even with the addition of transport molecules, MDPs remain electrically insulating up to very large applied electric fields. Thus, dopant molecules in these materials do not directly add carriers to the system, as they would in typical p-type or n-type semiconductors. To act as a charge transport layer, as in a xerographic photoreceptor, e.g., carriers must be *injected*, either electronically or optically, into the otherwise insulating material, where they are then able to move through the manifold of localized electronic states associated with the transport molecules introduced into the material for that purpose.

In the work presented in this dissertation, several features of charge transport in MDPs are theoretically studied and several new theoretical and numerical results are presented. To aid in the presentation of these results, which appear in the body of the dissertation, this introductory section provides a basic description of the underlying physics of photo-injected charge transport in molecularly-doped polymers, emphasizing the important role of *energetic and spatial disorder* in the transport

process. After describing basic experimental observations, including a number of essentially universal features common to many MDPs, key theoretical ideas that have been previously developed to explain these observations are reviewed. This review reveals an interesting fact: very different statistical (i.e., microscopic) models of the disorder have been used to explain different commonly-observed features of the experimental data. Indeed, this evident dichotomy in the theoretical literature forms the basic motivation for the theoretical and numerical studies that are presented in this dissertation, which attempts to answer the question as to whether the different kinds of disorder invoked to explain the different classes of experimental observation are, in fact, *compatible*, i.e., could they actually co-exist; or would the presence of one type of disorder modify or destroy the characteristic features that arise naturally with the other.

The rest of this section is laid out as follows. In the next subsection properties associated with the electronic structure of molecularly doped polymers that allows for the process of photo-injection (or photogeneration) of charge carriers, and for their subsequent motion through a MDP film are briefly discussed. Following this, a description of the basic experimental set-up associated with the time-of-flight measurements that are commonly used to measure transport properties in these materials is presented. This is followed by a description of universal features that emerge from these measurements, and a review of transport models that have been developed to explain them. This section concludes with a subsection outlining the motivation for the research presented here, and an overview of the material presented in the remaining sections of the dissertation.

1.1. CHARGE TRANSPORT IN MOLECULARLY-DOPED POLYMERS

Charge transport in metals and other types of ordered solids (i.e., crystals) was initially explained using a simple model proposed by Drude, soon after the discovery of the electron. In the Drude model [47], collisions between electrons were neglected, and essentially free electrons were assumed to undergo collisions only with metal ions. The mean free path was thus assumed to be governed by the lattice spacing in the crystal, independent of the speed of the electron. The erroneous assumption that the scattering was due to the ions was corrected later in the quantum description [48], in which it came to be understood that electrons in an ordered lattice form energy bands, and are better described by Bloch waves that scatter not from the ordered array of ions but from deviations from the ordered structure arising from defects, impurities, and lattice vibrations (i.e., phonons). Thus, the basic picture of charge transport in many ordered materials is one in which electrons travel considerable distances in extended momentum-like states, between scattering events that lead, e.g., to normal electrical conduction.

In contrast to ordered crystalline materials, with well defined Bloch states and their associated energy bands, amorphous organic materials like MDPs have no translational symmetry, and the relative "softness" of the organic molecules making up the material increases the importance of the electronic coupling of charge carriers to vibrational modes of the material. Both of these effects favor the formation of *localized*, rather than *extended*, electronic states. Thus, charge transport in MDPs occurs not through extended free-particle-like motion, but by hopping transitions of carriers between localized states associated with the dopant molecules [30, 46].

The spatial energy structure of a typical molecularly-doped polymer material is indicated schematically in Fig. 1.2. In this figure, localized electronic states of the polymer repeat units and those of the dopant molecules are seen to be of two types:

those which are filled or occupied by electrons and those which are not. For each molecular unit there is a highest occupied molecular orbital (or HOMO) and a lowest unoccupied molecular orbital or (LUMO). Because of the different local environments experienced by different molecules in the amorphous material, there is an energetic distribution of localized HOMO and LUMO states randomly distributed throughout the doped polymer.

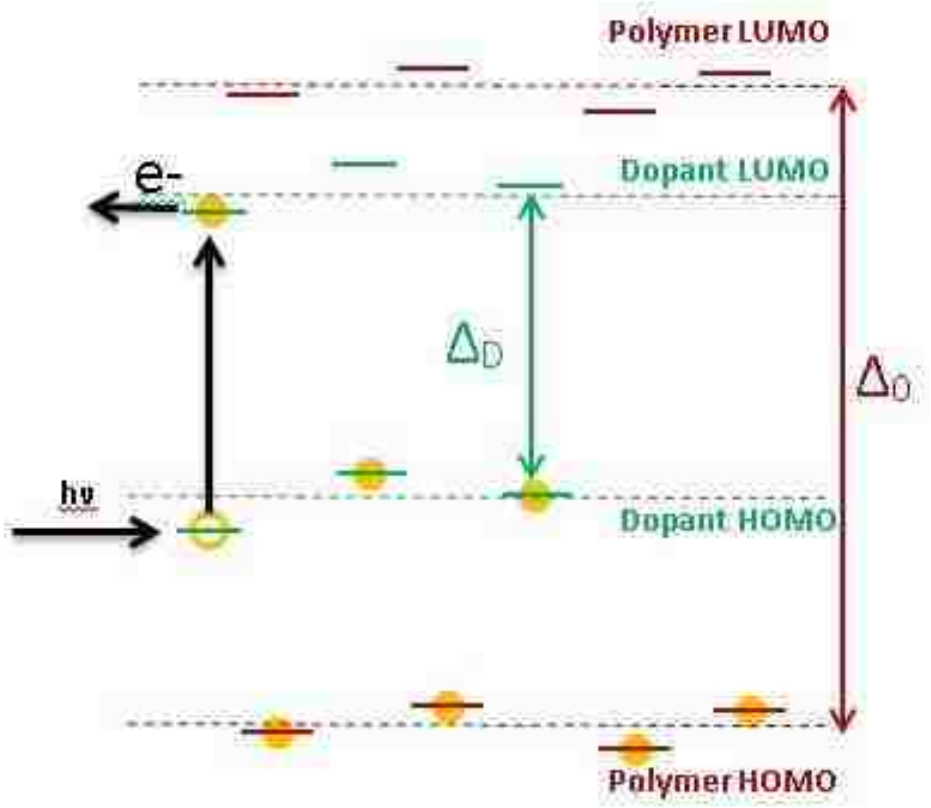

Figure 1.2. Energy structure of molecularly-doped polymer.

In the polymers of interest, the energy difference $\Delta_0 >> kT$ between polymer LUMO and HOMO states is sufficiently large that at any accessible temperature the polymer HOMO states are all occupied and the polymer LUMO states are all

unoccupied. This is the localized state analog to having a filled valence band, an empty conduction band, and a large band gap; as a consequence, the undoped polymer is strongly insulating.

The energy difference Δ_D between the HOMO and LUMO levels of dopant molecules is also much larger than kT, but it is smaller than that of the polymer, and the relative location of its energy levels with those of the polymer plays an important role. For hole transporting materials like DEH:PC, as indicated in the figure, the HOMO level of the dopant molecule is considerably higher than the HOMO levels of the polymer, and the LUMO of the dopant is lower than that of the polymer. It is this fact that allows for efficient photo-injection of mobile holes in the doped material. This occurs when, as indicated in the figure, a dopant molecule lying near a transparent (positively charged) contact is photo-excited (e.g., with a laser tuned to a frequency for which $\Delta_P > \hbar\omega > \Delta_D$) forming a Frenkel exciton (a particle-hole excitation localized on the dopant molcule). In the presence of the strong electric fields applied in an experiment, this exciton can undergo field-ionization, with the photo-excited electron leaving the dopant molecule and entering the positive contact of the anode to which it is attracted. The photo-ionized dopant molecule now has a positively charged hole in its HOMO level, that can subsequently make a hopping transition into the HOMO levels of other dopant molecules in its neighborhood (a process in which an electron on one of the neighboring molecules actually makes a transition onto the photo-ionized dopant molecule, neutralizing it in the process, but allowing the positive hole to now reside on the dopant molecule from which the electron came). Thus, photo-injected hole conduction in, e.g., DEH:PC takes place as a sequence of hopping transitions occurring among the impurity "band" of localized states associated with the dopant molecules.

The localized charge carrier states of interest are associated with molecular orbitals that fall off exponentially with distance from the dopant molecule. The

tunneling transition probability per unit time, W_{mn}, of an electron moving from a localized state n to a state m associated with a different dopant molecule (Fig. 1.3) is proportional to the square of an appropriate transition matrix element taken between these two states, and is thus expected to depend exponentially

$$W_{mn} \propto \exp\left(-\frac{2r_{mn}}{\alpha}\right) \tag{1}$$

upon the spatial separation $r_{mn} = |\vec{r}_m - \vec{r}_n|$ between them. In this last expression, α is the localization length associated with the exponential decay of the molecular orbital associated with the HOMO levels of the dopant molecules.

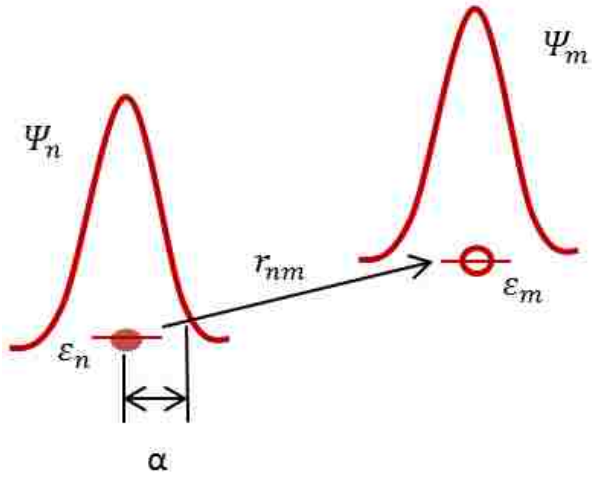

Figure 1.3. Hopping transition between two localized states separated by r_{nm}, with energies ε_n and ε_m and localization radius α.

As mentioned earlier, due to the different local environments surrounding each dopant molecule, there are local variations in the energy ε_n of the dopant states involved in the transition. Naturally, the transition rate also depends on the energy difference $\varepsilon_{mn} = \varepsilon_m - \varepsilon_n$ between the two states, but its functional form depends

on the nature and strength of the electron-phonon coupling. Indeed, it is only by absorbing or emitting phonons that a transition between electronic states of different energy can occur while still conserving the total energy of the system. For molecularly doped polymers, the nature of this coupling is still somewhat of an open question, with two different microscopic pictures commonly invoked to describe individual hopping transitions.

In one picture, the disordered material is assumed to have a broad spectrum of vibrational modes, so that is always possible to absorb or emit a single phonon having the energy $|\varepsilon_{mn}| \sim \hbar\omega_i$ needed for an electronic transition. In this picture, hopping rates are assumed to take the form

$$W_{mn} = v_0 \exp\left(-\frac{2r_{nm}}{\alpha}\right) \exp\left(-\frac{\varepsilon_m - \varepsilon_n + |\varepsilon_m - \varepsilon_n|}{2kT}\right) \tag{2}$$

derived by Miller and Abrahams to describe one-phonon thermally-assisted tunneling [49]. With Miller-Abrahams rates, hops downward in energy are independent of the energy mismatch, while hops upward in energy are reduced by a Boltzmann factor $\exp - |\varepsilon_{mn}| / kT$, that reflects the availability in the medium of phonons of the required energy. In this expression ν_0 is a prefactor that is usually treated as a phenomenological parameter that describes the attempt frequency for hops between states of the same energy.

The second picture commonly used to describe transitions between localized states in molecularly doped polymers takes into account the relative softness of the organic molecules involved, and theoretical evidence that suggests that the spatial configuration of the atoms in a typical organic dopant molecule can change considerably depending on whether it is electrically neutral, or ionized, i.e., whether there is a charge carrier occupying it or not. This molecular distortion, which occurs due to a lowering of the overall molecular potential energy in the presence of the altered

electronic distribution arising from the presence of absence of the carrier, constitutes a non-perturbative, multi-phonon interaction. The applicability of multiphonon rates is supported by electronic structure calculations on organic molecules that show significant reorganization energies (in the range of a few hundred to several hundred meV) between the lowest energy state of the neutral organic molecule and its corresponding cation [50]. Since this molecular distortion occurs on any dopant molecule occupied by the carrier it is often viewed as "following" the carrier as it migrates between different sites. The combined entity consisting of the charge carrier and the molecular distortion which accompanies it is referred to as a molecular *polaron* (in this case, a small polaron, to distinguish it from carriers, e.g., in semi-conductors in which the coupling is weaker, and the accompanying distortion is of larger radius and involves displacments of many neighboring atoms) [51–54]. A hopping transition of a small polaron of this type requires that thermal fluctations lead to appropriate molecular distortions in a pair of dopant molecules, so that a carrier on one molecule can resonantly tunnel to the other. The small polaron transition rate has been calculated by Holstein and Emin [55, 56] in a form

$$W_{n,m} = \frac{J_0^2 e^{-2\lambda r_{nm}}}{\sqrt{2\hbar^2 \varepsilon_B kT/\pi}} \exp\left[-\frac{\varepsilon_B + \varepsilon_{nm}}{2kT} - \frac{\varepsilon_{nm}^2}{8\varepsilon_B kT}\right] \tag{3}$$

which is equivalent to the chemical reaction rate formula derived by Marcus [57]. In this expression, J_0 characterizes the strength of the transition matrix element connecting the two states, and E_B is a measure of the rearrangement energy that occurs in the presence of the charge carrier, and is referred to as the polaron binding energy.

It is worth pointing out that the two rates described above, i.e., the Miller-Abraham rates and the small polaron or Marcus rates share an important feature that arises from any microscopic model of electron-phonon coupling, and which is

necessary in order for the electronic system (in the absence of an applied field) to be able to come to thermal equilibrium. This feature is expressed in the condition of detailed balance [58],

$$\frac{W_{nm}}{W_{mn}} = \frac{P_n}{P_m} = \exp\left(-\frac{\varepsilon_m - \varepsilon_n}{2kT}\right)$$

which relates transitions in opposite directions, and which ensures that in equilibrium that number of transitions per unit time from state m to n is the same as the number occurring in the reverse direction. In this expression, P_n represents the equilibrium probability that a carrier injected into the system occupies site n. In the presence of the electric field $\vec{E}$, the system is no longer in equilibrium, but the transition rates are assumed to continue to locally obey detailed balance, but with site energies modified in the usual way, i.e., $\varepsilon_m \to \varepsilon_m - e\vec{E} \cdot \vec{r}_m$.

The transition rates described above exponentially reduce the likelihood of transitions from a given transport site to another one far away in distance, and to sites much higher in energy. In general this favors transitions to a relatively small group of nearest-neighbors lying in the immediate vicinity of a given dopant molecule, unless those sites are all of an energy much higher than the initial site. In such a circumstance, the most likely transition can be to a state which is further away in space, but closer in energy. This competition between states which are closer in space or in energy is generally referred to as "variable range hopping" [59], and the transport that results can be strongly influenced by the density of transport sites of different energy (the density of states, or DOS), and the degree to which the energies of states arranged close together in space have similar or different energies, i.e., it can depend strongly on any existing *correlations* in the distribution of site energies. In any case, the rates introduced above describe the transition rate for individual hops, with the evolution of carriers in the system as a whole generally understood to be

described by a set of rate equations

$$\frac{dP_n}{dt} = \sum_m (W_{nm}P_m - W_{mn}P_n)$$

collectively referred to as a master equation [58].

1.2. EXPERIMENTAL OVERVIEW

The efficiency of a wide variety of applications that use molecularly doped polymers depends upon the ability of charge carriers to move through the material. An experimental quantity commonly used to characterize their ability to do so is the charge carrier mobility $\mu = v_d/E$, where v_d is the drift velocity that carriers develop in the presence of an applied electric field E. The mobility is the main parameter of interest used to characterize transport in molecularly-doped polymers, both in studies of the underlying physics of charge transport in disordered systems and for device optimization. A number of techniques have been developed to measure the mobility, such as the time-of-flight (TOF) method, the dark-injection space-charge limited current (DI-SCLC) technique [60], and the steady-state trap-free space-charge-limited current (TF-SCLC) method [61].Here, the time-of-flight method is discussed because it has been by far the most widely used, and because its description is of considerable importance to some of the theoretical results presented in this dissertation.

1.2.1. Time-of-Flight Measurements of the Drift Mobility. The time-of-flight method was first introduced by Haynes and Shockley [62]. Using this conceptually very simple technique one can study the transit of charge carriers across a sample directly over a relatively wide range of electric fields and temperatures. The set-up of a typical TOF measurement for MDPs [30] is shown schematically in Fig. 1.4. In short, the experiment is performed by coating a thin layer of the MDP material on both sides with semitransparent electrodes, usually gold or aluminum. This layered

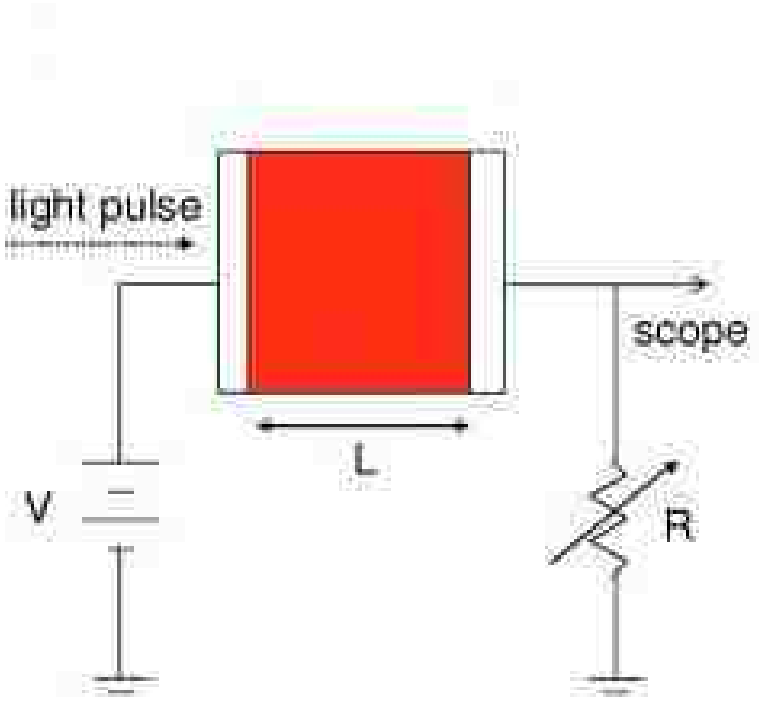

Figure 1.4. Schematical representation of the time-of-flight technique.

system is then used as a capacitor in an RC circuit in which an applied voltage V charges the capacitor, and produces an electric field $E = V/L$ inside the MDP material, of (measureable) thickness L. If the MDP is itself used as a photo-generator, a highly absorbent laser is used to illuminate the surface of the sample, injecting carriers as previously described. While this photo-generated charge carrier sheet drifts (and spreads) across the sample, the current flowing through it (proportional to the instantaneous drift velocity and the number of carriers in the sample) can be monitored by measuring the voltage across the resistor. As carriers leave the sample at the collecting electrode, the current begins to decrease. If all carriers in the sample moved, at all times, with the same drift speed v_d, the TOF current transient would appear as illustrated in Fig. 1.5. This idealization is not very realistic, however, since real carriers undergo both drift and diffusion, the latter of which rounds the sharp

edge of the decay of TOF current decay. In a sufficiently thick sample, however, if normal Fickian diffusion were taking place, the diffusive rounding would be small compared to the width of the plateau, and hence the time of flight, or transit time τ could be determined without difficulty. From the transit time, one can determine the drift velocity $v_d = L/\tau$, and thus the TOF mobility, given by

$$\mu = \frac{L^2}{V\tau}. \tag{4}$$

In practice, there are a number of difficulties associated with this simple picture. First, as discussed below, in most measurements on MDPs the tail of the current transient is very broad, often wider than the current plateau itself. While deviations from the idealized current shape could arise from several influences, including the RC circuit response time, variation in mobility due to sample inhomogeneity, local electric field variations, etc., it is generally believed that the wide tails seen in experiment are associated with disorder in the system. In addition to this effect which is important to the physics, there are a number of strictly technical issues that go into the design of a clean experiment. For example, the resistance R of the resistor clearly has to be chosen so that the RC time constant of the circuit is much less than the transit time, so the response observed is due to charge carriers in the MDP and not due to the

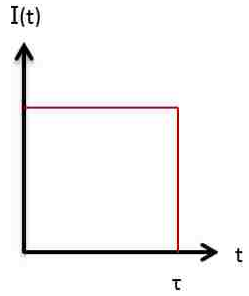

Figure 1.5. Idealized TOF photocurrent transient.

response of the circuit itself. Typically, the sample relaxation time is greater than 1s. the circuit response time can be designed to be less than 10^{-4} s by using $R \sim 10^6\ \Omega$. The transit time of many MDPs is in the range $10^{-4} - 10^{-1}$s for reasonable voltages and sample thicknesses $(1 - 100\ \mu\text{m})$.

In addition, the applied electric field E should not be perturbed by the generated charges; it needs to be uniform across the sample, and given by $E = V/L$. To ensure this, the quantity of charge produced by the laser should be much less than the product of the sample voltage and capacitance and at the same time the amount of charge should be large enough to give unequivocal signals. Also, at high temperatures the field has to be kept below the dielectric breakdown strength of the material. Satisfying these two conditions simultaneously is the major constraint of this technique. On the other hand, one of the advantages of the TOF method is that by choosing the direction of the electric field (or the electrode at which the charge carriers are generated) it is possible to measure electron as well as hole mobilities independently in the same sample.

The results of a large number of TOF experiments on photoinjected hole transport in molecularly-doped polymers reveal a number of essentially universal features. These features fall into two classes, with different theoretical models developed to explain features from each class. The first deals with the temperature and electric field dependence of the measured TOF mobility, while the second focuses on features associated with the shape of the TOF transients, and in particular on the broad tails of observed transients, mentioned briefly above. In what follows, these commonly observed features are reviewed.

1.2.2. Electric Field and Temperature Dependence of the Mobility. Time-of-flight experiments performed on a large class of MDPs reveal a universal dependence of the hopping mobility μ on temperature T and applied field E . At fixed temperature the hopping mobility has a field dependence that for a wide range

of electric fields ($E \sim 10^4 - 10^6$) V/cm obeys a Poole-Frenkel-like law [63]

$$\mu \propto \exp\left(\gamma\sqrt{E}\right) \tag{5}$$

where the "Poole-Frenkel factor" γ is found to be a decreasing function of the temperature. Figure 1.6 shows a semi-logarithmic plot of μ *vs.* $E^{1/2}$ at different temperatures for 30% DEH:PC, taken from the work of Mack, et al. [2]. The experimental data, all

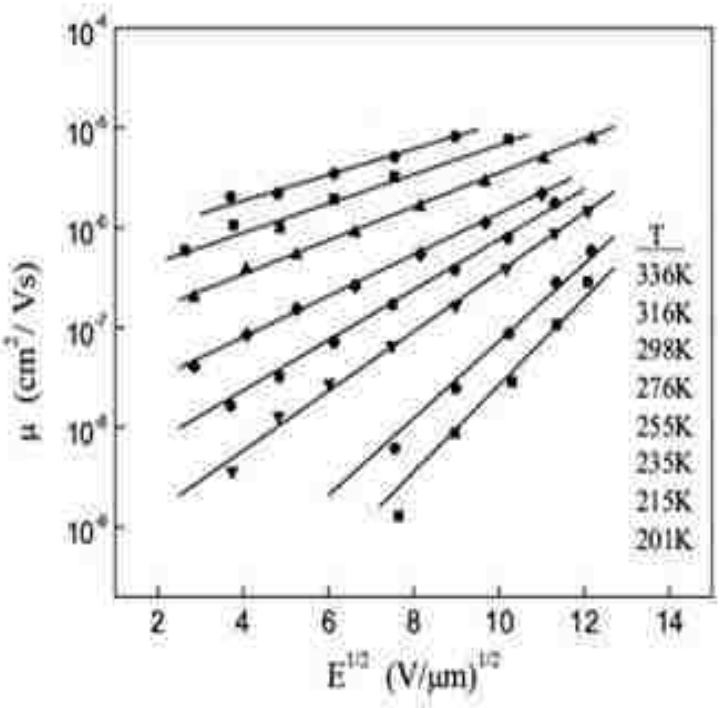

Figure 1.6. Mobility *vs.* Field for 30% DEH:PC [2].

lying on straight lines, clearly demonstrate the PF field dependence (5) of the hopping

mobility. At fixed field, the temperature dependence of the mobility is activated and can generally be described by an expression of the form

$$\mu \propto \exp\left[-\left(\frac{T_0}{T}\right)^n\right] \tag{6}$$

where $1 \leqslant n \leqslant 2$, and T_0 is a characteristic temperature. Figure 1.7 shows two semi-log plots of measured mobility data for PVK-TNF of Pfister [3] plotted assuming an Arrhenius law (linearly activated) and also plotted as a function of the square of the inverse temperature (which is referred as quadratically activated). Neither plot fits a straight line perfectly, and it is likely that the actual temperature dependence involves a product of both quadratically and linearly activated terms, a form that emerges in the theoretical work presented in this dissertation.

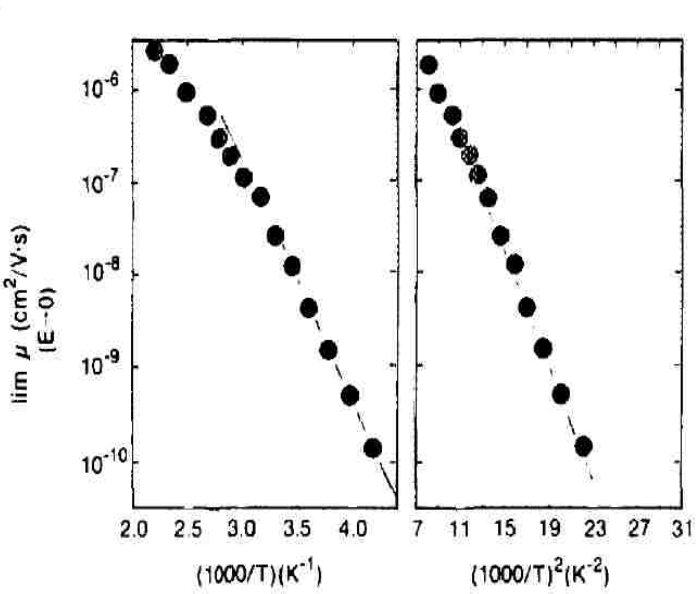

Figure 1.7. Arrhenius type and non-Arrhenius type temperature dependence plots for PVK-TNF [3].

1.2.3. Universality of Time-of-flight Photocurrent Transients and the Non-dispersive to Dispersive Transition. In addition to the characteristic features associated with the temperature and field dependence of the mobility itself, current-time transients $J(t)$ obtained in time-of-flight measurements display their own universal features. As shown in Fig. 1.8, typical room temperature TOF transients [4], following the initial laser pulse, start with an initial injection "spike" that rapidly decays into a nearly flat plateau extending out to a time τ, (the time of flight, or transit time) at which the photocurrent turns over and begins a broad algebraic decay $J \sim t^{-s}$, or "tail", characterized by a power $s \sim 2$. The decay of the initial injection spike occurs as carriers, initially photoinjected into a broad distribution of states, thermalize or equilibrate into an approximately thermal distribution of

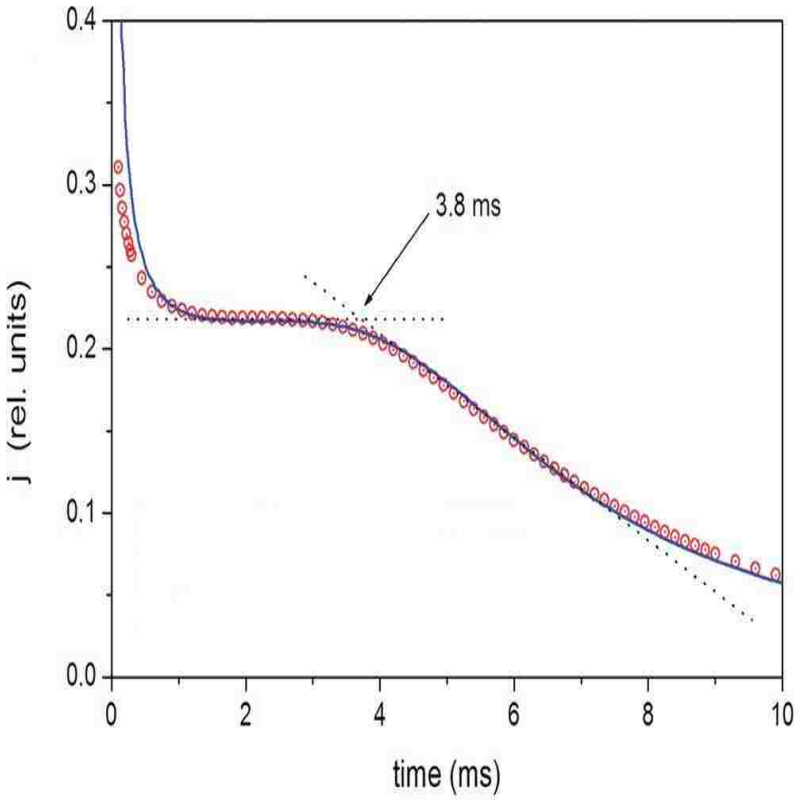

Figure 1.8. Current transient due to holes in 30% DEH:PC presented in linear current-linear time representation [4].

energy states that they subsequently maintain as they cross the sample. The observed plateau thus describes the thermalized average drift of carriers across the sample, and the tail emerges as a result of the very broad distribution of arrival times associated with carriers that experience very different local environments in the sample that are either easier or harder to traverse. Photocurrent TOF transients that display these three distinct regimes, and in particular those that exhibit a well-defined plateau, are referred to as "non-dispersive". In this regime the resulting transit time τ is experimentally identified with the time of intersection of asymptotes fitted to the plateau and tail regions of the TOF transient [30].

As the temperature is lowered, the shape of MDP current-time transients begins to change. In particular, the temporal width of the plateau region decreases, at the expense of an increasingly prolonged initial equilibration phase and a similarly broadened tail. At some critical temperature T_c, the plateau disappears entirely, so that below this temperature the current transient exhibits a monotonic decrease with time. This change in the character of the TOF transients from non-dispersive at high temperatures to "dispersive" at low temperatures is shown in Fig. 1.9.

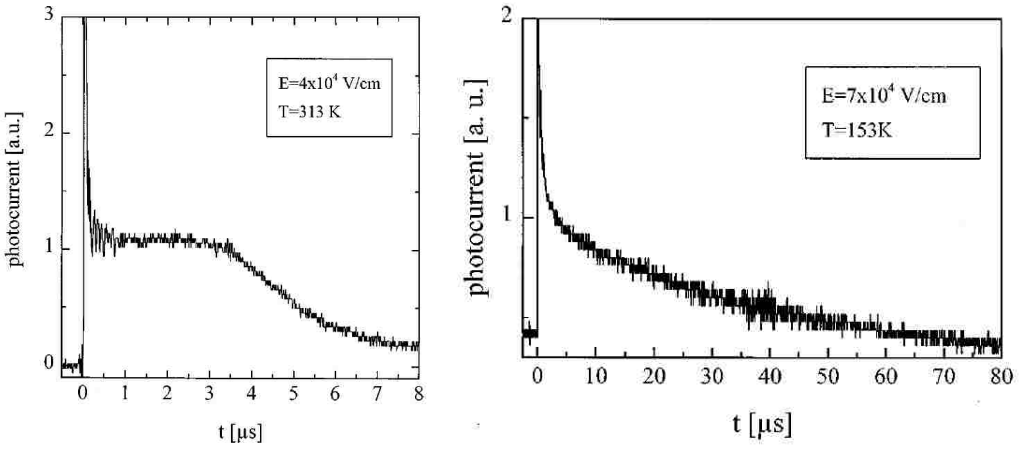

(a) Non-Dispersive (b) Dispersive

Figure 1.9. Non-dispersive to dispersive transition. [5]

The non-dispersive plateau seen at room temperature thus smears at lower temperatures into a monotonic dispersive decay that, when plotted on linear axes, does not allow for a clear determination of the transit time. In the dispersive regime, however, it has been found that when the current-time transient is plotted on log-log axis, as shown in Fig. 1.10, the different power-law decays of the injection spike and of the tail allow for a more-or-less unambiguous determination of a "mean transit time" from which an effective time-of-flight mobility can be determined. This "non-dispersive to dispersive transition" is usually interpreted as a failure or inability of the initially injected charge carriers to equilibrate during the average time that it takes for carriers to traverse the sample. Indeed, in a sample of infinite length it has been suggested that there is a temperature below which carriers *cannot actually equilibrate*-i.e., as they traverse the sample they progressively sample states deeper and deeper in energy, at which they reside for longer and longer dwell times before being able to acquire the thermal energy to escape. In such a situation the bulk steady-state mobility would vanish. Thus, the non-dispersive to dispersive transition represents a kind of photo-conducting/photo-insulating transition for the material.

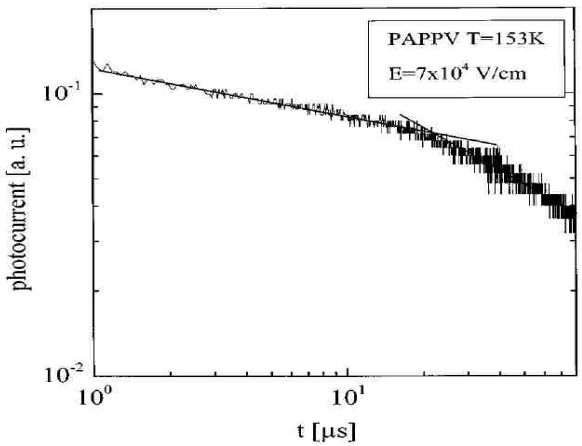

Figure 1.10. Log-log plot for dispersive transient. [5]

In addition to this well-documented non-dispersive-dispersive transition involving the shape of the current-time transients, the TOF transients of a large number of MDPs, on either side of the transition, exhibit a scaling law, referred to as *universality*, in which normalized current transients $j = J(t)/J(\tau)$ obtained for different electric fields on the same sample, when plotted together as a function of the scaled time t/τ, lie on a single universal curve. This universality is clearly demonstrated in data on 30% DEH:PC taken by Tutnyev, et al. [4] in Fig. 1.11.

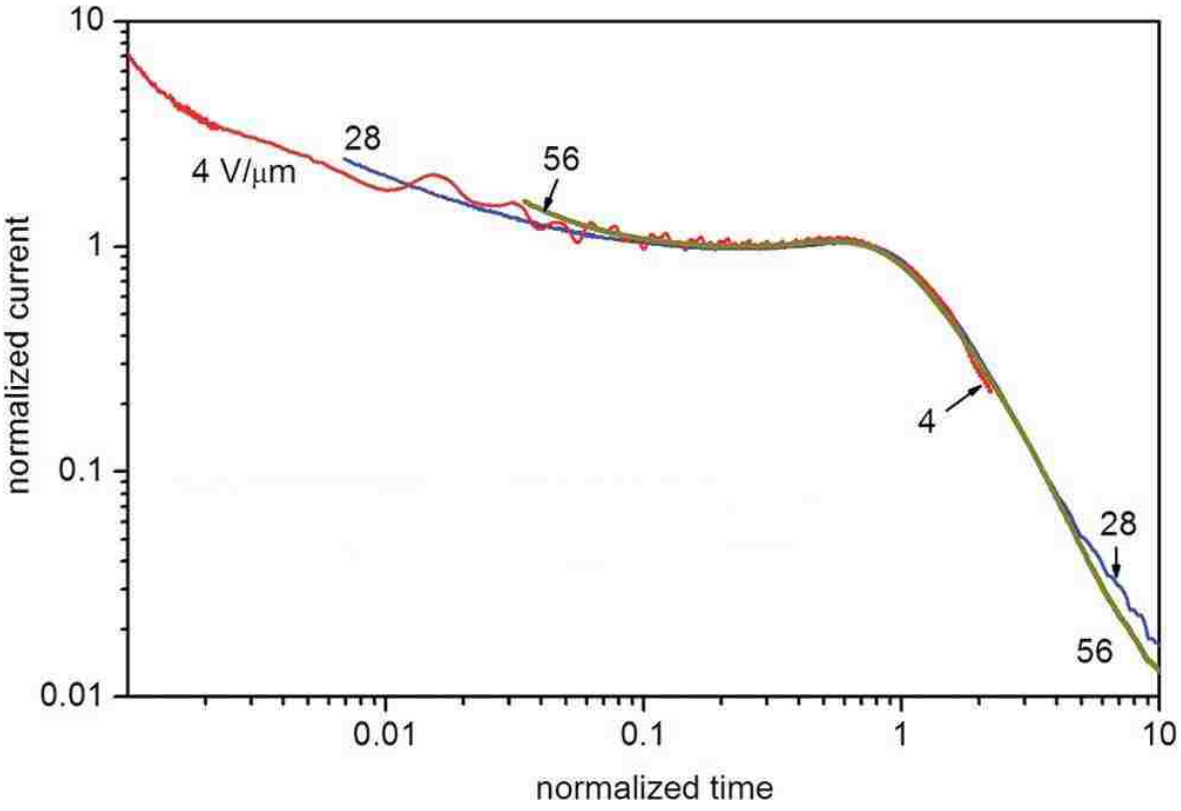

Figure 1.11. Log-Log plot of a 17.5 μm sample for electric fields of 4, 28,and 56 V/μm showing universality over an electric field range spanning more than one decade [4].

1.3. THEORETICAL MODELS DEVELOPED TO EXPLAIN THE EXPERIMENTAL OBSERVATIONS

As of yet, no single microscopic theory has been shown to lead to all of these observed features, i.e., a Poole-Frenkel (PF) field and temperature dependence, a dispersive to non-dispersive transition, and universality of current-time transients. While there do exist robust disorder-based theoretical models capable of predicting either of these two sets of features independently, the class of models that explain the field dependence of the mobility seem to require very different microscopic assumptions about the underlying disorder than those that have been shown to lead to universality of photocurrent transients.

The observed field and temperature dependence are well-predicted in some models [64–66] with a Gaussian density of transport site energies (schematically indicated in Fig. 1.12). Dispersive transport and universality of TOF transients, by contrast, are well-predicted in so-called multiple trapping models [4,67] that postulate an exponential distribution of low energy (trap) states (as in Fig. 1.13). In what follows, a brief review of each of these two different classes of models is presented.

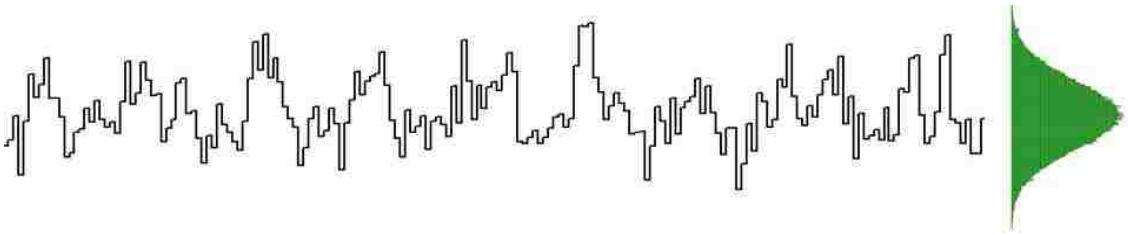

Figure 1.12. Gaussian density of transport site energies.

1.3.1. Gaussian Models. The first serious model developed in an attempt to describe the temperature and field dependence of the mobility of MDPs was the Gaussian Disorder Model (GDM) introduced by Baessler and coworkers [30, 68],

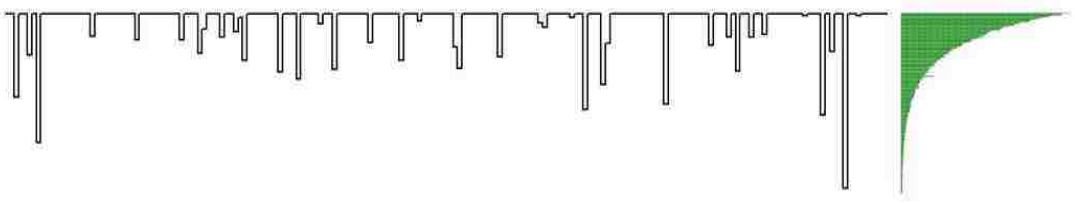

Figure 1.13. Exponential distribution of low energy (trap) states.

which describes charge transport as a biased random walk among sites arranged on a cubic lattice, with each site having a random site energy ε_i independently drawn from an uncorrelated Gaussian distribution of energetic width σ. Among the various mechanisms proposed as the source of this kind of disorder, it has been shown [69] that the interaction of charge carriers with permanent dipoles can give rise to a Gaussian-like density of states. In theoretical papers on charge carrier hopping in MDPs the question inevitably arises as to the functional form to take for the hopping rate $W_{n,m}$ governing transitions between two localized states of the system, as discussed earlier. The GDM employs Miller-Abrahams rates (2) that describe single-phonon assisted tunneling. Miller-Abrahams rates are independent of temperature for hops downward in energy, and thermally suppressed by a Boltzman factor $\exp\left[-\left(\varepsilon_{nm}\right)/kT\right]$ for hops up in energy. In the absence of the field rates in the GDM take the form:

$$W_{n,m} = \begin{cases} \nu_0 \exp(-\Gamma_{nm} r_{nm}/a) \exp\left(-\varepsilon_{nm}/k_B T\right), & \varepsilon_{nm} > 0 \\ \nu_0 \exp(-\Gamma_{nm} r_{nm}/a), & \varepsilon_{nm} < 0. \end{cases} \tag{7}$$

In this expression ν_0 is a (constant) attempt frequency, a is the lattice spacing (identified with the mean distance between dopant molecules embedded in the polymer), $\varepsilon_{nm} = \varepsilon_n - \varepsilon_m$, and $\Gamma_{nm} = \Gamma_n + \Gamma_m$ is the sum of independent Gaussian random variables Γ_n, characterized by a specified mean $\langle \Gamma_n \rangle = \gamma a$ and statistical width $\delta\Gamma_n$. The parameters Γ_n are included in the GDM to incorporate the effects of geometric

disorder arising from random molecular orientations and intersite distances r_{nm}, while the overlap parameter γ characterizes the exponential decay of the transition strength with increased inter-site separation. The strength of the geometrical disorder in the GDM is traditionally characterized by the parameter $\Sigma = \sqrt{2}\delta\Gamma_n = \delta\Gamma_{nm}$. In the presence of the electric field $\vec{E}$, site energies and transition rates are appropriately modified, with $\varepsilon_n \rightarrow \varepsilon_n - e\vec{E}\cdot\vec{\rho}_n$. In the GDM it is assumed that the electron-phonon coupling is sufficiently weak that polaronic effects can be neglected.

In practice, the GDM is a numerical model which has formed the basis for a large number of Monte Carlo simulations [30,68] that have attempted to replicate the temperature and field dependence seen in experiment. The results of those simulations (usually performed at one lattice spacing, and one temperature, but for different disorder strengths) clearly show a quadratically activated mobility emerging from the Gaussian distribution of transport sites. The electric field dependence of the GDM has always shown much less convincing agreement with the observed PF field dependence. While the numerical results exhibit a PF-like region at very high fields, they always tend to flatten out "Ohmically" at low fields. In spite of this failure at low fields, Baessler and co-workers have developed an empirical PF-like fitting formula characterizing the high field region that has been used extensively in comparison with experimental data [30, 68].

Due to the large computer effort associated with performing Monte Carlo simulations to obtain mobility data accurate enough to compare to experiment, it has not been possible until recently to actually fit the predictions of the GDM, or any disorder-based theories, to actual TOF mobility data taken for real molecularly-doped polymers. Such a fit, using an alternative computational technique, has recently been performed by Chowdhury and Parris [70], for the mobility data of 30% DEH:PC of Mack, et al. [2]. Their results are shown in Fig. 1.14. In this fit, the lattice spacing was computed based upon the mean DEH interdopant spacing, the wavefunction

decay parameter was obtained from independent measurements of the concentration dependence (i.e., on the mean interdopant spacing) of the mobility [71], and only the parameters (ν_0, σ, Σ) were varied to fit the data at high fields. In the figure, filled symbols are the experimental data shown earlier, while open symbols connected by solid curves show numerical predictions of the GDM optimized to fit the data. While the results agree quite well at high fields, the characteristic flattening predicted by the GDM at low fields emphasizes the inadequacy of the model.

Attempts to understand the failure of the GDM at low fields led to further analysis of the energetic disorder generated by the unscreened multipole moments of molecular charge distributions of dopants and polymer host molecules (dipole mo-

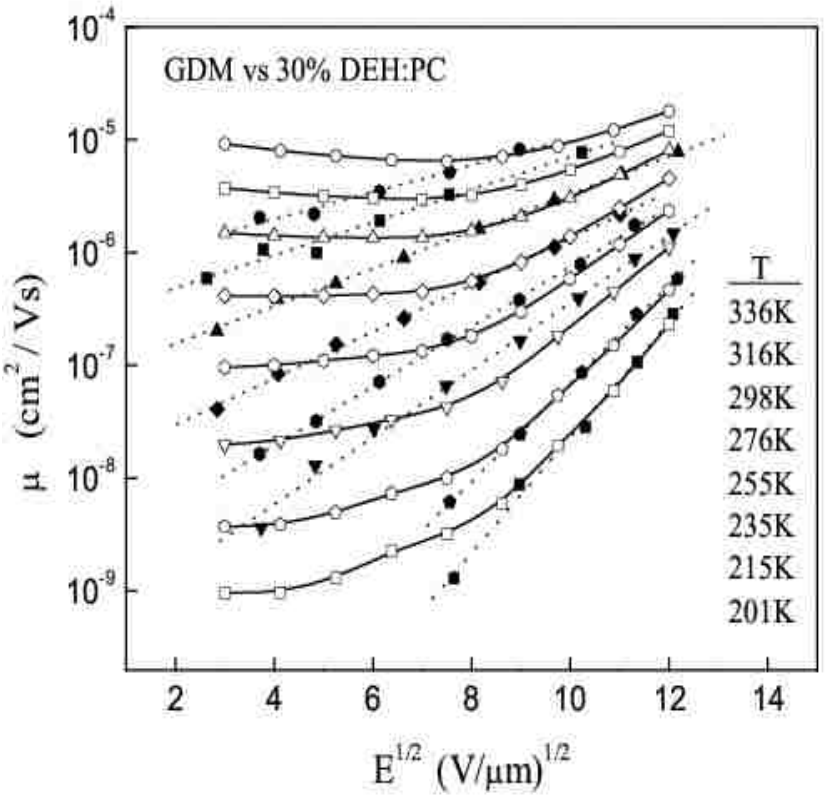

Figure 1.14. Theoretical fit of the GDM to experimental data of Mack, et al. [2] for 30% DEH:PC.

ments in particular). The work of a number of research groups, notably Gartstein and Conwell [72], Novikov and Vanikov [73], and Dunlap, Kenkre, and Parris [64] showed how a random distribution of randomly oriented electric dipole moments associated with molecular units in the material produce a random electrostatic potential energy landscape $u(\vec{r})$ that is approximately Gaussian (as had been assumed in the GDM), but which also possesses long range spatial correlations not included in the GDM. Theoretical studies of subsequently developed correlated Gaussian disorder models (CGDMs), such as the dipole glass model (DGM) of Novikov et al. [65], and the polaron correlated disorder model (PCDM) of Parris, et al. [66], have shown, both analytically and numerically, that a Gaussian energy landscape with correlations [73]

$$\langle u(\vec{r})\, u(0)\rangle \sim \sigma^2 a_0 r^{-1} \tag{8}$$

of the type that arise from the dominant dipolar contributions, leads to a convincing PF field dependence over a very broad range of electric fields. This PF field dependence has been shown to arise independently of whether the hopping rates used are of the Miller-Abrahams single-phonon type [65], as assumed in the GDM, or are of the multi-phonon type (3) described [66] by small-polaron theory or Marcus reaction rate theory [57].

As with the GDM, the different correlated disorder models were studied through the use of numerical simulations and model calculations in an attempt to replicate the observed field and temperature dependence. Like the GDM, until recently the numerically intensive nature of the models made them unwieldy instruments to attempt a direct analysis of real TOF data. The recent work of Chowdhury and Parris [70] cited above includes a comparison of how well the GDM and several correlated models (the dipole glass model of Novikov et al. [74] and the PCDM of Parris et al. [66]) are able to actually fit the experimental data of Mack et al. [2] for 30% DEH:PC.

The conclusion of the study was that models that use Miller-Abrahams rates, with or without correlations, are unable to quantitatively fit the full electric field and temperature dependence of the mobility, but that a correlated polaron model which includes the effects of the molecular distortion does a satisfactory job of capturing the field and temperature dependence observed experimentally. The results of a fit of the PCDM theory of Parris et al. [66] to the experimental data of Mack, et al. [2] is reproduced in Fig. 1.15. As in the previous figure, the filled symbols are the experimental data and the open symbols are numerical predictions of the PCDM with the parameters $(J_0, \sigma, E_b, \Sigma)$ varied to optimize agreement with experiment.

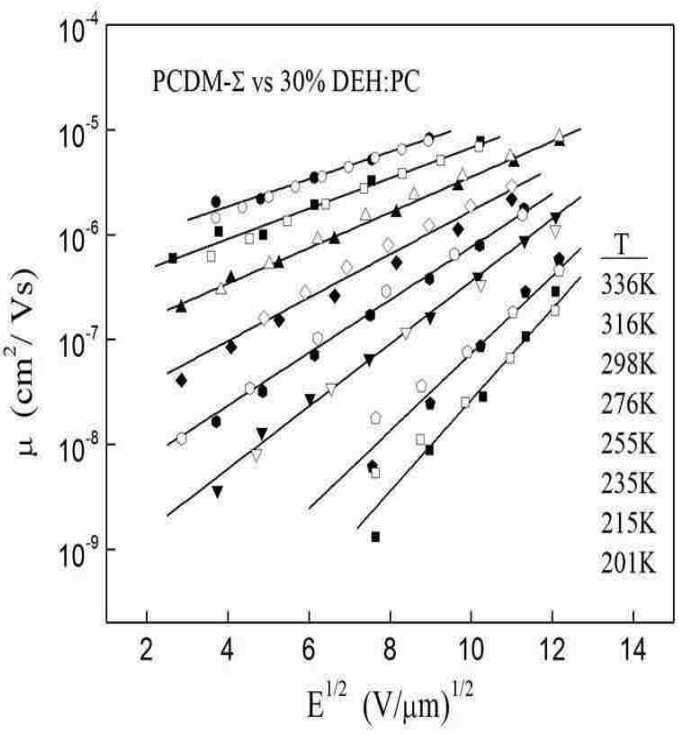

Figure 1.15. Comparison of theoretical PCDM model with experimental data of Mack et al. [2] for 30% DEH:PC.

1.3.2. Multiple Trapping (Exponential) Models. Although Gaussian disorder models that include spatial correlations and appropriate hopping rates appear to do a good job describing the temperature and electric field dependence of the mobility in real MDPs, they have not been used, typically, as a model for understanding the characteristic features exhibited by the time-of-flight transients (from which the temperature and field dependent mobility are actually deduced). Instead, analysis of dispersive features of the TOF photocurrent transients, i.e., their universal scaling with electric field and the non-dispersive to dispersive transition, have been analyzed using a very different model of energetic disorder. Indeed, it appears that dispersive features associated with charge transport in MDPs are most easily explained in the context of so-called multiple-trapping models (MTMs) [4] that assume an *uncorrelated exponential distribution* of localized energy states. In the MTMs that were introduced following the early work on dispersive transport by Scher and Montroll [67], carriers were assumed to move through a medium containing a random distribution of *traps*, i.e., localized states characterized by an energetic depth ε and a release time $\tau \sim \exp(\varepsilon/kT)$ that depends exponentially on the trap depth. Straightforward analysis [4] on one-dimensional MTMs reveals that when the distribution

$$\rho(\varepsilon) \sim \exp(-\varepsilon/\varepsilon_0) \tag{9}$$

of trap depths is itself exponentially dependent on ε, appropriately scaled TOF transients exhibit universality with respect to the electric field, and exhibit a dispersive-to-nondispersive transition as the temperature is lowered.

Above the transition, in the non-dispersive regime, MTMs do an excellent job of reproducing the shape of real TOF transients. In the TOF transient exhibited in Fig. 1.8 the solid curve represents experimental data [4] for 30% DEH:PC, while

the open symbols are the result of calculations performed using a multiple trapping model with an exponential distribution of trap depths.

In the MTM, as the temperature is lowered to a point where the mean thermal energy kT falls below the average trap depth ε_0, a transition to a dispersive transport regime occurs. In this regime, the bulk steady-state mobility vanishes, but in a sample of finite thickness carriers will eventually traverse the sample, and the photocurrent transient will show a knee on a double-log plot (as in Fig. 1.10). Scher and Montroll [67] showed that the current $I(t)$ before the knee, in this case, takes the form

$$I(t) \propto t^{-(1-\alpha)} \tag{10}$$

while the current after the knee is given by

$$I(t) \propto t^{-(1+\alpha)} \tag{11}$$

where in both expressions $\alpha = kT/\varepsilon_0$ is a "dispersion parameter" determined by the width of the underlying exponential distribution of trap energies. In this dispersive regime, if the location of the knee is identified as the mean transit time, an effective TOF mobility can be defined within the MTM. Rather than the Poole-Frenkel form predicted by correlated Gaussian disorder models, the MTM mobility has a much weaker algebraic dependence

$$\mu \propto \upsilon \left(\frac{E}{L}\right)^{(1-\alpha)/\alpha} \tag{12}$$

on the electic field. In this expression, $\upsilon = \upsilon_0 \exp(-\beta\varepsilon_0)$ is an effective detrapping rate.

Thus, while the MTM does an excellent job of describing characteristic features of TOF photocurrent transients themselves, it clearly fails as a model for predicting the temperature dependence and the universal Poole-Frenkel field dependence observed in experiment.

Similarly, Gaussian models have not been shown to exhibit a transition to dispersive transport, and there are good reasons to believe that they do not. Indeed, the physical mechanism that underlies the transition that occurs in MTMs is an inability of the charge carriers to equilibrate once the temperature falls below the critical temperature $T_c = \varepsilon_0/k$. For particles occupying an exponential distribution of trap states, the mean energy of a carrier in equilibrium would be proportional to the integral

$$\langle \varepsilon \rangle \propto \int_0^\infty (-\varepsilon) \rho(\varepsilon) e^{\varepsilon/kT} d\varepsilon = -\int_0^\infty \varepsilon e^{-\varepsilon/\varepsilon_0} e^{\varepsilon/kT} d\varepsilon \tag{13}$$

where the Boltzmann factor has a positive exponent, since the energy of a state with trap depth ε is $-\varepsilon$. For high enough temperatures, the integral is well-behaved, since the density of states makes the integrand exponentially small at large values of ε. For $T > T_c$, however, the integral diverges and the mean energy of a carrier falls to negative infinity. This cannot happen in a Gaussian density of states, because the Gaussian factor always modulates the integral. Thus, in a Gaussian model there is no critical temperature below which the mean energy is not finite, and the bulk mobility should not vanish at any finite temperature.

1.4. MOTIVATION FOR PRESENT RESEARCH AND OVERVIEW

The simultaneous presence of these two different features, i.e., a PF field dependence, and universality of current time transients leads to the question of whether

the energy distribution associated with the localized states frequented by carriers in these materials contains contributions from both kinds of disorder.

One can imagine, e.g., a situation in which transport sites are embedded in a medium possessing a spatially-correlated Gaussian background field $u(\vec{r})$ arising from random molecular charge distributions, but which also includes a perhaps small intrinsic concentration of uncorrelated low energy traps characterized by an exponential distribution of trap depths. Shallow and deep traps of this sort are frequently known to arise in organic materials, e.g., from broken bonds, chemical impurities, and other short-range defects.

In a two component medium of this sort, each of the two characteristic features commonly observed in MDPs could arise from the particular part of the energetic distribution of localized states to which it is sensitive, providing a natural explanation for their coexistence. Of course this is not guaranteed *a priori*, since inclusion of the type of disorder associated with one feature could significantly alter or destroy the behavior associated with the other. Thus, for such a theoretical explanation to be plausible it must be first established that these two mechanisms do not significantly *interfere* with one another.

It is this question that is addressed in this research. In particular, analytical and numerical calculations are presented of the field and temperature dependent mobility of carriers that undergo hopping transport on an ordered lattice with site energies $\varepsilon_n = u_n + \upsilon_n$ that are the sum of two independent components. The first component u_n is drawn from a spatially-correlated Gaussian distribution of energetic width σ_0, as in CDMs previously studied. The second component assigns to each site, with probability c, an additional energy υ_n drawn from an exponential distribution of energetic width ε_0. In this way one can able to study the degree to which the trap distribution alters or destroys the PF field dependence that would otherwise arise from the correlated component. In the process, it allows to determine the dependence of

the mobility on the additional parameters that characterize the distribution of traps in the system.

The rest of this dissertation is laid out as follows. The next section focuses on a description of statistical features associated with the energy distributions that characterize the energetic landscape on which the transport studies presented in the rest of the dissertation are based. Following that, a series of analytical calculations on quasi-one dimensional systems characterized by several different distributions of site energies is presented. In order to separate out characteristic effects associated with each, transport in systems containing (i) only an exponential distribution of traps, (ii) only an exponential distribution of barriers, and (iii) a combined exponential distribution of traps and barriers embedded in a correlated Gaussian energy landscape are separately considered. The results of that last investigation contain some of the main analytical results, which suggest that a hybrid model of this sort can, in fact, capture the main features seen in experiment. Unfortunately, analytical results are only possible in a one-dimensional calculation, and it is well known that 1D results do not always provide a reliable (qualitative or quantitative) indication of what actually happens in a 3D system. In section 4, therefore, the result of extensive numerical calculations that largely confirm the basic features observed in the 1D calculations is presented. The last section contains a brief summary.

2. STATISTICAL PROPERTIES

The focus of this section is on deriving properties of the site energy distribution functions that will be used later in the dissertation to describe a carrier moving through a correlated Gaussian energy landscape in which are distributed a fixed concentration of exponentially distributed traps. Thus, the possibility that the energy of a carrier located at the nth site in the system is allowed to be a sum $\varepsilon_n = u_n + \upsilon_n$ of two terms. The first term is the correlated component u_n, which is an element of a correlated Gaussian field $\mathbf{u} = (u_1, u_2, \ldots, u_N)$ characterized by a joint probability distribution function

$$\rho\left(\mathbf{u}\right) = \frac{\exp\left(-\frac{1}{2}\mathbf{u}\cdot\Sigma^{-1}\cdot\mathbf{u}\right)}{\sqrt{2\pi\left|\Sigma\right|}} \tag{14}$$

in which Σ is the correlation matrix with diagonal elements $\Sigma_{n,n} = \langle u_n^2\rangle = \sigma_0^2$ equal to the variance of the marginal distribution

$$\rho_1\left(u_n\right) = \frac{e^{-u_n^2/2\sigma_0^2}}{\sqrt{2\pi\sigma_0^2}}, \tag{15}$$

of site energies, while the off-diagonal elements of Σ describe the long range spatial correlations [73]

$$\Sigma_{n,m} = \langle u_n u_m\rangle = \sigma_0^2\left[a_0 r_{nm}^{-1}\right] \qquad m \neq n \tag{16}$$

that are assumed to arise from unscreened molecular charge distributions in the medium, and thus have a form that has been shown to arise from the interaction between a carrier and random molecular dipole moments [73] in the material. In this last expression, a_0 is a minimum separation distance between transport sites,

comparable to the size of the dopant molecules themselves, which is generally smaller than or equal to the mean separation distance a between nearest neighbors. As described elsewhere [73], the long range (i.e., r^{-2}) dependence of the charge dipole interaction on distance makes this the dominant contribution to the correlated component of the potential energy background in which the transport sites are embedded.

In addition to this correlated component, a certain fraction c of sites in the system represent either traps or "anti-traps", i.e., barriers. At trap sites, the energy is altered relative to the correlated background in which it is embedded, by a random negative amount υ_n drawn from an exponential distribution of trap depths. At a barrier site, the random energy is positive and drawn from an exponential distribution of barrier heights. In principle, these could be two different distributions. Taking into account the fractional occupation of traps or barriers along the path, the energies υ_n are assumed to be independently drawn from a distribution

$$\rho_2(\upsilon_n) = c\rho_e(\upsilon_n) + (1-c)\,\delta(\upsilon_n) \tag{17}$$

where for traps ($\upsilon_n < 0$)

$$\rho_e(\upsilon_n) = \varepsilon_0^{-1} \exp\left(-|\upsilon_n|/\varepsilon_0\right), \tag{18}$$

for barriers ($\upsilon_n > 0$),

$$\rho_e(\upsilon_n) = \varepsilon_0^{-1} \exp\left(-\upsilon_n/\varepsilon_0\right),$$

and in the presence of a symmetric distribution of traps and barriers

$$\rho_e(\upsilon_n) = (2\varepsilon_0)^{-1} \exp\left(-|\upsilon_n|/\varepsilon_0\right). \tag{19}$$

Note that $\upsilon_n = 0$ for sites that are not traps (or barriers), which occur in fractional concentration $(1-c)$. For mathematical convenience, both positive and negative trap depths, are allowed and calculations later in the dissertation that correspond to both of these situations are presented. In the numerical results presented in section 4 on 3D systems both traps and barriers are included, both of which are documented components of disordered organic solids [46]. This purely mathematical assumption makes the mean value $\langle \upsilon_n \rangle = 0 = \langle u_n \rangle$ of the uncorrelated component equal to that of the correlated component, and allows the full width σ of the total distribution of site energies in the system to be more easily to characterized. In the rest of this section, the details of the statistical description associated with this symmetrical exponential distribution are worked out. The anlysis for the situation where there are only traps, or only barriers, follows along similar lines.

For the symmetric distribution, the uncorrelated energies υ_n are characterized by vanishing first moments $\langle \upsilon_n \rangle = 0$ and second moments $\langle v_n^2 \rangle$ that can be calculated using Eq.(18) and (17)

$$\left\langle v_n^2 \right\rangle = \frac{c}{2\varepsilon_0} \int_{-\infty}^{\infty} d\upsilon_n \; \upsilon_n^2 \exp\left(-\frac{|\upsilon_n|}{\varepsilon_0} \right) = 2c \left(\varepsilon_0\right)^2 . \tag{20}$$

Thus, one can write

$$\langle \upsilon_n \upsilon_m \rangle = 2c\varepsilon_0^2 \; \delta_{n,m} = \sigma_t^2 \delta_{n,m},$$

in which $\sigma_t = \sqrt{2c}\varepsilon_0$.

With the assumption that the two contributions to the full site energy $\varepsilon_n = u_n + \upsilon_n$ are uncorrelated with each other, the moments of the full distribution are then also readily computed

$$\langle \varepsilon_n \rangle = 0 \qquad\qquad \langle \varepsilon_n^2 \rangle = \sigma_0^2 + \sigma_t^2 = \sigma_0^2 + 2c\varepsilon_0^2 \tag{21}$$

The corresponding correlation function is

$$\langle \varepsilon_n \varepsilon_m \rangle = \sigma_0^2 (a_0 r_{nm}^{-1}) \qquad\qquad n \neq m.$$

Figure 2.1 shows a spatial plot of site energy as a function of position, i.e., the energy landscape, for the two parent distributions and for the combined distribution. For these plots, the width of the correlated Gaussian component is $\sigma_0 = 0.1$ eV, the width of the uncorrelated exponential distribution is $\varepsilon_0 = 0.1$ eV, and the concentration of traps and barriers is $c = 0.1$. The combined distribution contains characteristics of

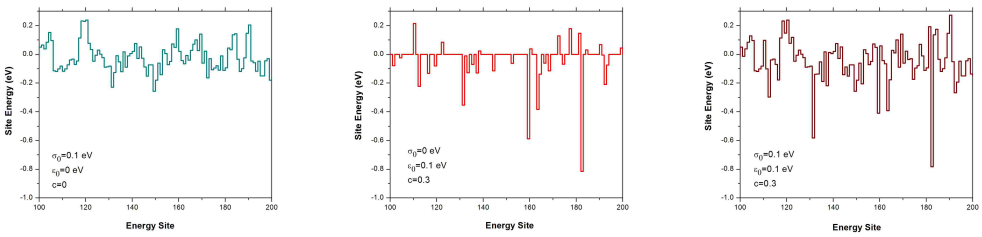

Figure 2.1. Energy Landscape for the correlated Gaussian, the uncorrelated exponential, and the combined distribution.

the two parent distributions, a fact that can be seen more easily if the frequency axis of the histogram for each distribution is plotted using a logarithmic axis, as in Fig. 2.2, in which the Gaussian distribution appears as an inverted parabola, and the exponential distribution as a linear "tent" function. The combined distribution remains very Gaussian near the centroid, but has tails of exponential character.

The combined site energy distribution function $\rho(\varepsilon)$ itself is given by the convolution

$$\rho(\varepsilon) = \int_{-\infty}^{\infty} dv_n \rho_2(v_n) \int_{-\infty}^{\infty} du_n \; \rho_1(u_n) \delta[\varepsilon - (u_n + v_n)]. \tag{22}$$

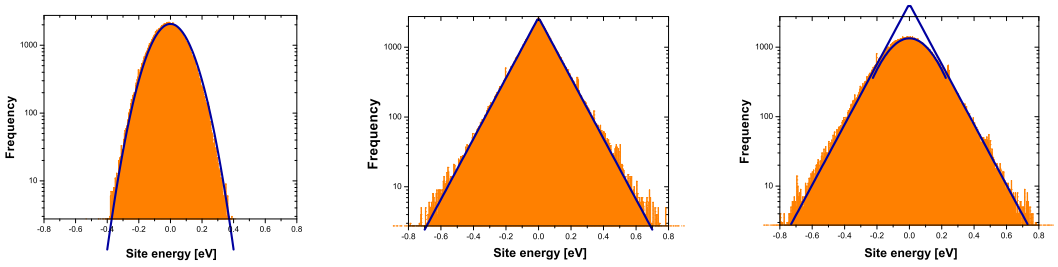

Figure 2.2. Log frequency histogram for the correlated Gaussian, uncorrelated exponential and the combined distribution.

Substituting the parent distributions from (15), (17), and (19) into this expression one finds that

$$\begin{aligned}
\rho(\varepsilon) &= \frac{1)}{\sqrt{2\pi\sigma_0^2}} \int_{-\infty}^{\infty} dv_n \ \left[c\rho_e\left(v_n\right) + \left(1-c\right)\delta(v_n)\right] \int_{-\infty}^{\infty} du_n \exp(-u_n^2/2)\delta[u_n - (\varepsilon - v_n)] \\
\rho(\varepsilon) &= \frac{1}{\sqrt{2\pi\sigma_0^2}} \int_{-\infty}^{\infty} \left[c\frac{1}{2\varepsilon_0}\exp\left(-\frac{|v_n|}{\varepsilon_0}\right) + \left(1-c\right)\delta(v_n)\right] \exp(-\frac{\left(\varepsilon - v_n\right)^2}{2\sigma_0^2})dv_n \\
&= \frac{1}{\sqrt{2\pi\sigma_0^2}} \left[\int_{-\infty}^{\infty} \frac{c}{2\varepsilon_0}\exp\left(-\frac{|v_n|}{\varepsilon_0}\right)\exp(-\frac{\left(\varepsilon - v_n\right)^2}{2\sigma_0^2})dv_n\right] \\
&\quad + \frac{1}{\sqrt{2\pi\sigma_0^2}} \left[\frac{(1-c)}{\varepsilon_0}\exp(-\frac{\varepsilon^2}{2\sigma_0^2})\right]
\end{aligned}$$

The remaining integrals are all of Gaussian form, and thus expressable in terms of the regular and complementary error function. Details are worked out in an Appendix; the final result can be expressed in the following relatively compact form

$$\rho(\varepsilon) = c\widehat{\rho}(\varepsilon) + \left(1-c\right)\rho_1(\varepsilon) \tag{23}$$

with

$$\widehat{\rho}(\varepsilon) = \frac{1}{4\varepsilon_0}\exp\left(\frac{\sigma_0^2}{2\varepsilon_0^2}\right) f(\varepsilon) \tag{24}$$

$$\rho_1(\varepsilon) = \frac{1}{\sqrt{2\pi\sigma_0^2}} \exp(-\frac{\varepsilon^2}{2\sigma_0^2}) \tag{25}$$

and

$$f(\varepsilon) = \exp\left(\frac{\varepsilon}{\varepsilon_0}\right)\left[1 - \mathrm{erf}\frac{\left(\varepsilon + \frac{\sigma_0^2}{\varepsilon_0}\right)}{\sqrt{2\sigma_0^2}}\right] + \exp\left(\frac{-\varepsilon}{\varepsilon_0}\right)\left[1 + \mathrm{erf}\frac{\left(\varepsilon - \frac{\sigma_0^2}{\varepsilon_0}\right)}{\sqrt{2\sigma_0^2}}\right].$$

Note from Fig. 2.2 that, because an exponential function falls off more slowly than a Gaussian, the tails of the total distribution are dominated by the *exponential* energy dependence of the uncorrelated component. To see this, substitute the asymptotic expansion $\mathrm{erf}\,(x) \sim 1 - x^{-1}\pi^{-1/2}e^{-x^2}$ of the error function into the expression for $f(\varepsilon)$ to obtain, after some algebra, the relation valid for $|\varepsilon| >> \sigma_0^2/\varepsilon_0$

$$f(\varepsilon) \sim 2\exp\left(\frac{-\varepsilon}{\varepsilon_0}\right)$$

which asymptotically gives for the combined distribution when $c > 0$,

$$\rho(\varepsilon) \simeq c\widehat{\rho}(\varepsilon) \simeq \frac{c}{2\varepsilon_0}\exp\left(\frac{\sigma_0^2}{2\varepsilon_0^2}\right)\exp\left(\frac{-\,|\varepsilon|}{\varepsilon_0}\right).$$

3. ANALYTICAL CALCULATIONS IN ONE-DIMENSION

In this section a number of new results relevant to photo-injected carriers moving at high electric fields through disordered energy landscapes of the type described in the Introduction are derived. The assumption of high electric fields is important, since it implies that longitudinal motion in the direction of the applied field is much larger than the diffusional spreading that takes place transverse to it. Intuitively, in this situation, the transport path taken by a carrier is asymptotically well-approximated by a quasi-one dimensional path through the material that begins on the injecting contact and ends on the collecting one. Analysis of motion along such a path allows for the derivation of some essentially exact results that allow us to gain insight into what could happen in bulk materials.

As mentioned in the introduction, the main concern is with the situation in which the energy landscape through which the particle moves contains two contributions, a correlated Gaussian one arising from unscreened dipole moments associated with the molecular constituents of the MDP, and an uncorrelated exponential component associated with chemical defects, broken bonds, and other short-range contributions to the energetic disorder. To that end, it is useful to develop some intuition regarding what happens when each of these components occurs separately.

Motion in a 1D *trap-free* correlated Gaussian potential was analytically studied in Refs. [75] and [76]. Those calculations were, themselves, based upon an exact solution due to Derrida [77] to the so-called "random bias problem" involving steady-state motion along a rather arbitrary 1D nearest-neighbor chain of transport sites. The theoretical translation of those exact results to a form appropriate to the description of motion in a correlated energy landscape of the type associated with MDPs led

in Refs. [75] and [76] to exact analytical results that, for the first time, predicted the Poole-Frenkel response to the electrical field commonly observed in those materials.

In view of these earlier results, here a series of three separate 1D calculations are presented, each similar in many ways to those presented in Refs. [75] and [76], but which differ from the earlier calculations in the details regarding the energy landscape through which the particle moves. The three cases consider here include situations where the energy landscape is (i) entirely described by a concentration c of randomly distributed traps drawn from an exponential distribution of trap depths, (ii) entirely described by a concentration c of randomly distributed barriers with an exponential distribution of barrier heights, and (iii) described by a hybrid two component system containing both a correlated Gaussian energy landscape as studied in Refs. [75] and [76], as well as a fractional concentration c of randomly distributed traps and barriers drawn from the symmetric exponential distribution described in the last section.

The first two calculations, which do not include the correlated Gaussian component, do not predict a Poole-Frenkel response to the driving field, but they each exhibit a transition as the temperature is lowered to a regime where the bulk mobility vanishes. For the case of exponentially distributed traps, this is to be expected since this calculation contains essentially the same physics included in multiple-trapping models (although the specific calculation presented here is new). Naturally, the transition in this case can be identified with the nondispersive to dispersive transition predicted by MTMs. The second case considered here, provides a high-field example of a "random barrier model" and shows that, at least in 1D, an exponential distribution of barriers can also lead to a transition to a "non-conducting", or dispersive regime, even though the mean energy of a carrier in such a system is always well defined and finite. Hence, it suggests the possibility of another mechanism for dispersive transport other than the normal picture where the carriers fail to equilibrate.

The third calculation, in which traps and barriers are embedded in a correlated Gaussian landscape, is the primary focus of the research contained in this dissertation since it holds the possibility of explaining the disparate features commonly observed in MDPs. In this case, due to the traps and barriers, one also finds a transition to a dispersive regime. For this particular model, the transition appears to dominated by the presence of the traps, which by themselves lead to a higher critical temperature than do barriers alone. In spite of the transition, which suggests trap-dominated transport, the analysis continues to predict a Poole-Frenkel field dependence, and a temperature dependence that has both quadratic and linear activation factors, as observed experimentally, provided that small polaron transport rates are assumed. The temperature and field dependence is predicted, moreover, to persist right up to the transition point, as is also observed in experiments. The analytical calculations presented in this section, therefore, sets the stage, and provides an impetus for the 3D numerical calculations presented in the next section, which are designed to verify whether these features are maintained in higher dimensions.

3.1. MOTION THROUGH A 1D MEDIUM CONTAINING A RANDOM DISTRIBUTION OF TRAPS

In this section a carrier moving in 1D through a medium containing a finite concentration c of traps is considered, each with a trap depth independently drawn from an exponential distribution of width ε_0. As in section 2, the site energy distribution function for individual sites along this 1D path can be written in the form

$$\rho\left(\varepsilon_n\right) = c\rho_e\left(\varepsilon_n\right) + \left(1-c\right)\delta\left(\varepsilon_n\right), \tag{26}$$

where, for $\varepsilon < 0$

$$\rho_e\left(\varepsilon\right) = \varepsilon_0^{-1}\exp\left(\varepsilon/\varepsilon_0\right). \tag{27}$$

The calculation starts with the master equation

$$\frac{dP_n}{dt} = \sum_m \left[W_{n,m}P_m\left(t\right) - W_{m,n}P_n\left(t\right)\right] \tag{28}$$

governing the evolution of the probability $P_n\left(t\right)$ of finding the carrier at the nth site along the path at time t, in which the hopping rate $W_{n,m}$ from site m to site n is assumed to depend on the separation distance and on the energies of the two sites as in Eq. (3). In view of the exponential dependence of the transition rate on separation distance, transitions are restricted to nearest neighbors , which are assumed to be separated by a mean separation distance a. Also, for mathematical convenience one can follow the authors of Ref. [75] and drop the "inversion term" in Eq. (3) and re-express the resulting polaron hopping rate in a symmetric form which can be written as

$$W_{n,m} = \nu_0 \exp\left[-\frac{\varepsilon_{nm}}{2kT}\right] \tag{29}$$

in which an overall prefactor is introduced

$$\nu_0 = \frac{J_0^2 e^{-2\lambda a}}{\sqrt{2\hbar^2\varepsilon_B kT/\pi}} \exp\left[-\frac{\varepsilon_B}{2kT}\right] \tag{30}$$

that is linearly activated due to the dependence on the polaron binding energy, but is independent of the energy mismatch between neighboring sites. In this approximation, taking the field E to be directed towards increasing n, and taking into account the detailed balance relation $W_{n,n+1}/W_{n+1,n} = e^{-\beta(\varepsilon_n - \varepsilon_{n+1} + eEa)}$ obeyed by the transition rates in the presence of the field, the authors of Ref. [75] claim, based on exact results of Derrida [77], that at the field strengths typically used in the experiments

of interest, the drift velocity for such a system can be written in the form

$$v = \mu E = \frac{\nu_0 a e^{\frac{1}{2}\beta e E a}}{\sum_{m=0}^{N-1} e^{-m\beta e E} \left\langle e^{-\beta\varepsilon_n} e^{\frac{1}{2}\beta\varepsilon_{n+m}} e^{\frac{1}{2}\beta\varepsilon_{n+m+1}} \right\rangle}, \tag{31}$$

where, according to Ref. [75], the correlation function

$$\left\langle e^{-\beta\varepsilon_n} e^{\frac{1}{2}\beta\varepsilon_{n+m}} e^{\frac{1}{2}\beta\varepsilon_{n+m+1}} \right\rangle = \frac{1}{N} \sum_{n=1}^{N} e^{-\beta\varepsilon_n} e^{\frac{1}{2}\beta\varepsilon_{n+m}} e^{\frac{1}{2}\beta\varepsilon_{n+m+1}} \tag{32}$$

is to be identified with a particular sum of products of Boltzmann factors that arise in the course of the calculation. With this identification, the correlation function itself can be computed as an average taken with respect to the distribution (26). Interestingly, the basic result (31) does not appear to have been derived anywhere in the literature. In the interest of completeness, therefore, the opportunity is taken to provide such a derivation here.

A derivation of (31) begins with an exact result due to Derrida [77] for the steady-state drift velocity v for a general 1D nearest neighbor chain with transition rates $W_{n,n+1}$ and $W_{n,n-1}$ governing hopping transitions into site n from sites $n+1$ and $n-1$, respectively. For a chain of length N subject to periodic boundary conditions, Derrida derives the following expression for the drift velocity

$$v = \frac{aN}{\sum_{n=1}^{N} r_n} \left[1 - \prod_{n=1}^{N} \left(\frac{W_{n,n+1}}{W_{n+1,n}} \right) \right] \tag{33}$$

where the quantities r_n are given by the expression

$$r_n = \frac{1}{W_{n+1,n}} \left[1 + \sum_{i=1}^{N-1} \prod_{j=1}^{i} \left(\frac{W_{n+j-1,n+j}}{W_{n+j+1,n+j}} \right) \right]. \tag{34}$$

As described above, one can assume a symmetric detailed balance relation that, in the presence of the field can be written

$$W_{n\pm1,n} = \upsilon_0 \exp\left[-\frac{1}{2}\beta\left(\varepsilon_{n\pm1} - \varepsilon_n \mp F\right)\right] \tag{35}$$

where $F = eEa$ is the potential energy change induced across two sites by the field. Substituting these hopping rates into Eq. (33) one finds

$$v = \frac{aN}{\sum_{n=1}^{N} r_n}\left[1 - \prod_{n=1}^{N}\left(\frac{e^{-\frac{1}{2}\beta\varepsilon_n}e^{\frac{1}{2}\beta\varepsilon_{n+1}}e^{-\frac{1}{2}\beta F}}{e^{-\frac{1}{2}\beta\varepsilon_{n+1}}e^{\frac{1}{2}\beta\varepsilon_n}e^{\frac{1}{2}\beta F}}\right)\right]$$

$$= \frac{aN}{\sum_{n=1}^{N} r_n}\left[1 - \prod_{n=1}^{N} e^{-\frac{1}{2}\beta[\varepsilon_n - \varepsilon_{n+1}]}e^{-\beta F}\right]$$

$$= \frac{aN}{\sum_{n=1}^{N} r_n}\left[1 - e^{-N\beta F}\prod_{n=1}^{N} e^{-\frac{1}{2}\beta[\varepsilon_n - \varepsilon_{n+1}]}\right]$$

$$= \frac{aN}{\sum_{n=1}^{N} r_n}\left[1 - e^{-N\beta F}e^{-\frac{1}{2}\beta[\varepsilon_1 - \varepsilon_N]}\right]$$

in which the r_n must now be obtained using Eq. (34). Expanding, and using detailed balance,

$$r_n = \frac{1}{W_{n+1,n}}\left[1 + \left(\frac{W_{n,n+1}}{W_{n+2,n+1}}\right) + \left(\frac{W_{n,n+1}}{W_{n+2,n+1}}\right)\left(\frac{W_{n+1,n+2}}{W_{n+3,n+2}}\right) + \ \ldots\right]$$

$$= \frac{1}{W_{n+1,n}}\left[1 + \left(\frac{e^{\left[-\frac{1}{2}\beta(\varepsilon_n - \varepsilon_{n+1} + F)\right]}}{e^{\left[-\frac{1}{2}\beta(\varepsilon_{n+2} - \varepsilon_{n+1} - F)\right]}}\right) + \left(\frac{e^{\left[-\frac{1}{2}\beta(\varepsilon_n - \varepsilon_{n+1} + F)\right]}}{e^{\left[-\frac{1}{2}\beta(\varepsilon_{n+2} - \varepsilon_{n+1} - F)\right]}} \times \frac{e^{\left[-\frac{1}{2}\beta(\varepsilon_{n+1} - \varepsilon_{n+2} + F)\right]}}{e^{\left[-\frac{1}{2}\beta(\varepsilon_{n+3} - \varepsilon_{n+2} - F)\right]}}\right)\right]$$

This last expression can be systematically simplified.

$$r_n = \frac{e^{\frac{1}{2}\beta\varepsilon_{n+1}} e^{-\frac{1}{2}\beta\varepsilon_n} e^{-\frac{1}{2}\beta F}}{\upsilon_0} \Big[1 + e^{-\frac{1}{2}\beta\varepsilon_n} e^{-\frac{1}{2}\beta\varepsilon_{n+2}} e^{-\beta F} + e^{-\frac{1}{2}\beta\varepsilon_n} e^{-\frac{1}{2}\beta\varepsilon_{n+1}} e^{-\frac{1}{2}\beta\varepsilon_{n+2}} e^{-\frac{1}{2}\beta\varepsilon_{n+3}} e^{-2\beta F} + \ldots\Big]$$

and so

$$r_n = \frac{e^{-\frac{1}{2}\beta F}}{\upsilon_0} \left[\left(e^{\frac{1}{2}\beta\varepsilon_{n+1}} e^{-\frac{1}{2}\beta\varepsilon_n}\right) + \left(e^{-\beta\varepsilon_n} e^{\frac{1}{2}\beta\varepsilon_{n+1}} e^{\frac{1}{2}\beta\varepsilon_{n+2}}\right) e^{-\beta F} + \left(e^{-\beta\varepsilon_n} e^{\frac{1}{2}\beta\varepsilon_{n+2}} e^{\frac{1}{2}\beta\varepsilon_{n+3}}\right) e^{-2\beta F} + \ldots\right]$$

The final expression for r_n then takes the form

$$r_n = \frac{e^{-\frac{1}{2}\beta F}}{\upsilon_0} \sum_{m=0}^{N-1} e^{-m\beta F} e^{-\beta\varepsilon_n} e^{\beta\varepsilon_{n+m}} e^{\beta\delta_{n+m}}$$

where $2\delta_n = \varepsilon_{n+1} - \varepsilon_n$. Substituting the quantities r_n into the equation for the drift velocity, one finds without approximation

$$v = \frac{\upsilon_0 \rho e^{\frac{1}{2}\beta F} \left[1 - e^{-\left[N\beta F + \frac{1}{2}\beta[\varepsilon_1 - \varepsilon_N]\right]}\right]}{\frac{1}{N}\sum_{m=0}^{N-1} e^{-m\beta F} \sum_{n=1}^{N} e^{-\beta\varepsilon_n} e^{\beta\varepsilon_{n+m}} e^{\beta\delta_{n+m}}}. \tag{36}$$

Here $N\beta F = N\beta eEa = \beta eEL$ is the ratio of the potential energy drop across the entire sample (which may be tens of electron volts) to the mean thermal energy kT (which is measured in meV). Hence the exponential term in the bracket of the numerator is completely negligible. Dropping this term, and introducing the definition (32) reduces this last expression to (31), as desired.

With this derivation of Eq. (31), it remains to carry out the computation of the correlation function (32), using the distribution defined by (26) and (27). As it turns out, the necessary integrals over the trap distribution are all of exponential form, and easily evaluated. To this end it is useful to note that for any $\lambda > 0$,

$$\langle e^{\lambda\beta\varepsilon}\rangle = (1-c) + \frac{c}{1+\lambda\beta\varepsilon_0}, \qquad \lambda > 0. \tag{37}$$

For $\lambda > 0$ and $\lambda\beta\varepsilon_0 < 1$, on the other hand,

$$\langle e^{-\lambda\beta\varepsilon}\rangle = (1-c) + \frac{c}{1-\lambda\beta\varepsilon_0}, \qquad \lambda > 0, \quad \lambda\beta\varepsilon_0 < 1. \tag{38}$$

Finally, for $\lambda > 0$ and $\lambda\beta\varepsilon_0 > 1$, the mean value $\langle e^{-\lambda\beta\varepsilon}\rangle$ diverges, i.e.,

$$\langle e^{-\lambda\beta\varepsilon}\rangle \to \infty, \qquad \lambda > 0, \quad \lambda\beta\varepsilon_0 > 1. \tag{39}$$

Thus, e.g., for $m = 0$ the correlation function (32) can be computed as

$$\langle e^{-\beta\varepsilon_n} e^{\frac{1}{2}\beta\varepsilon_n} e^{\frac{1}{2}\beta\varepsilon_{n+1}}\rangle = \langle e^{-\frac{1}{2}\beta\varepsilon}\rangle\langle e^{\frac{1}{2}\beta\varepsilon}\rangle \tag{40}$$

where using the fact that energies at different sites are uncorrelated. Using (37) and (38) obtaining from this last expression for $\beta\varepsilon_0 < 2$,

$$\langle e^{\frac{1}{2}\beta\varepsilon}\rangle = \frac{2+\beta\varepsilon_0\,(1-c)}{2+\beta\varepsilon_0} \tag{41}$$

and

$$\langle e^{-\frac{1}{2}\beta\varepsilon}\rangle = \frac{2-\beta\varepsilon_0\,(1-c)}{2-\beta\varepsilon_0}. \tag{42}$$

For $\beta\varepsilon_0 > 2$, the first term (41) remains unchanged, while (42) diverges. Thus, for $m = 0$ and $\beta\varepsilon_0 < 2$ the correlation function (32) can be written

$$\langle e^{-\beta\varepsilon_n} e^{\frac{1}{2}\beta\varepsilon_n} e^{\frac{1}{2}\beta\varepsilon_{n+1}} \rangle = \frac{4 - \beta^2\varepsilon_0^2 (1-c)^2}{4 - \beta^2\varepsilon_0^2} \tag{43}$$

while for $\beta\varepsilon_0 > 2$ it diverges. For $m > 0$ one needs to evaluate

$$\langle e^{-\beta\varepsilon_n} e^{\frac{1}{2}\beta\varepsilon_{n+m}} e^{\frac{1}{2}\beta\varepsilon_{n+m+1}} \rangle = \langle e^{-\beta\varepsilon} \rangle \langle e^{\frac{1}{2}\beta\varepsilon} \rangle^2. \tag{44}$$

For $\beta\varepsilon_0 > 1$ this diverges, according to (39). For $\beta\varepsilon_0 < 1$, using (37) and (38), one finds that

$$\langle e^{-\beta\varepsilon_n} e^{\frac{1}{2}\beta\varepsilon_{n+m}} e^{\frac{1}{2}\beta\varepsilon_{n+m+1}} \rangle = \left(\frac{1 - \beta\varepsilon_0 (1-c)}{1 - \beta\varepsilon_0} \right) \left(\frac{2 + \beta\varepsilon_0 (1-c)}{2 + \beta\varepsilon_0} \right)^2 \tag{45}$$

Substituting these correlation functions into the denominator of (31), one finds that most of the terms factor out of the sum, which can then be computed as a geometric series in powers of $\exp(-\beta eEa)$. Performing the resulting sum, one finds that for $\beta\varepsilon_0 < 1$,

$$\begin{aligned} v = \nu_0 a e^{\frac{1}{2}\beta eEa} \Bigg[& \frac{4 - \beta^2\varepsilon_0^2 (1-c)^2}{4 - \beta^2\varepsilon_0^2} \\ & + 2 \left(\frac{1 - \beta\varepsilon_0 (1-c)}{1 - \beta\varepsilon_0} \right) \left(\frac{2 + \beta\varepsilon_0 (1-c)}{2 + \beta\varepsilon_0} \right)^2 \operatorname{csch} (\beta eEa/2)\, e^{-\frac{1}{2}\beta eEa} \Bigg]^{-1} \end{aligned} \tag{46}$$

For $\beta\varepsilon_0 > 1$ the drift velocity and mobility vanish, as a result of the diverging correlation functions that appear in the denominator of (31) in that regime. This is the signature, in this steady-state calculation, of the non-dispersive to dispersive transition predicted by multiple trapping models, and indeed the transition deduced here occurs at the same critical temperature $T_c = \varepsilon_0/k$ as predicted by those models. This

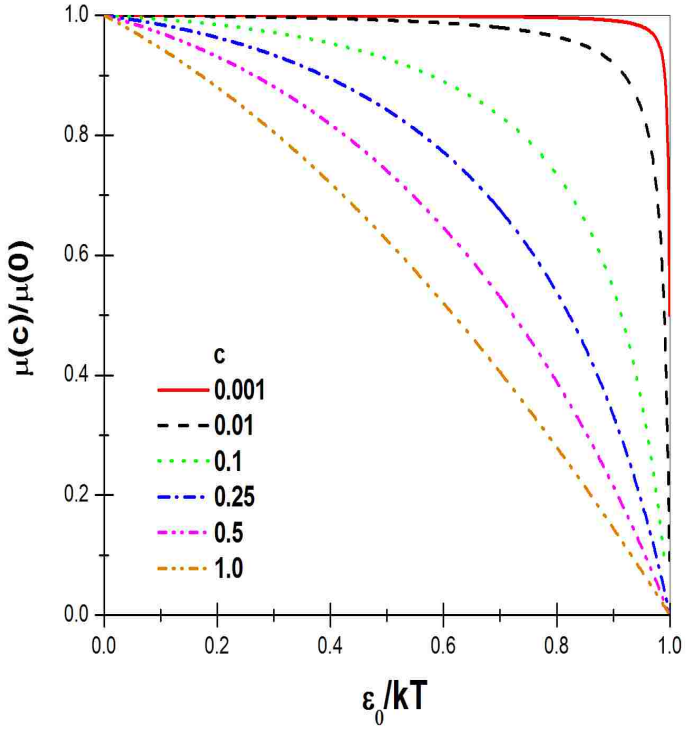

Figure 3.1. Normalized mobility $\mu(T)/\mu(0)$ as a function of ε_0/kT.

behavior is shown in Fig. 3.1 which shows the normalized mobility as a function of ε_0/kT. The concentration dependence of the mobility is shown in Fig. 3.2.

The field dependence of the mobility is governed by the hyperbolic and exponential factors that appear in this expression. Interestingly, the arguments of these functions are independent of any disorder parameters and just depend on the ratio of the potential energy drop eEa due to the field across a single lattice spacing, to the thermal energy kT.

At low fields, as $E \to 0$, the hyperbolic cosecant diverges as the inverse of its argument, and the exponential function approaches unity. In this limit the system

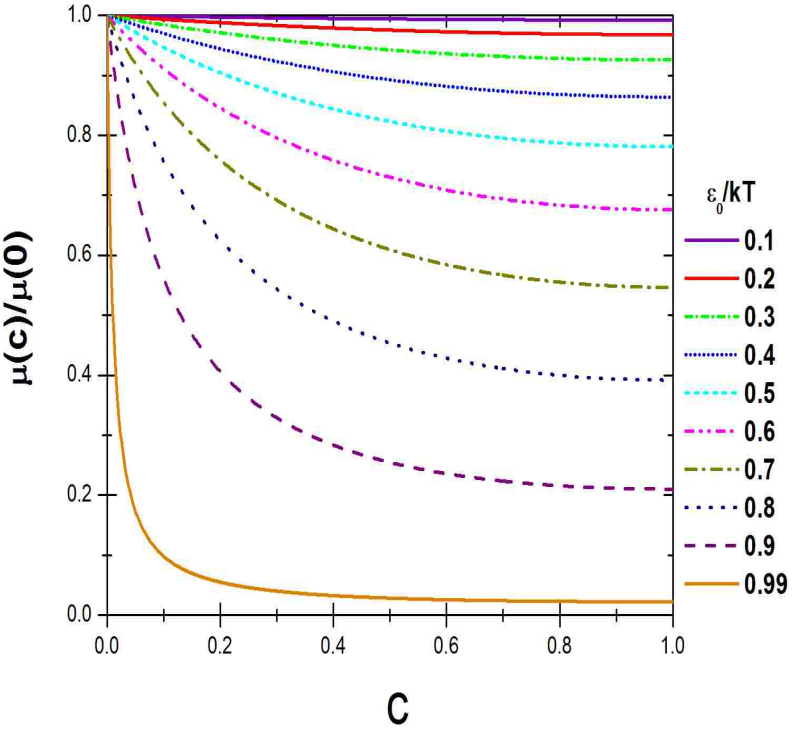

Figure 3.2. Normalized mobility $\mu(c)/\mu(0)$ as a function of trap concentration c.

exhibits a linear (Ohmic) response:

$$v \sim \frac{\nu_0 a}{4\left(\frac{1-\beta\varepsilon_0(1-c)}{1-\beta\varepsilon_0}\right)\left(\frac{2+\beta\varepsilon_0(1-c)}{2+\beta\varepsilon_0}\right)^2}\beta eEa \tag{47}$$

$$\mu = \frac{\beta\nu_0 a^2 e}{4\left(\frac{1-\beta\varepsilon_0(1-c)}{1-\beta\varepsilon_0}\right)\left(\frac{2+\beta\varepsilon_0(1-c)}{2+\beta\varepsilon_0}\right)^2} = \beta eD \tag{48}$$

where

$$D = \frac{\nu_0 a^2}{4\left(\frac{1-\beta\varepsilon_0(1-c)}{1-\beta\varepsilon_0}\right)\left(\frac{2+\beta\varepsilon_0(1-c)}{2+\beta\varepsilon_0}\right)^2} \tag{49}$$

is the low-field diffusion constant. This reduces to $D_0 = \nu_0 a^2$ when $c = 0$ and to the following when $c = 1$.

$$D_1 = \frac{\nu_0 a^2}{4\left(\frac{1}{1-\beta\varepsilon_0}\right)\left(\frac{2}{2+\beta\varepsilon_0}\right)^2}$$

When the arguments of the hyperbolic cosecant and the exponential function become of the order of unity, the drift velocity (Fig. 3.3) eventually increase because of the $e^{\frac{1}{2}\beta eEa}$ term. Thus, with a random distribution of exponentially distributed traps, the mobility increases exponentially with field from its Ohmic limit. This behavior is shown in Fig. 3.4.

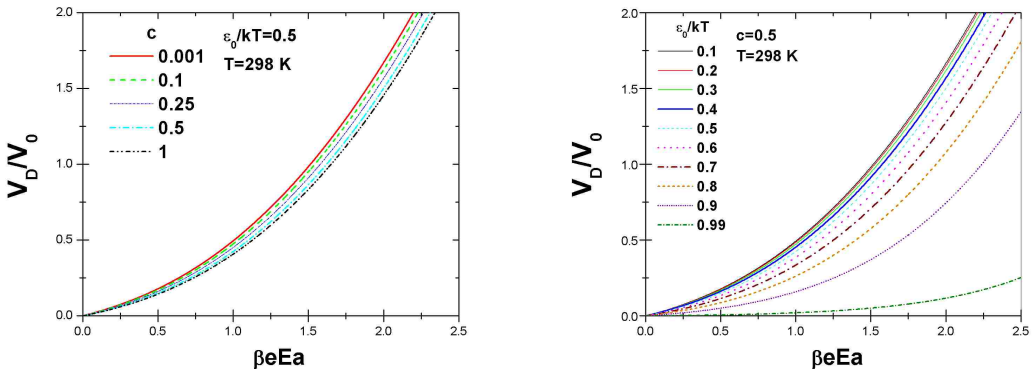

Figure 3.3. Normalized Drift Velocity as a function of E.

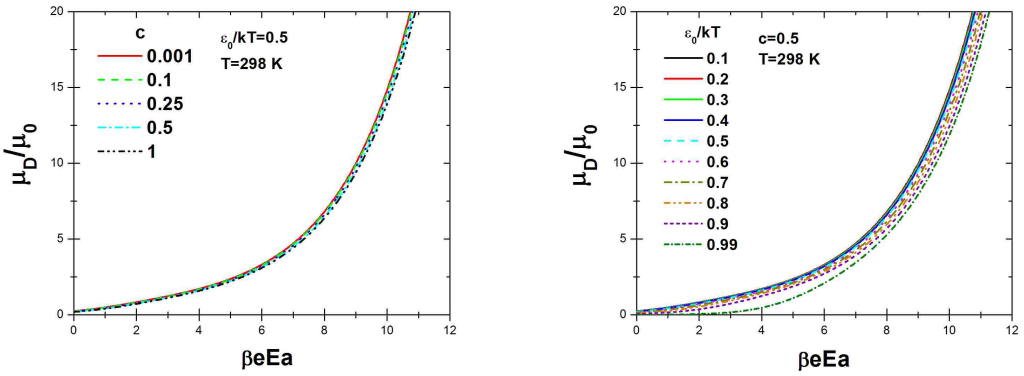

Figure 3.4. Normalized Mobility as a function of E.

3.2. MOTION THROUGH A 1D MEDIUM CONTAINING A RANDOM DISTRIBUTION OF BARRIERS

In this section the calculation presented above is repeated for the case in which the exponentially distributed site energies that appear in concentration c are positive, and thus potentially represent barriers to transport. For this situation, the relevant site energy distribution function takes a form similar to that of the last calculation

$$\rho\left(\varepsilon_n\right) = c\rho_e\left(\varepsilon_n\right) + \left(1-c\right)\delta\left(\varepsilon_n\right), \tag{50}$$

except that now, for positive energies $\varepsilon > 0$

$$\rho_e\left(\varepsilon\right) = \varepsilon_0^{-1}\exp\left(-\varepsilon/\varepsilon_0\right). \tag{51}$$

The calculation proceeds as in the last section. Starting with the master equation (28) one obtains, as shown in the last section, the drift velocity

$$v = \mu E = \frac{\nu_0 a e^{\frac{1}{2}\beta eEa}}{\sum_{m=0}^{N-1} e^{-m\beta eEa}\left\langle e^{-\beta\varepsilon_n} e^{\frac{1}{2}\beta\varepsilon_{n+m}} e^{\frac{1}{2}\beta\varepsilon_{n+m+1}}\right\rangle}, \tag{52}$$

where

$$\langle e^{-\beta\varepsilon_n} e^{\frac{1}{2}\beta\varepsilon_{n+m}} e^{\frac{1}{2}\beta\varepsilon_{n+m+1}}\rangle = \frac{1}{N}\sum_{n=1}^{N} e^{-\beta\varepsilon_n} e^{\frac{1}{2}\beta\varepsilon_{n+m}} e^{\frac{1}{2}\beta\varepsilon_{n+m+1}}. \tag{53}$$

In this case, for $m = 0$ the correlation function can be computed as

$$\langle e^{-\beta\varepsilon_n} e^{\frac{1}{2}\beta\varepsilon_n} e^{\frac{1}{2}\beta\varepsilon_{n+1}}\rangle = \langle e^{-\frac{1}{2}\beta\varepsilon}\rangle\langle e^{\frac{1}{2}\beta\varepsilon}\rangle \tag{54}$$

where each average is now over the distribution given by (50) and (51). Again, the integrals required to carry out the average are of exponential form, and one finds,

e.g., that

$$\begin{aligned}\langle e^{\frac{1}{2}\beta\varepsilon}\rangle &= \int_0^\infty \rho(\varepsilon)\, e^{\frac{1}{2}\beta\varepsilon} d\varepsilon \\ &= \int_0^\infty \left[\frac{c}{\varepsilon_0} e^{-\varepsilon/\varepsilon_0} + (1-c)\,\delta(\varepsilon)\right] e^{\frac{1}{2}\beta\varepsilon} d\varepsilon \\ &= \frac{c}{\varepsilon_0}\int_0^\infty \exp\left[-\varepsilon\left(\frac{2-\beta\varepsilon_0}{2\varepsilon_0}\right)\right] d\varepsilon + (1-c)\end{aligned}$$

which diverges when $\beta\varepsilon_0 > 2$ and simplifies for $\beta\varepsilon_0 < 2$ to

$$\langle e^{\frac{1}{2}\beta\varepsilon}\rangle = (1-c) + \frac{2c}{2-\beta\varepsilon_0} = \frac{2-\beta\varepsilon_0(1-c)}{2-\beta\varepsilon_0}, \quad \beta\varepsilon_0 < 2. \tag{55}$$

Similarly, at any temperature:

$$\langle e^{-\frac{1}{2}\beta\varepsilon}\rangle = (1-c) + \frac{2c}{2+\beta\varepsilon_0} = \frac{2+\beta\varepsilon_0(1-c)}{2+\beta\varepsilon_0}. \tag{56}$$

Thus, for $m = 0$ the correlation function (53) diverges for $\beta\varepsilon_0 > 2$ and otherwise is given by

$$\langle e^{-\beta\varepsilon_n} e^{\frac{1}{2}\beta\varepsilon_n} e^{\frac{1}{2}\beta\varepsilon_{n+1}}\rangle = \frac{4-\beta^2\varepsilon_0^2(1-c)^2}{4-\beta^2\varepsilon_0^2}, \quad \beta\varepsilon_0 < 2. \tag{57}$$

For $m > 0$ evaluate:

$$\langle e^{-\beta\varepsilon_n} e^{\frac{1}{2}\beta\varepsilon_{n+m}} e^{\frac{1}{2}\beta\varepsilon_{n+m+1}}\rangle = \langle e^{-\beta\varepsilon}\rangle\langle e^{\frac{1}{2}\beta\varepsilon}\rangle^2 \tag{58}$$

which also diverges for $\beta\varepsilon_0 > 2$ and otherwise reduces to

$$\langle e^{-\beta\varepsilon_n} e^{\frac{1}{2}\beta\varepsilon_{n+m}} e^{\frac{1}{2}\beta\varepsilon_{n+m+1}}\rangle = \left(\frac{1-\beta\varepsilon_0(1-c)}{1+\beta\varepsilon_0}\right)\left(\frac{2-\beta\varepsilon_0(1-c)}{2-\beta\varepsilon_0}\right)^2. \tag{59}$$

With this last expression, the denominator of (52) can be written

$$\sum_{m=0}^{N-1} e^{-m\beta eEa}\langle e^{-\beta\varepsilon_n} e^{\frac{1}{2}\beta\varepsilon_{n+m}} e^{\frac{1}{2}\beta\varepsilon_{n+m+1}}\rangle$$

$$= \frac{4-\beta^2\varepsilon_0^2(1-c)^2}{4-\beta^2\varepsilon_0^2} + \left(\frac{1-\beta\varepsilon_0(1-c)}{1+\beta\varepsilon_0}\right)\left(\frac{2-\beta\varepsilon_0(1-c)}{2-\beta\varepsilon_0}\right)^2 \sum_{m=1}^{\infty} e^{-m\beta eEa}$$

$$= \frac{4-\beta^2\varepsilon_0^2(1-c)^2}{4-\beta^2\varepsilon_0^2}$$

$$+\left(\frac{1-\beta\varepsilon_0(1-c)}{1+\beta\varepsilon_0}\right)\left(\frac{2-\beta\varepsilon_0(1-c)}{2-\beta\varepsilon_0}\right)\left(\frac{e^{-\beta eEa}}{1-e^{-\beta eEa}}\right)$$

$$= \frac{4-\beta^2\varepsilon_0^2(1-c)^2}{4-\beta^2\varepsilon_0^2}$$

$$+\frac{1}{2}\left(\frac{1+\beta\varepsilon_0(1-c)}{1+\beta\varepsilon_0}\right)\left(\frac{2-\beta\varepsilon_0(1-c)}{2-\beta\varepsilon_0}\right)^2 \operatorname{csch}(\beta eEa/2)\, e^{-\frac{1}{2}\beta eEa}$$

giving, for exponentially distributed barriers of mean barrier height ε_0 in concentration c, the result, valid for $\beta\varepsilon_0 < 2$,

$$v = \nu_0 a e^{\frac{1}{2}\beta eEa}\left[\frac{4-\beta^2\varepsilon_0^2(1-c)^2}{4-\beta^2\varepsilon_0^2}\right.$$
$$\left.+\frac{1}{2}\left(\frac{1+\beta\varepsilon_0(1-c)}{1+\beta\varepsilon_0}\right)\left(\frac{2-\beta\varepsilon_0(1-c)}{2-\beta\varepsilon_0}\right)^2 \operatorname{csch}(\beta eEa/2)\, e^{-\frac{1}{2}\beta eEa}\right]^{-1}. \quad (60)$$

Thus, in the random barrier problem a mobility transition occurs at a critical temperature $T_c = \varepsilon_0/2k$, which is half of that which arises in the random trap problem. Thus barriers are less effective than traps in reducing the mobility. This behavior is shown in Fig. 3.5 which shows the normalized mobility as a function of ε_0/kT. The concentration dependence of the mobility is shown in Fig. 3.6. One can note that this transition occurs even though, in this problem, the mean energy of a carrier in

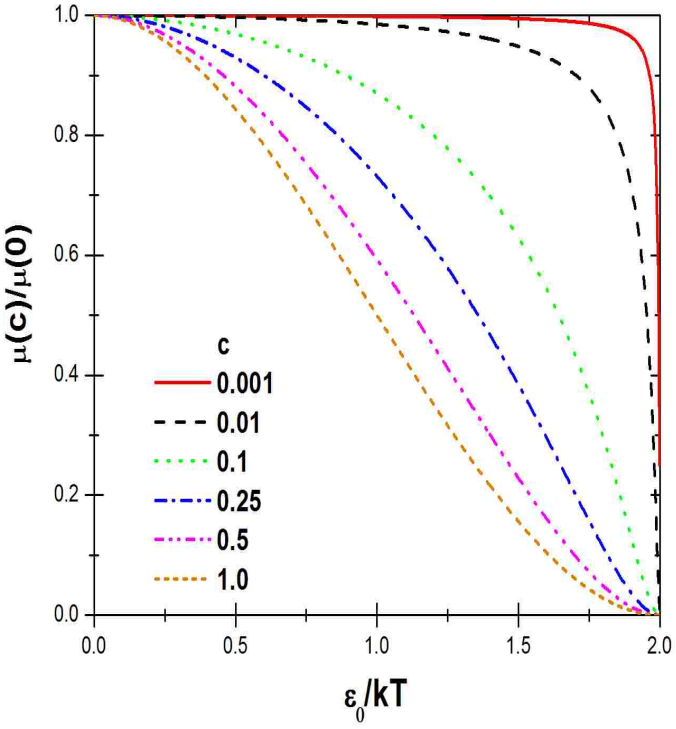

Figure 3.5. Normalized mobility as a function of ε_0.

thermal equilibrium remains finite at all positive temperatures–so in this case the mobility transition is not due to an inability of carriers to come to thermal equilibrium.

Above the transition, the field dependence of the mobility (60) is clearly very similar to that predicted by (46). Thus, e.g., a similar low field (Ohmic) response is found:

$$v = \frac{\nu_0 a}{4\left(\frac{1+\beta\varepsilon_0(1-c)}{1+\beta\varepsilon_0}\right)\left(\frac{2-\beta\varepsilon_0(1-c)}{2-\beta\varepsilon_0}\right)^2}\beta e E a, \tag{61}$$

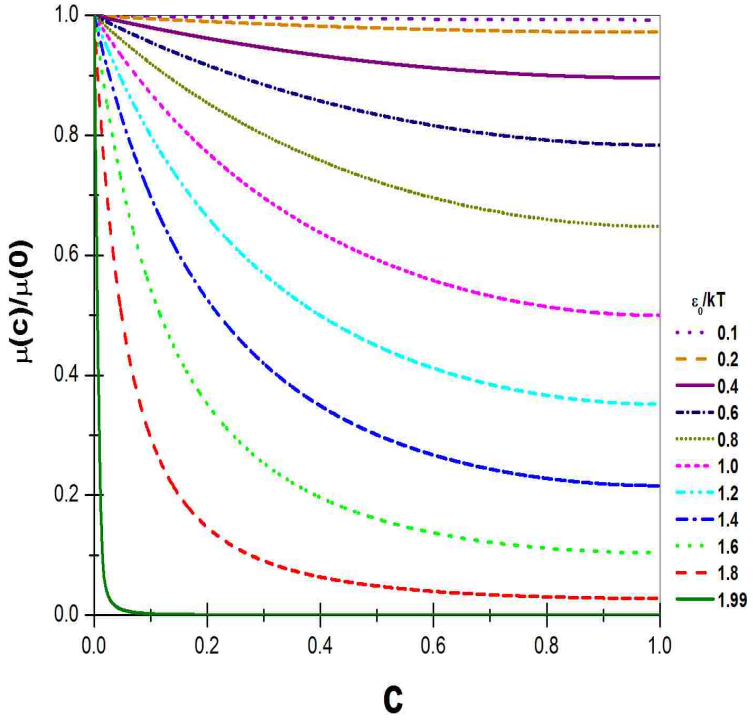

Figure 3.6. Normalized mobility as a function of barrier concentration.

and so

$$\mu = \frac{\beta\nu_0 a^2 e}{4\left(\frac{1+\beta\varepsilon_0(1-c)}{1+\beta\varepsilon_0}\right)\left(\frac{2-\beta\varepsilon_0(1-c)}{2-\beta\varepsilon_0}\right)^2} = \beta e D, \tag{62}$$

where

$$D = \frac{\nu_0 a^2}{4\left(\frac{1+\beta\varepsilon_0(1-c)}{1+\beta\varepsilon_0}\right)\left(\frac{2-\beta\varepsilon_0(1-c)}{2-\beta\varepsilon_0}\right)^2}$$

reduces to $D_0 = \nu_0 a^2$ when $c = 0$ and to

$$D_1 = \frac{\nu_0 a^2}{4\left(\frac{1}{1+\beta\varepsilon_0}\right)\left(\frac{2}{2-\beta\varepsilon_0}\right)^2}$$

for $c = 1$. The drift velocity (shown in Fig. 3.7) and mobility (shown in Fig. 3.8) increase exponentially with electric field deviating from PF like behavior.

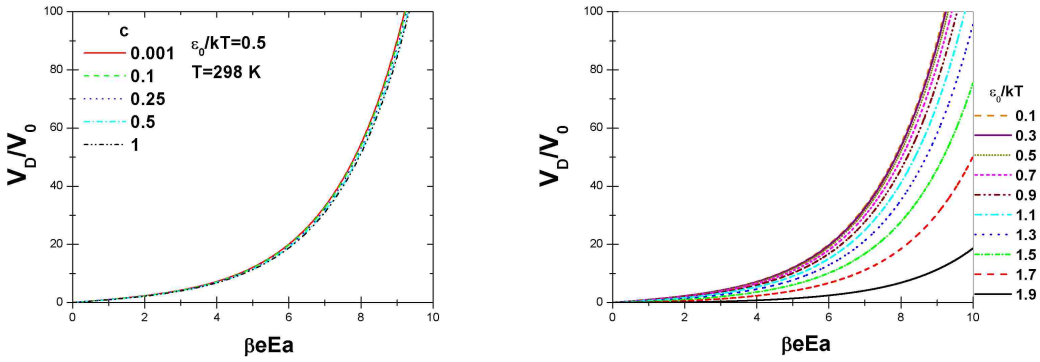

Figure 3.7. Normalized Drift Velocity as a function of E.

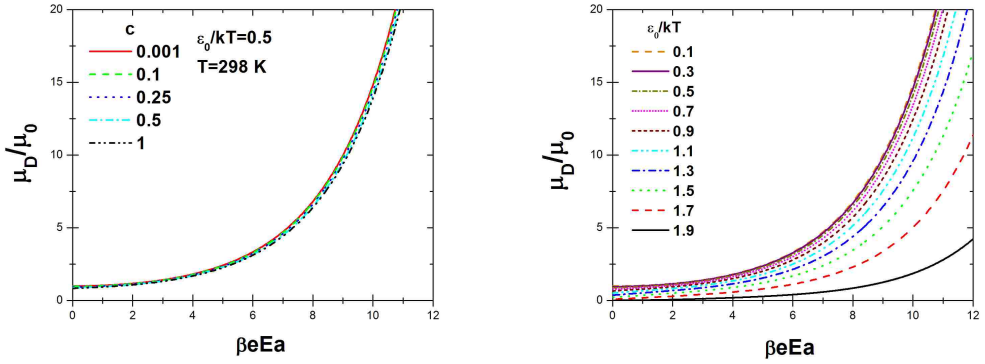

Figure 3.8. Normalized Mobility as a function of E.

3.3. MOTION THROUGH A 1D CORRELATED GAUSSIAN POTENTIAL WITH A FINITE CONCENTRATION OF EXPONENTIALLY DISTRIBUTED TRAPS AND BARRIERS

The previous calculations of this section have established that a finite concentration of traps and/or barriers with depths/heights distributed according to an exponential distribution gives rise in 1D to a steady-state mobility that undergoes a transition to an essentially insulating phase as the temperature is lowered below a critical temperature that depends on the average trap depth or barrier height. In such a system, the electric field dependence of the mobility is very different from the Poole-Frenkel form commonly observed in molecularly-doped polymers. In this section the motion of carriers which undergo hopping transport through a correlated Gaussian potential landscape in the presence of traps and barriers is considered, that could in principle, give rise to a transition of the type previously analyzed.

As in previous subsections of this section, using the same conventions already introduced, the calculation starts with the master equation (28) governing the evolution of the probability $P_n(t)$ of finding the carrier at the nth site at time t, which leads in steady state to an expression for the drift velocity

$$v = \mu E = \frac{\nu_0 a}{\sum_{m=0}^{N-1} e^{-m\beta eEa} \left\langle e^{-\beta\varepsilon_n} e^{\frac{1}{2}\beta\varepsilon_{n+m}} e^{\frac{1}{2}\beta\varepsilon_{n+m+1}} \right\rangle}, \tag{63}$$

where

$$\langle e^{-\beta\varepsilon_n} e^{\frac{1}{2}\beta\varepsilon_{n+m}} e^{\frac{1}{2}\beta\varepsilon_{n+m+1}} \rangle = \frac{1}{N} \sum_{n=1}^{N} e^{-\beta\varepsilon_n} e^{\frac{1}{2}\beta\varepsilon_{n+m}} e^{\frac{1}{2}\beta\varepsilon_{n+m+1}}. \tag{64}$$

The correlation functions (64) required are now more complicated then in the previous two calculations because, as described in section 2, the energy $\varepsilon_n = u_n + v_n$ at a site is now assumed to arise from two components, a correlated part u_n with values drawn from a Gaussian marginal distribution of width σ as described in section 2, and an

uncorrelated part v_n drawn from a distribution

$$\rho\left(v_n\right) = c\rho_v\left(v_n\right) + \left(1-c\right)\delta\left(v_n\right), \tag{65}$$

where

$$\rho_v\left(v\right) = \left(2\varepsilon_0\right)^{-1}\exp\left(-\left|v\right|/\varepsilon_0\right). \tag{66}$$

Nonetheless, with the assumption that the two components are independent of each other, the correlation functions factor. Re-expressing the correlation function in the form $\left\langle e^{-\beta\varepsilon_n}e^{\beta\varepsilon_{n+m}}e^{\beta\delta_{n+m}}\right\rangle$, where $2\delta_{n+m} = \varepsilon_{n+m+1} - \varepsilon_{n+m}$, one can write

$$\left\langle e^{-\beta\varepsilon_n}e^{\beta\varepsilon_{n+m}}e^{\beta\delta_{n+m}}\right\rangle = \left\langle e^{-\beta u_n}e^{\beta u_{n+m}}e^{\beta\delta u_{n+m}}\right\rangle\left\langle e^{-\beta v_n}e^{\beta v_{n+m}}e^{\beta\delta v_{n+m}}\right\rangle.$$

The part of the correlation function

$$\left\langle e^{-\beta u_n}e^{\beta u_{n+m}}e^{\beta\delta u_{n+m}}\right\rangle \tag{67}$$

associated with the correlated part of the potential was calculated in Ref. [75] in the approximation that the site-energy difference $u_{n+1} - u_n$ between neighboring sites is small compared to kT (as occurs when energies of neighboring sites are correlated) so that exponential factors involving δu_{n+m} can be set equal to unity. With this approximation, one finds that for $m = 0$, the correlated part (67) of the correlation function reduces to unity, while for $m > 0$, one has [75]

$$\langle e^{-\beta u_n}e^{\beta u_{n+m}}\rangle = \exp\left(\beta^2\sigma_0^2\left[1-\alpha m^{-1}\right]\right) \qquad m>0,\ \alpha = a_0/a \tag{68}$$

There is no reason to expect the part of energy difference between neighboring sites due to the uncorrelated part to be small, and so one refrains from making that

approximation for the v_n. Thus, in terms of the uncorrelated part of the correlation function, taking into account our results for the correlated part, one can write for $m = 0$

$$\left\langle e^{-\beta\varepsilon_n} e^{\beta\varepsilon_{n+m}} e^{\beta\delta_{n+m}} \right\rangle = \left\langle e^{-\frac{1}{2}\beta v_n} \right\rangle \left\langle e^{\frac{1}{2}\beta v_{n+1}} \right\rangle \tag{69}$$

and for $m > 0$

$$\begin{aligned}
\left\langle e^{-\beta\varepsilon_n} e^{\beta\varepsilon_{n+m}} e^{\beta\delta_{n+m}} \right\rangle &= \left\langle e^{-\beta u_n} e^{\beta u_{n+m}} \right\rangle \left\langle e^{-\beta v_n} e^{\frac{1}{2}\beta v_{n+m}} e^{\frac{1}{2}\beta v_{n+m+1}} \right\rangle \\
&= \exp\left(\beta^2\sigma_0^2\left[1-\alpha m^{-1}\right]\right) \left\langle e^{-\beta v_n} \right\rangle \left\langle e^{\frac{1}{2}\beta v_{n+m}} \right\rangle \left\langle e^{\frac{1}{2}\beta v_{n+m+1}} \right\rangle \\
&= \exp\left(\beta^2\sigma_0^2\left[1-\alpha m^{-1}\right]\right) \left\langle e^{-\beta v_n} \right\rangle \left\langle e^{\frac{1}{2}\beta v_n} \right\rangle^2
\end{aligned}$$

To compute the remaining parts of the correlation function, first evaluate, using the distributions (65) and (66), the mean value

$$\begin{aligned}
\left\langle e^{\lambda v} \right\rangle &= \int_{-\infty}^{\infty} \rho\left(v\right) e^{\lambda v} dv \\
\left\langle e^{\lambda v} \right\rangle &= \int_{-\infty}^{\infty} c\rho_e\left(v\right) e^{\lambda v} dv + \left(1-c\right) \int_{-\infty}^{\infty} \delta\left(v\right) e^{\lambda v} dv \\
&= \frac{c}{2\varepsilon_0} \left\{ \int_{-\infty}^{0} \exp\left(v\left[\frac{1+\lambda\varepsilon_0}{\varepsilon_0}\right]\right) dv + \int_{0}^{\infty} \exp\left(-v\left[\frac{1-\lambda\varepsilon_0}{2\varepsilon_0}\right]\right) dv \right\} + \left(1-c\right).
\end{aligned}$$

Evaluating the integral one finds

$$\left\langle e^{\lambda v} \right\rangle = \frac{1-\lambda^2\varepsilon_0^2\left(1-c\right)}{\left(1-\lambda^2\varepsilon_0^2\right)}. \tag{70}$$

Using this result, respectively, with $\lambda = -\beta/2, \beta/2$ and $-\beta$ one finds that for $\beta\varepsilon_0 < 1$

$$\left\langle e^{-\frac{1}{2}\beta v_n} \right\rangle = \frac{4-\beta^2\varepsilon_0^2\left(1-c\right)}{\left(4-\beta^2\varepsilon_0^2\right)} \tag{71}$$

$$\left\langle e^{-\frac{1}{2}\beta v_{n+1}} \right\rangle = \frac{4-\beta^2\varepsilon_0^2\,(1-c)}{(4-\beta^2\varepsilon_0^2)} \tag{72}$$

$$\left\langle e^{-\beta v_n} \right\rangle = \frac{1-\beta^2\varepsilon_0^2\,(1-c)}{(1-\beta^2\varepsilon_0^2)}. \tag{73}$$

Using these results in our earlier expression for the correlation function one can write for $m = 0$, and $\beta\varepsilon_0 < 1$

$$\left\langle e^{-\beta\varepsilon_n} e^{\beta\varepsilon_{n+m}} e^{\beta\delta_{n+m}} \right\rangle = \left[\frac{4-\beta^2\varepsilon_0^2\,(1-c)}{(4-\beta^2\varepsilon_0^2)}\right]^2, \tag{74}$$

while for $m > 0$ and $\beta\varepsilon_0 < 1$

$$\left\langle e^{-\beta\varepsilon_n} e^{\beta\varepsilon_{n+m}} e^{\beta\delta_{n+m}} \right\rangle = e^{\beta^2\sigma_0^2\left[1-\alpha m^{-1}\right]} \left[\frac{1-\beta^2\varepsilon_0^2\,(1-c)}{(1-\beta^2\varepsilon_0^2)}\right] \left[\frac{4-\beta^2\varepsilon_0^2\,(1-c)}{(4-\beta^2\varepsilon_0^2)}\right]^2 \tag{75}$$

Based upon our previous results for traps and barriers, one can already anticipate that the divergence of correlation functions for $\beta\varepsilon_0 > 1$ will lead to a mobility transition. In the rest of what follows it is understood that the expressions are considered only in the regime for which $\beta\varepsilon_0 < 1$. Although some of the expressions do not diverge until $\beta\varepsilon_0 > 2$, this regime cannot be reached before the transition at $\beta\varepsilon_0 = 1$ occurs, and need not, therefore, be considered.

With the results (74) and (75), the denominator in the expression (63) for the drift velocity can be written

$$\left[\frac{4-\beta^2\varepsilon_0^2\,(1-c)}{(4-\beta^2\varepsilon_0^2)}\right]^2 + \left[\frac{1-\beta^2\varepsilon_0^2\,(1-c)}{(1-\beta^2\varepsilon_0^2)}\right] \left[\frac{4-\beta^2\varepsilon_0^2\,(1-c)}{(4-\beta^2\varepsilon_0^2)}\right]^2 e^{\beta^2\sigma_0^2} \sum_{m=1}^{\infty} e^{-m\beta eEa} e^{-\beta^2\sigma_0^2\alpha m^{-1}} \tag{76}$$

where the term with $m = 0$ is displayed explicitly. For typical values of the energetic disorder in MDPs, $\beta\sigma_0 \sim 3{-}5$, and so the the exponential factor $e^{\beta^2\sigma_0^2}$ in the remaining terms will tend to enhance their contribution relative to the $m = 0$ term.

Because of the correlations in the potential, the remaining sum can now no longer be computed as a simple geometric series. However, because of the competition between the two exponential factors appearing in it, the summand will rise and decay relatively slowly over a large number of sites, so that the sum itself can be approximated by an integral

$$\sum_{m=1}^{\infty} e^{-m\beta eEa} e^{-\beta^2\sigma_0^2\alpha m^{-1}} \sim a^{-1} \int_a^{\infty} \exp\left[-\left(Fy + \hat{\sigma}^2 a_0 y^{-1}\right)\right] dy \tag{77}$$

over a continuous position variable $y \sim y_m = ma$. Here $F = \beta eE$ and $\hat{\sigma} = \sigma_0/kT$. For sufficiently large disorder and at fields of interest, the integrand in this last expression becomes strongly peaked and can be evaluated using a saddle point integration. Thus setting

$$a^{-1} \int_a^{\infty} \exp\left[-\left(Fy + \hat{\sigma}^2 a_0 y^{-1}\right)\right] dy = a^{-1} \int_a^{\infty} \exp\left[-g\left(y\right)\right] dy$$

with $g = \left(Fy + \hat{\sigma}^2 a_0 y^{-1}\right)$, one determines the location of the peak, which occurs when

$$\frac{d}{dy}\left(Fy + \hat{\sigma}^2 a_0 y^{-1}\right) = 0, \tag{78}$$

at $y = y_0 = \sqrt{\hat{\sigma}^2 a_0 / F}$. Using this, calculate

$$g(y_0) = 2\sqrt{\hat{\sigma}^2 F a_0} \tag{79}$$

$$g'(y_0) = 0 \tag{80}$$

$$g''(y_0) = \frac{2\hat{\sigma}^2 a_0}{y_0^3} \tag{81}$$

so that one can write, near y_0,

$$g(y) \sim g(y_0) + \frac{1}{2}\frac{2\hat{\sigma}^2 a_0}{y_0^3}(y - y_0)^2 = g(y_0) + \frac{(y - y_0)^2}{2\alpha^2} \tag{82}$$

where $\alpha^2 = y_0^3 / 2\hat{\sigma}^2 a_0$. With this the expression one finds that

$$\begin{aligned} & a^{-1}\int_a^\infty \exp\left[-g(y)\right] dy \\ & = a^{-1}\exp\left(-2\sqrt{\hat{\sigma}^2 F a_0}\right)\int_{-\infty}^{\infty} \exp\left[-\frac{(y - y_0)^2}{2\alpha^2}\right] dy. \end{aligned}$$

Evaluating the Gaussian integral and substituting the definitions introduced above, an approximation to the sum in (76)is obtained:

$$\sum_{m=1}^{\infty} e^{-m\beta eEa} e^{-\beta^2\sigma_0^2 \alpha m^{-1}} \sim (a_0/a)\sqrt{\pi\beta\sigma_0}\,(\beta eEa_0)^{-3/4}\exp\left(-\sqrt{4\beta^2\sigma_0^2(\beta eEa_0)}\right). \tag{83}$$

By inserting this last expression into (76), and the resulting expression into the denominator of (63), one obtains, after dividing by the field E, the mobility:

$$\mu = \frac{\upsilon_0 a E^{-1}\left[\left(4 - \beta^2\varepsilon_0^2(1-c)\right)/\left(4 - \beta^2\varepsilon_0^2\right)\right]^2}{1 + \left[\frac{1-\beta^2\varepsilon_0^2(1-c)}{\left(1-\beta^2\varepsilon_0^2\right)}\right] e^{\beta^2\sigma_0^2}(a_0/a)\sqrt{\pi\beta\sigma_0}\,(\beta eEa_0)^{-3/4} \times \exp\left(-\sqrt{4\beta^2\sigma_0^2(\beta eEa_0)}\right)} \tag{84}$$

As discussed above, when the $m = 0$ term can be neglected, this can be simplified further. Making this approximation and using the definition (30) of υ_0 the following results are obtained

$$\mu = \frac{\mu_0 \exp\left[-\varepsilon_B/2kT\right] \exp\left(-\beta^2\sigma_0^2\right) \exp\left(\sqrt{4\beta^2\sigma_0^2\left(\beta e E a_0\right)}\right)}{\left[\frac{1-\beta^2\varepsilon_0^2(1-c)}{\left(1-\beta^2\varepsilon_0^2\right)}\right]\left[\frac{4-\beta^2\varepsilon_0^2(1-c)}{\left(4-\beta^2\varepsilon_0^2\right)}\right]^2} \tag{85}$$

in which

$$\mu_0 = \frac{J_0^2 e^{-2\lambda a} a^2 \left(\beta e E a_0\right)^{3/4}}{E a_0 \sqrt{2\hbar^2 \varepsilon_B \sigma_0}} \tag{86}$$

is algebraic in the field and temperature, and thus slowly varying with respect to the exponential terms appearing in (85).

Equation (85) is one of the main results of this dissertation. It predicts, analytically, most of the features observed in MDPs: (i) a Poole-Frenkel field dependence, with a Poole-Frenkel factor that decreases with increasing temperature, (ii) a temperature dependence at fixed field which has a combination of quadratically and linearly activated components, and (iii) a non-dispersive to dispersive transition as the temperature is lowered below a critical value $T_c = \varepsilon_0/k$ (Fig. 3.9). Although the model has both barriers and traps the critical temperature exhibited in the
presence of both is the higher value associated with the traps alone. The steady-state calculation presented here does not allow for a determination regarding the universality of current-time transients in this model, but since the transition is driven by the exponential distribution of traps it is reasonable to expect that it shares the dispersive features of multiple trapping models.

In Figs. 3.9 - 3.12 the predictions of this 1D model are graphically illustrated. Figure 3.9 shows the mobility transition that occurs as the value of ε_0/kT approaches the critical value of unity, below which the system is not thermodynamically stable.

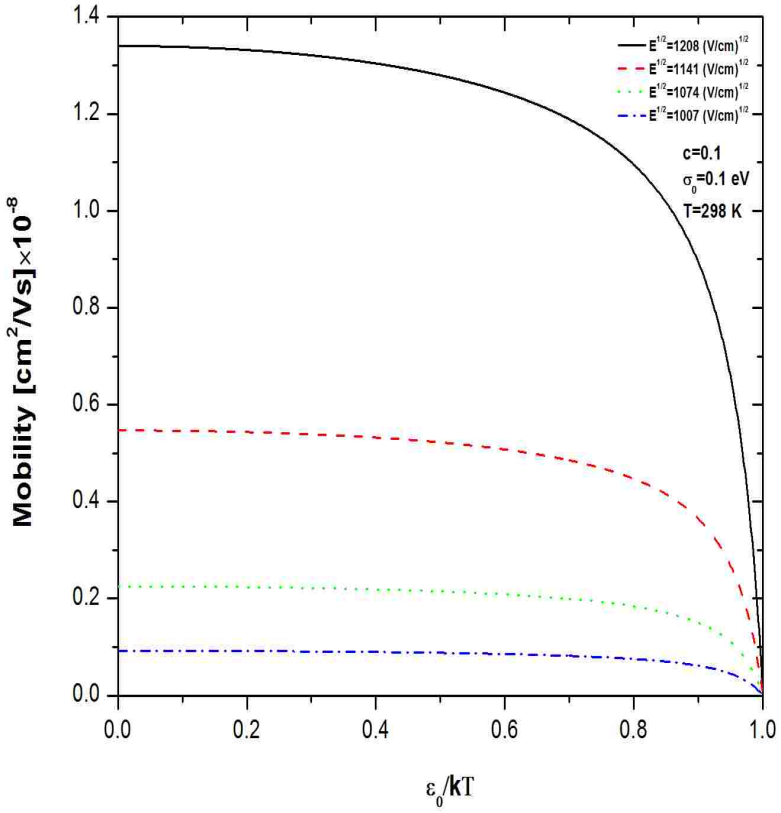

Figure 3.9. Mobility as a function of ε_0/kT for different values of the electric field.

The steady-state drift mobility smoothly approaches zero at this point, as the terms proportional to c in the denominator of Eq. (85) diverge. The data in this figure were computed for four different values of the electric field for a system with Gaussian disorder $\sigma_0 = 0.1$ eV, a combined trap/barrier concentration $c = 0.1$ and a constant temperature of $T = 298\ K$, by varying the trap depth ε_0.

The dependence of the trap or barrier concentration c on the mobility is illustrated in Fig.3.10. Here $\mu(0)$ is the mobility when c is zero. Here one can see that the drop in mobility with increasing concentration c becomes more drastic with increasing values of ε_0.

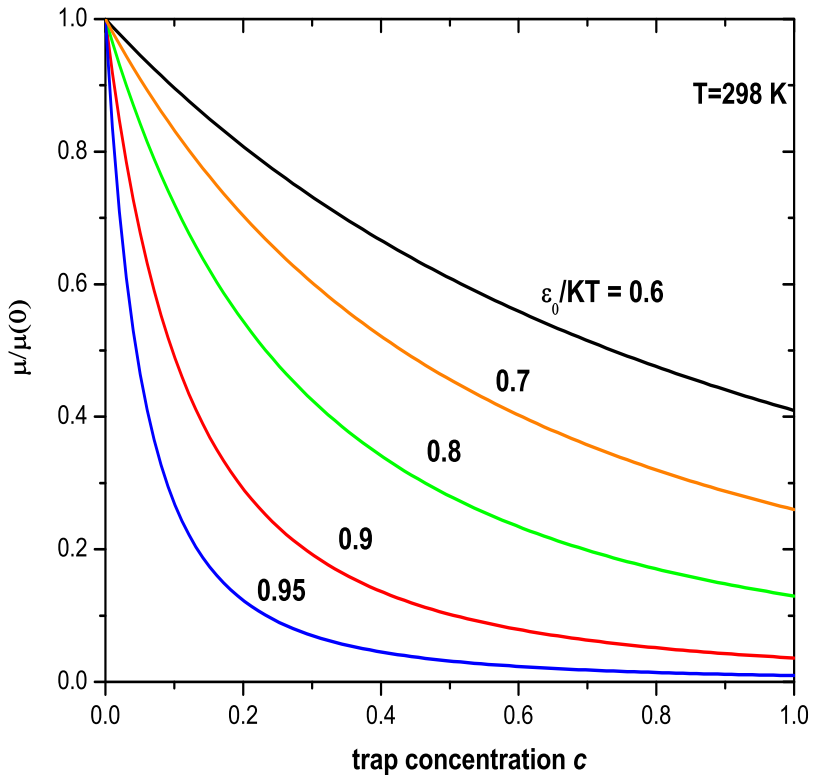

Figure 3.10. Mobility as a function of trap concentration.

The activated field dependence, aside from algebraic prefactors, is contained entirely in the Poole-Frenkel factor in Eq. (85), which can be written in the form $\exp\sqrt{\gamma E}$ where $\gamma = 4\beta^2\sigma e a_0$, depends only on the correlated Gaussian part of the distribution, and is insensitive to the presence of the traps. The PF dependence is shown in Fig. 3.11. For this computation, the concentration, the Gaussian width, and the temperature were kept at the same constant values as in the previous figure. In this figure, a dimensionless parameter $\varepsilon = |\varepsilon_c - \varepsilon_0|/\varepsilon_c$ is defined which provides the relative deviation of the width ε_0 of the exponential distribution from the critical value $\varepsilon_c = kT$. Starting from $\varepsilon = 1$ which is the pure Gaussian distribution, the

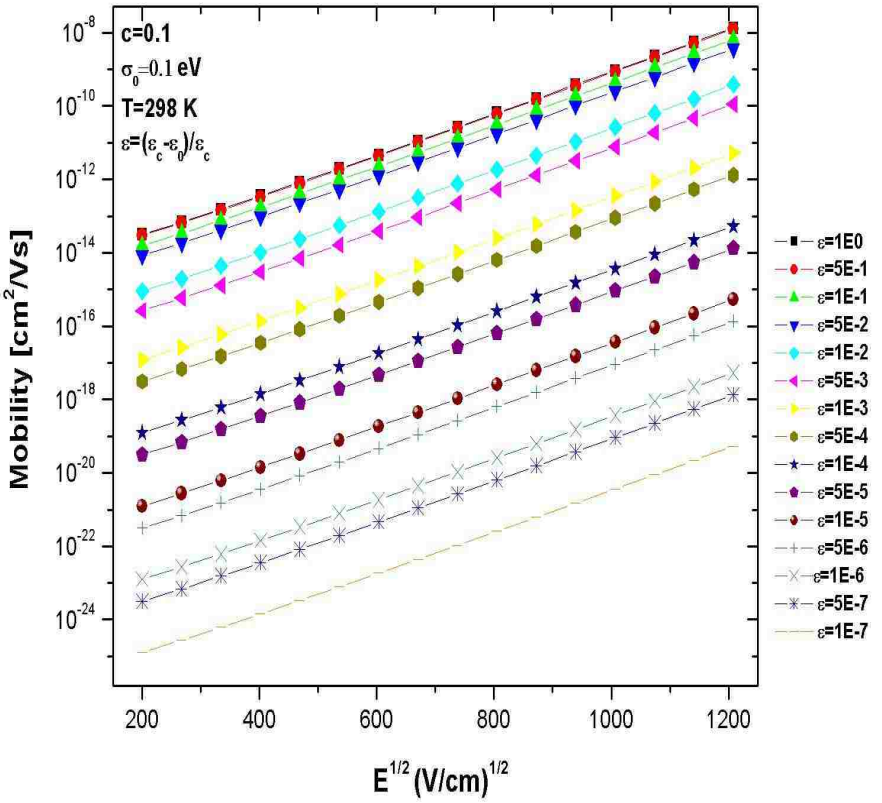

Figure 3.11. Mobility as a function of $E^{1/2}$ for different values of ε.

dimensionless parameter decreases as ε_0 approaches the critical value. The plot clearly shows that the mobility also approaches zero, and yet maintains the characteristic Poole-Frenkel behavior right up to the transition.

Finally, Fig. 3.12 shows how the PF field dependence changes as the temperature is lowered.

Previous comparisons of 1D analytic calculations of this sort with numerical simulations in 3D show that the 1D calculations generally capture the correct functional dependence on temperature and field, although they tend to overestimate the Poole-Frenkel coefficient γ. Physically, this results because the assumed

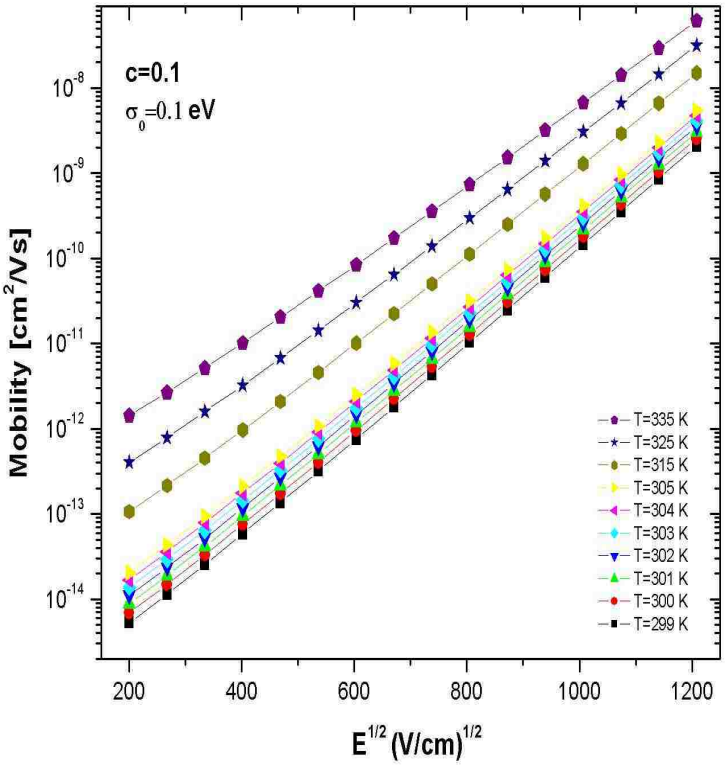

Figure 3.12. Mobility as a function of $E^{1/2}$ at different temperatures.

one-dimensional path through the material artificially eliminates the possibility that carriers can find alternate routes around difficult energetic barriers that they encounter, which they can, of course, do in higher dimensions.

In the next section 3D numerical calculations are presented that explore the degree to which the 1D calculation presented in this section captures the behavior of the full 3D system.

4. NUMERICAL CALCULATIONS FOR 3D SYSTEMS

In this section the result of numerical calculations are presented in order to test whether the features predicted by the 1D analytical calculations discussed in section 3 are also exhibited by 3D systems, and in particular whether a hybrid model which includes both a correlated Gaussian potential energy landscape as well as a finite concentration of exponentially distributed energetic defects might explain the main features observed in the measured time-of-flight mobility of molecularly-doped polymers.

It is not at all obvious that the predictions of the 1D calculation should extend to 3D systems without significant modification. Transport in disordered systems can depend very strongly on dimensionality, as can be seen by considering the very different behavior of percolating lattices in different dimensions. Indeed, the mobility of a 3D cubic lattice vanishes when a finite concentration $c \sim 75\%$ of its bonds are removed, because of the disappearance at that concentration of a connected cluster of transport sites that span the lattice. In 1D, this "transition" occurs with the removal of the first bond [78].

Unfortunately, analytical calculations of transport in disordered systems in higher dimensions are much more difficult than in 1D. It is sometimes possible to analytically construct an effective medium theory (as in the percolation problem) [79], which can often be quite accurate, but such theories become problematic with realistic hopping rates that connect sites that are greater than nearest neighbors, as occurs, e.g., in a real MDP. There is also the problem that with an effective medium theory the results involve an approximation the validity of which is usually difficult to determine in advance.

Hopping transport on *ordered lattices*, in which there is no energetic disorder, is well understood both in the absence of a field, where it leads to diffusion, and for fields of arbitrary strength, where it leads to a well-defined field dependent mobility. Indeed solutions to the master equation for ordered systems are often the starting point for the development of a useful effective medium theory. Both for reference purposes and to serve as a point of comparison with the numerical results of this section, the Appendix contains a section in which hopping transport on such an ordered lattice is worked out in considerable detail.

However, molecularly-doped polymers, are certainly not ordered, as emphasized earlier. Thus, to perform realistic calculations of hopping transport in 3D disordered materials of this sort it is necessary to perform numerical computations of some sort.

Most of the early numerical work on MDPs was done through Monte Carlo simulations [68] which use the microscopic transition rates to generate random moves by a particle executing a biased random walk on the underlying set of transport sites. Monte Carlo calculations have the advantage that they are conceptually simple, and they can be implemented on a realization of the disordered system which is arbitrarily large. Their main disadvantage is that they must be run for many realizations of the random walk in order to obtain sufficient statistics, and to ensure that one is sufficiently sampling the rare regions of the disordered medium.

An alternative method for computing the mobility is through numerical solutions to the master equation that governs the evolution of the site probabilities themselves, and as has already been described in this dissertation. This is the approach taken in the research presented in this section. Advantages of the approach are that, first, if a large enough region of the disorder material is simulated, only one realization of the disordered system needs to be implemented (or a few, if statistical error bars are desired), and secondly, that the numerical solution to the master

equation automatically includes information about all possible random walks that could take place on the disordered structure that is the target of the computation. The main disadvantage is that the size of the system that one can simulate is considerably smaller than is possible using Monte Carlo simulations. At any rate, in the next section the numerical approach that has implemented here as a tool for studying hopping transport in a correlated Gaussian energy landscape possessing a finite concentration of exponentially distributed traps and barriers is described. Following that, the results of numerical calculations that appear to confirm many, although perhaps not all, of the essential features seen in the 1D analytical results developed in the last section are presented.

4.1. NUMERICAL APPROACH

In this section, the numerical approach that has been implemented here to compute the mobility for 3D disordered systems is described. Briefly, the approach is to solve, in steady-state and with periodic boundary conditions, the equations of motion for the transport site occupation probabilities $p_{\vec{n}}$ of a sufficiently large realization of the disordered system of interest. For the computations presented in this paper, this was done for sites located on a periodically repeated cubic lattice having edge lengths L_x,L_y, and L_z, where the edge lengths varied (for reasons described below) in powers of 2 from $L = 2^4 = 16$ to $L = 2^7 = 256$ and containing a total of $N = L_x L_y L_z$ sites. Typical calculations are performed with $L = 64$ which incorporates $N \sim 2.6 \times 10^5$ transport sites.

In the presence of the field, the steady-state probabilities describe a non-equilibrium condition of constant average particle flow along the direction of the applied field. For each realization of the lattice, and at each value of the magnitude of the electric field $\vec{E} = E\hat{x}$ (directed along the x axis of the cubic lattice), the

longitudinal component of the mobility is numerically computed.

$$\mu = \langle v_\ell \rangle / E$$

from the corresponding component $\langle v_\ell \rangle = \langle \vec{v} \rangle \cdot \hat{x}$ of the steady-state drift velocity $\langle \vec{v} \rangle$. The latter is obtained from the steady-state solution to the master equation

$$\frac{dP_{\vec{n}}}{dt} = \sum_{\vec{m}} \left[W_{\vec{n},\vec{m}} P_{\vec{m}}(t) - W_{\vec{m},\vec{n}} P_{\vec{n}}(t) \right] \equiv \sum_{\vec{m}} H_{\vec{n},\vec{m}} P_{\vec{m}}(t) , \tag{87}$$

in which $\vec{n} = (n_x, n_y, n_z)$ is a vector lattice index having integer components labeling the lattice point at $\vec{r}_{\vec{n}} = \vec{n}a$, the quantity $W_{\vec{n},\vec{m}}$ denotes the transition rate from site $\vec{m}$ to site $\vec{n}$, which in the results presented here is assumed to depend on the separation distance and energy of the two sites involved according to Eq. (3), and $P_{\vec{n}}(t)$ is the probability that the carrier is at lattice site $\vec{n}$ at time t. For a given initial condition $P_{\vec{n}}(0)$ the carrier's mean position $\langle \vec{r}(t) \rangle$ and velocity $\langle \vec{v}(t) \rangle$ can then be expressed as

$$\begin{aligned} \langle \vec{r}(t) \rangle &= \sum_{\vec{n}} \vec{r}_{\vec{n}} P_{\vec{n}}(t) , \\ \langle \vec{v}(t) \rangle &= \frac{d}{dt} \langle \vec{r}(t) \rangle = \sum_{\vec{n},\vec{m}} \vec{r}_{\vec{n}} H_{\vec{n},\vec{m}} P_{\vec{m}}(t) , \end{aligned}$$

and the required steady-state drift velocity

$$\langle \vec{v} \rangle = \lim_{t \to \infty} \langle \vec{v}(t) \rangle = \sum_{\vec{n},\vec{m}} \vec{r}_{\vec{n}} H_{\vec{n},\vec{m}} p^{(s)}_{\vec{m}} \tag{88}$$

can be computed from the transition rates and the steady-state site occupation probabilities

$$p^{(s)}_{\vec{m}} = \lim_{t \to \infty} P_{\vec{m}}(t) . \tag{89}$$

The latter can be obtained by solving the linear set of equations

$$\sum_{\vec{m}} H_{\vec{n},\vec{m}} p_{\vec{m}}^{(s)}(t) = 0 \tag{90}$$

that result from (87) by setting $dP_{\vec{n}}/dt = 0$. Thus, once the site energies have been assigned, as described below, and the field specified, transition rates $W_{\vec{n},\vec{m}}$ are computed, according to Eq. (3), connecting each site to its 27 nearest neighbors lying within a $3 \times 3 \times 3$ cube centered on that site. With the transition rates determined, Eq. (90) is solved using an over-relaxation algorithm, and the resulting occupation probabilities used to compute the drift velocity and the mobility as outlined above.

For the calculations of mobility performed in the current study, the zero-field energy of each site of the lattice was computed as the sum $\varepsilon_{\vec{n}} = \varepsilon_{\vec{n}}^{(1)} + \varepsilon_{\vec{n}}^{(2)}$ of two randomly drawn energies.

The uncorrelated trap energies $\varepsilon_{\vec{n}}^{(2)}$ were drawn as discussed in section 2, independently from a distribution

$$\rho\left(\varepsilon^{(2)}\right) = c\varepsilon_0^{-1} \exp\left(-\left|\varepsilon^{(2)}\right|/\varepsilon_0\right) + (1-c)\,\delta\left(\varepsilon^{(2)}\right)$$

that randomly assigns exponentially distributed traps (or barriers) of mean depth (or height) ε_0 to transport sites in fractional concentration c. The remaining sites, in fractional concentration $(1-c)$, have $\varepsilon^{(2)} = 0$.

The spatially correlated component of the energy was obtained by producing individual realizations of a discrete Gaussian potential energy field $\varepsilon_{\vec{n}}^{(1)} = u_{\vec{n}}$ of zero mean having the desired (translationally invariant) correlations $C_{\vec{m}} \equiv \langle u_{\vec{n}} u_{\vec{n}+\vec{m}} \rangle$, defined on our integer lattice with $\vec{n} = (n_1, n_2, n_3)$, and $n_i = 1, 2, \ldots, L$. To accomplish

this, for each realization one first generates what ends up being the Fourier transform

$$\hat{u}_{\vec{k}} = \frac{1}{\sqrt{N}} \sum_{\vec{n}} u_{\vec{n}}\, e^{-i\vec{k}\cdot\vec{n}} \tag{91}$$

of the desired energy field. Here the discrete complex field $\hat{u}_{\vec{k}}$ is defined on the set Ω of N wavevectors $\vec{k} = (k_1, k_2, k_3)$ in the 1st Brillouin zone of the associated reciprocal lattice, with $k_i = 2\pi m_i/L$ and $m_i \in \{-M, -M+1, \cdots, M-1\}$, and $M = L/2$. The field $\hat{u}_{\vec{k}}$ is constructed as follows: for each wavevector $\vec{k}$ with positive z component, a complex value $\hat{u}_{\vec{k}} = \eta_{\vec{k}} e^{i\phi_{\vec{k}}}$ for the random field at wavevector $\vec{k}$ is numerically determined in two steps. In the first step the real quantity $\eta_{\vec{k}}$ is independently chosen from a Gaussian distribution

$$P_{\vec{k}}(\eta) = \frac{1}{\sqrt{2\pi\sigma_{\vec{k}}^2}}\, e^{-\eta^2/2\sigma_{\vec{k}}^2} \tag{92}$$

having zero mean and a $\vec{k}$-dependent variance

$$\sigma_{\vec{k}}^2 = \frac{1}{\sqrt{N}} \sum_{\vec{n}} C_{\vec{n}}\, e^{-i\vec{k}\cdot\vec{n}} = \frac{1}{\sqrt{N}} \sum_{\vec{n}} \langle u_{\vec{m}} u_{\vec{m}+\vec{n}} \rangle\, e^{-i\vec{k}\cdot\vec{n}} \tag{93}$$

that is the Fourier transform of the desired correlation function. In the second step an independent random phase $\phi_{\vec{k}}$ is chosen uniformly in the interval $[0, 2\pi]$. For the value $\hat{u}_0$ of the field at $\vec{k} = 0$, the phase ϕ_0 is set equal to zero. The values of $\hat{u}_{\vec{k}}$ for wavevectors $\vec{k}$ with negative z component are then assigned according to the relation $\hat{u}_{\vec{k}} = \hat{u}^*_{-\vec{k}}$. When averaged over many realizations, the moments of the complex fields thus constructed satisfy the relations

$$\langle \hat{u}_{\vec{k}} \rangle = \langle \eta_{\vec{k}} \rangle \langle e^{i\phi_{\vec{k}}} \rangle = 0 \tag{94}$$

$$\langle \hat{u}^*_{\vec{k}} \hat{u}_{\vec{k}'} \rangle = \langle |\hat{u}_{\vec{k}}|^2 \rangle \delta_{\vec{k}',\vec{k}} + \langle \hat{u}^*_{\vec{k}} \hat{u}^*_{\vec{k}} \rangle \delta_{\vec{k}',-\vec{k}} = \sigma^2_{\vec{k}} \delta_{\vec{k}',\vec{k}}, \tag{95}$$

where the average $\langle \hat{u}^*_{\vec{k}} \hat{u}^*_{\vec{k}} \rangle = \langle |\eta_{\vec{k}}|^2 \rangle \langle e^{2i\phi_{\vec{k}}} \rangle$ vanishes when $\phi_{\vec{k}}$ is chosen randomly on $[0, 2\pi]$.

With the $\hat{u}_{\vec{k}}$ chosen as described above, the values $u_{\vec{n}}$ of the energy field of interest are obtained as the inverse Fourier transform

$$u_{\vec{n}} = \frac{1}{\sqrt{N}} \sum_{\vec{k} \in \Omega} \hat{u}_{\vec{k}} \, e^{i\vec{k}\cdot\vec{n}} \tag{96}$$

of the discrete complex field $u_{\vec{k}}$. As required, the final energies are real, i.e.,

$$\begin{aligned} u^*_{\vec{n}} &= \frac{1}{\sqrt{N}} \sum_{\vec{k}} \hat{u}^*_{\vec{k}} \, e^{-i\vec{k}\cdot\vec{n}} = \frac{1}{\sqrt{N}} \sum_{\vec{k}} \hat{u}_{-\vec{k}} \, e^{-i\vec{k}\cdot\vec{n}} \\ &= \frac{1}{\sqrt{N}} \sum_{\vec{k}} \hat{u}_{\vec{k}} \, e^{i\vec{k}\cdot\vec{n}} = u_{\vec{n}} \end{aligned}$$

where the summation index is relabeled, with $\vec{k} \to -\vec{k}$, and used the fact that $\hat{u}_{-\vec{k}} = \hat{u}^*_{\vec{k}}$. Furthermore, being a sum of Gaussian variables, the values of the real discrete field $u_{\vec{n}}$ are themselves Gaussian distributed random variables that obey the relations

$$\begin{aligned} \langle u_{\vec{n}} \rangle &= \frac{1}{\sqrt{N}} \sum_{\vec{k}} \langle \hat{u}_{\vec{k}} \rangle \, e^{i\vec{k}\cdot\vec{n}} = 0 \\ \langle u_{\vec{n}} u_{\vec{n}'} \rangle &= \langle u^*_{\vec{n}} u_{\vec{n}'} \rangle = \frac{1}{\sqrt{N}} \sum_{\vec{k},\vec{k}'} \langle \hat{u}^*_{\vec{k}} \hat{u}_{\vec{k}'} \rangle \, e^{-i\vec{k}\cdot\vec{n}} e^{i\vec{k}'\cdot\vec{n}'} \\ &= \frac{1}{\sqrt{N}} \sum_{\vec{k},\vec{k}'} \sigma^2_{\vec{k}} \, \delta_{\vec{k},\vec{k}'} e^{-i\vec{k}\cdot\vec{n}} e^{i\vec{k}'\cdot\vec{n}'} \\ &= \frac{1}{\sqrt{N}} \sum_{\vec{k}} \sigma^2_{\vec{k}} \, e^{-i\vec{k}\cdot(\vec{n}-\vec{n}')} = C_{\vec{n}-\vec{n}'}. \end{aligned}$$

In our numerical implementation of these ideas, one (i) chooses

$$C_{\vec{n}-\vec{m}} = \langle u_{\vec{n}} u_{\vec{m}} \rangle = \frac{\sigma^2 a}{(|\rho_{\vec{n}} - \rho_{\vec{m}}| + a)} = \frac{\sigma^2}{(|\vec{n} - \vec{m}| + 1)} \tag{97}$$

equal to the autocorrelation function associated with charge-dipole interactions, (ii) numerically computes via fast Fourier transforms the variance

$$\sigma_{\vec{k}}^2 = \frac{1}{\sqrt{N}} \sum_{\vec{n}} C_{\vec{n}}\, e^{i\vec{k}\cdot\vec{n}}, \tag{98}$$

(iii) constructs a random energy field $\hat{u}_k$ as outlined above, and (iv) performs another fast (inverse) Fourier transform, as in (96), to obtain the discrete energy field $\varepsilon_{\vec{n}}^{(1)} = u_{\vec{n}}$ required.

4.2. NUMERICAL RESULTS

The numerical calculations presented in this section, obtained using the method outlined above, were performed for a system, which in the absence of traps (by which from here on refer to both traps and barriers) had parameter values chosen to match those which have been shown to give a good fit, as reported by Chowdhury and Parris [70], to the experimental TOF mobility measured for 30% DEH:PC by Mack et al. [2]. The calculation of Chowdhury and Parris [70], shown in Fig.1.14, was performed using the techniques described in the last section on a system with edge lengths of $L_x = L_y = L_z = 64$ sites. The lattice spacing a separating dopant molecules was determined using the relation

$$a = n^{-1/3} = \left(\frac{M}{c_0 A \rho_m} \right)^{1/3}$$

in which n is the number density of dopant molecules in the system, $c_0 = 0.30$ is the weight percent of dopant molecules in the material, $M = 1.12$ g/mol is the molecular weight of the DEH dopant molecules, A is Avogadro's constant, and $\rho_m = 1.12$ g/cm^3 the mass density of the resulting MDP. This relation gives a lattice spacing $a = 11.94$ Å. The wavefunction decay parameter $\lambda = 0.5$ Å^{-1} was taken from an analysis of the concentration dependence of the mobility by Borsenberger

and Schein [71]. In their fit to the data, Chowdhury and Parris determined values of the energetic disorder parameter $\sigma = 0.1$eV, the polaron binding energy $E_b = 0.37$eV, and the intersite matrix element $J_0 = 0.63$eV that gave good fits to the experimental data for this system. Since these values seem to characterize real MDPs, their use to define a baseline system from which to compute purely theoretical results seems to offer the best possibility of making the results of the calculation relevant to actual systems of interest. For most of the calculations performed, the temperature was kept constant at room temperature $T = 298\ K$, and the concentration and average trap depth were varied to study the general effects of trapping on the field and temperature dependence of the mobility.

A general finding from the numerical studies, is that the inclusion of a significant fraction (i.e., tens of percent) of traps into our baseline system have very little effect on the Poole-Frenkel field dependence that arises from the correlated Gaussian part of the distribution, provided that the trap depth does not significantly exceed the critical value predicted by the 1D calculation. Indeed, Fig. 4.1 shows a "Poole-Frenkel" plot (by which refer to a semi-log plot of the mobility plotted as a function of the square root of the electric field) for a series of systems in which an increasing concentration c of traps having a mean trap depth $\epsilon_0 = 0.9kT$ have been added to the baseline system described above. The results show, as one might expect, a monotonic decrease in the mobility with increasing trap concentration.

By carrying out calculations of this sort for different values of the mean trap depth, the plot presented in Fig. 4.2 is obtained which shows a plot of the mobility as a function of trap concentration for different values of the parameter ϵ_0/kT. The attentive reader will deduce from this plot that in our numerical calculations the mobility does not appear to vanish for $\epsilon_0/kT > 1$, as one might be led to expect from the predictions of the 1D calculation. Such a deduction on the part of the reader would be reinforced by the results shown in Fig. 4.3, which shows a plot of the mobility for

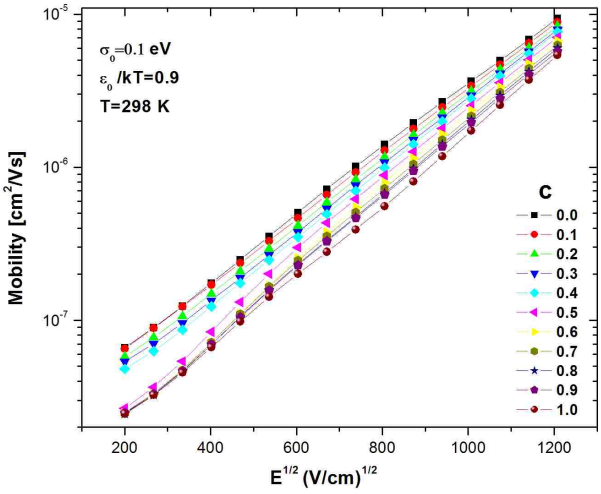

Figure 4.1. Field dependence of the mobility with an increasing concentration of traps of mean trap depth $\epsilon_0 = 0.9kT$.

four different electric fields plotted as a function of the dispersion parameter ϵ_0/kT for a system with a 10% concentration of traps. In this plot, the mobility does indeed exhibit the expected decrease with increasing values of the dispersion parameter, but the initial impression is that the point at which the mobility vanishes is not at $\epsilon_0/kT = 1$, but at $\epsilon_0/kT = 2$, which just happens to be the critical value that emerges in the 1D calculation for *random barriers*, not random traps.

Is the 1D calculation wrong? It is hard to imagine that it could be, given that the driving mechanism for the mobility transition, an inability of the carriers to equilibrate, should be operative in 3D as well as in 1D (and would for thermodynamic reasons give the same critical temperature). As it turns out, further investigation suggests that the actual critical point associated with *bulk material* is indeed at $\epsilon_0/kT = 1$ as predicted by the 1D calculation. The effects seen in these last two figures represent artifacts associated with finite-size effects.

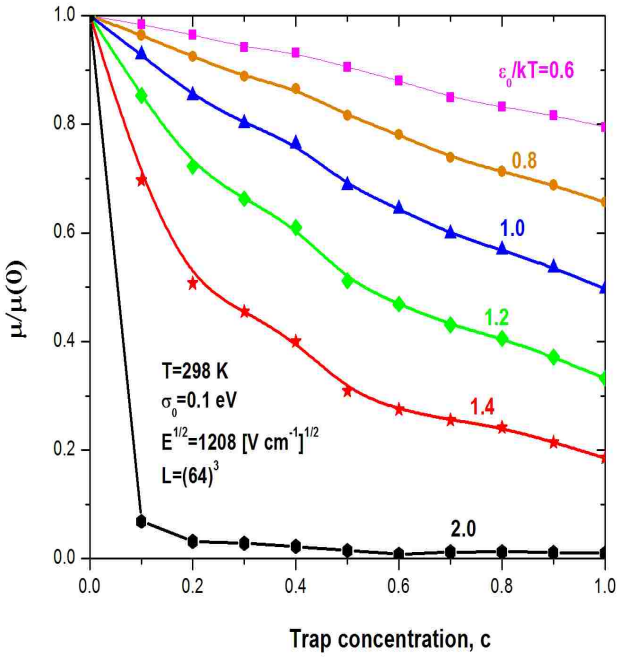

Figure 4.2. Mobility as a function of trap concentration for different values of the dispersion parameter ϵ_0/kT as shown.

Finite-size scaling is an important factor in simulations preformed on equilibrium systems, since it is generally understood that real phase transitions only occur in infinite systems. The transition occurring here is in a non-equiibrium system, but similar considerations apply.

Indeed, the calculations are performed for a large, but ultimately finite samples. Thus, every realization that has been generated has a lowest energy state, and any carrier in such a system has a finite energy. It is relatively easy to estimate the most probable value for the lowest energy in a system of N sites, but the important point to realize is that the mobility in these numerical simulations can never actually vanish, as it can in a bulk system, where a carrier can continue to sample states of lower and lower energy in the tails of the distribution.

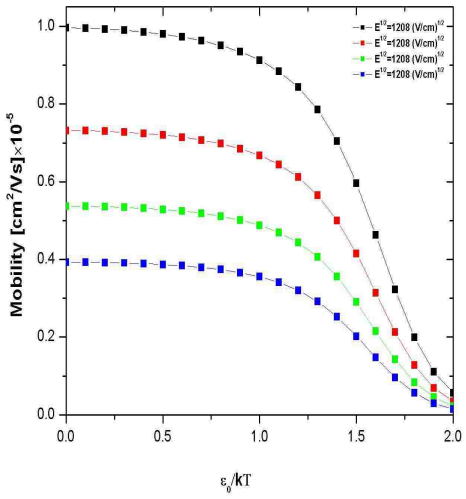

Figure 4.3. Mobility as a function of ϵ_0/kT for a system with a 10% concentration of traps and other parameters as indicated.

To numerically explore the dispersive to non-dispersive transition thus requires one to consider how the mobility should scale with the size of the system on either side of the transition (Fig. 4.4). Above the transition, one expects that as the system size is increased, the mobility should eventually converge to a stable value that represents the finite bulk mobility. Below the transition, however, as the system size increases, the mobility should continue to monotonically decrease, as lower energy states in the tail of the distribution are more thoroughly sampled by the larger number of sites in the system.

Motivated by these ideas a study of the dependence, above and below the transition on system size was carried out. Because of the Fast Fourier transform techniques that are used to generate the correlated Gaussian potential the system size can only be changed by factors of two. In doing this one has to be careful to maintain equal edge lengths transverse to the field direction (along the x axis) so as not to break the symmetry of the problem (this was motivated in part by the

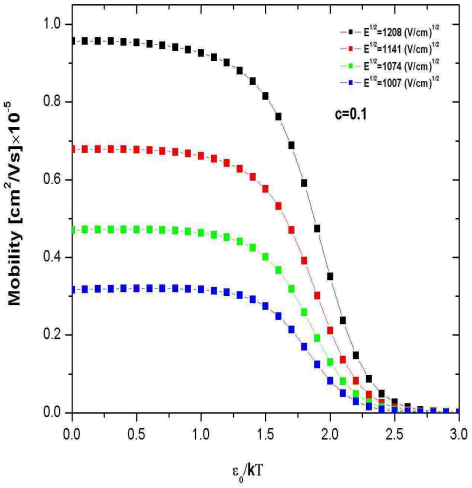

(a) $L_x = L_y = L_z = 32$.

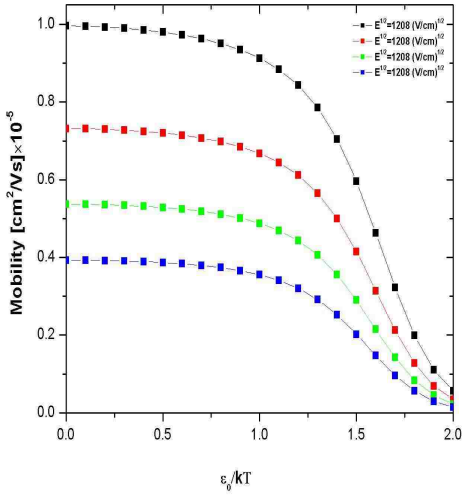

(b) $L_x = L_y = L_z = 64$.

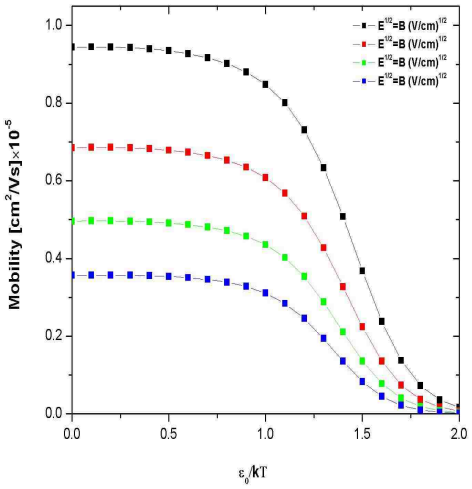

(c) $L_x = 128, L_y = L_z = 64$.

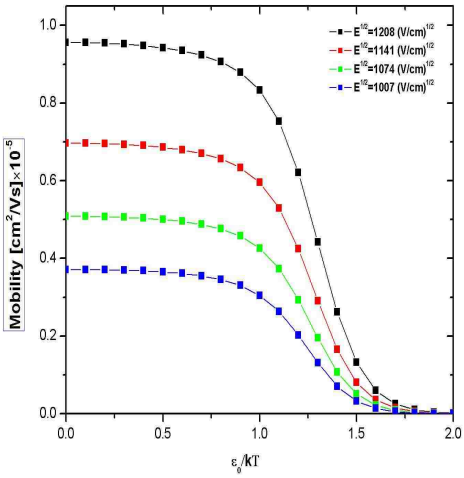

(d) $L_x = 64, L_y = L_z = 128$.

Figure 4.4. Mobility *vs.* ε_0/kT for different electric fields and different lattice sizes.

discovery of odd unphysical effects when this symmetry were broken). As an example of the effects of system size on the mobility on either side of the transition is presented in Fig. 4.4, which compares the effects of different lattice sizes. It is clear from this

figure that the apparent location of the transition moves to the right as the size of the system is increased.

Figure 4.5 which combines these data makes the behavior on either side of the transition even more apparent. Indeed, from this last figure it appears that the data to the left of the predicted transition point at $\epsilon_0/kT = 1$ are converging to a finite value, while to the data to the right of it appear to be continuing to fall with increasing size of the lattice. As an alternative way of presenting the data, in Fig. 4.6

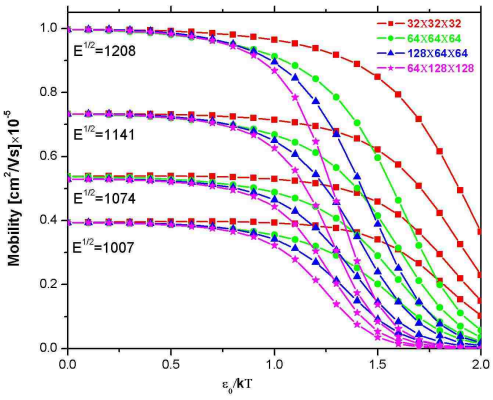

Figure 4.5. Mobility *vs.* ε_0/kT for different sizes of the lattice.

a double-log plot of the mobility at fixed field as a function of 1/N is illustrated. In this plot, the numerical data for $\epsilon_0/kT < 1$ appear to be approaching a limiting value as $1/N \to 0$, while the data for $\epsilon_0/kT > 1$ continues to decrease as $1/N \to 0$ at an increasing rate. Although this is not a proof, one can consider it as a convincing evidence that the actual transition point in the 3D system is, in fact, at $\epsilon_0/kT = 1$ as predicted by the 1D calculation.

Clearly it would be useful to continue these studies to larger system sizes. Unfortunately, the calculations that are presented thus far, in which the system size

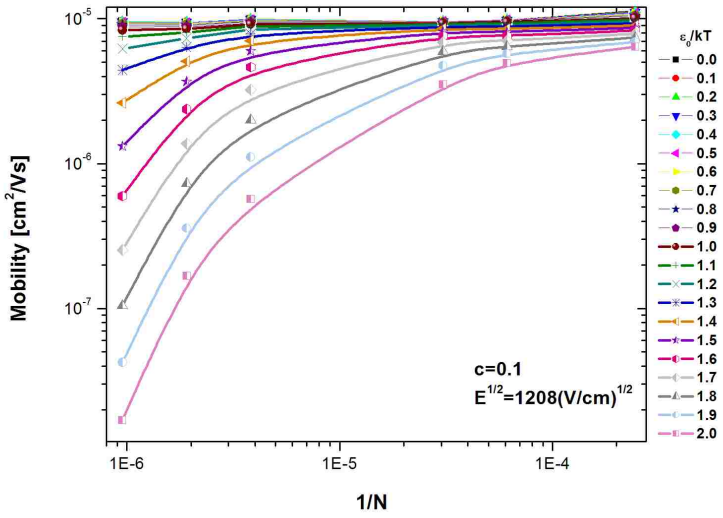

Figure 4.6. Mobility *vs.* $1/N$.

ranges up to $64 \times 128 \times 128$ sites seems to be as large as can be investigated using the current computational algorithm and the state of modern computational facilities.

Even if there remains, perhaps, some question as to the actual location of the critical point, it seems clear that such a point exists in the 3D system. In the 1D calculation, the Poole-Frenkel field dependence (and the associated temperature dependence) persists right up to the transition. Determining what actually happens at the transition point is clearly difficult numerically, for the reasons outlined above. However, if the critical point of the transition does, indeed, occur at $\epsilon_0/kT = 1$, then one can numerically examine the field dependence of the mobility up to and beyond this point. In Fig. 4.7 a calculation of the field dependence of the mobility for values of the dispersion parameter ϵ_0/kT that go right up to the critical value is presented, in panel (a), and which exceeds it by a factor of 2, in panel (b). These calculations were performed using the largest size lattice implemented, i.e, $L_x = 64, L_y = L_z = 128$. The results of panel (a) clearly show that, at least for this finite sized system, the

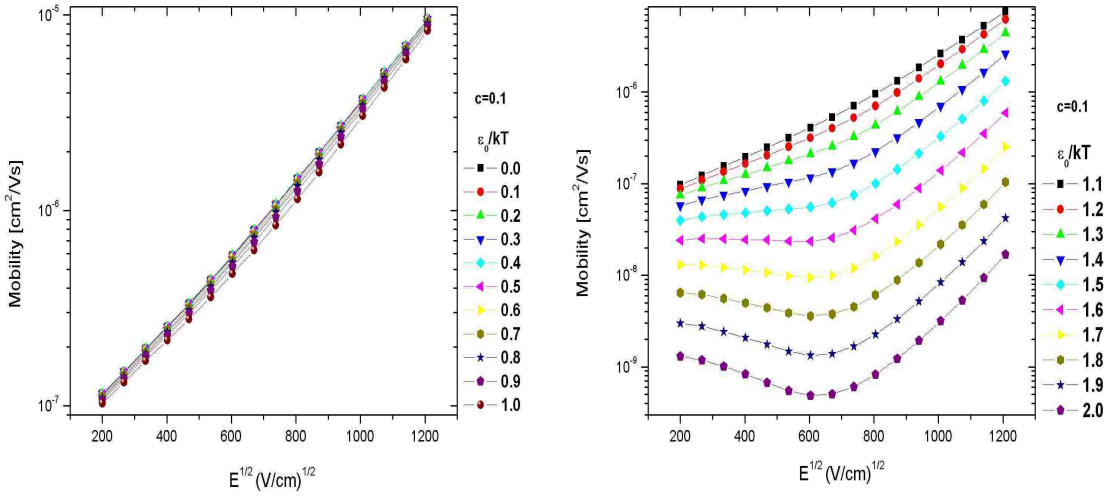

(a) $\varepsilon_0/kT = 0.0$ to 1.0.

(b) $\varepsilon_0/kT = 1.1$ to 2.0.

Figure 4.7. Mobility *vs.* $E^{1/2}$ for $L_x = 64, L_y = L_z = 128$.

PF field dependence is essentially unchanged as the critical point is approached. For values of the dispersion parameter greater than the critical value, there is a marked decrease in the mobility and the appearance of additional curvature that represents deviations from ideal PF behavior. It should be emphasized that this second panel, if it indeed represents the system below the actual transition point only gives the steady-state mobility for a periodically repeated system with a lower cut-off in the energy spectrum, and thus does not necessarily represent what would be measured in a time-of-flight experiment conducted on a sample with a length corresponding to some 10^4 sites. Nonetheless, the appearance of curvature in this region is additional evidence that the transition point really does occur at $\epsilon_0/kT = 1$. On the non-dispersive side of the transition the PF remains unchanged, as predicted by the 1D model.

5. CONCLUSIONS

In this dissertation, hopping transport of photo-injected charge carriers in molecularly doped polymers was studied for three different models of energetic disorder: two models described by different uncorrelated exponential energy distributions, and one described by a combination of correlated Gaussian energetic disorder and uncorrelated exponential energetic disorder. Previously, the commonly-observed temperature dependence and the Poole-Frenkel field dependence of the mobility had been explained using correlated Gaussian disorder models [64, 66], while universal features of current-time transients had been explained using multiple trapping models [4, 67] that postulate an uncorrelated exponential distribution of low energy sites. The main question this research has addressed is whether these two totally different kinds of energetic disorder can coexist in these materials without one component altering or destroying the characteristic features associated the other.

Analysis of the first model studied in this dissertation provides a theoretical description of the steady state mobility of carriers moving through an energy landscape entirely described by a concentration c of randomly distributed traps drawn from an exponential distribution of trap energies of average trap depth ε_0. For this system, a mobility transition is exhibited, i.e., the mobility vanishes as the temperature is lowered below a critical value $T_c = \varepsilon_0/k$, due to an inability of carriers at lower temperatures to achieve thermal equilibrium. As in multiple trapping models, this transition is identified with the nondispersive-to-dispersive transition seen in experimental measurements. A Poole-Frenkel response to the driving field is not observed for this system, which instead shows a field dependence that is exponential in the first power of the field. The resulting mobility monotonically decreases as c and $\beta\varepsilon_0$ are increased.

The second model analytically studied in this dissertation describes a particle moving through a medium with a finite concentration c of exponentially distributed barriers of average barrier height ε_0. As with traps, a transition occurs as the temperature is lowered, but in this model the mobility vanishes at a lower critical temperature $T_c = \varepsilon_0/2k$ than that which arises in the previous study. Moreover, in this barrier model the energy spectrum is bounded from below so, at any temperature, the carrier can always equilibrate to a finite mean carrier energy. Thus, at least in this 1D model, a transition to dispersive transport does not result from a thermodynamic instablity. For the barrier model, aside from the critical temperature, the electric field dependence, the concentration dependence, and the temperature dependence of the mobility exhibit features similar to the model that contains only traps.

The third model considered analytically was one in which both traps and barriers were embedded in a correlated Gaussian landscape. Analysis of this hybrid model leads to features that are qualitatively similar to those observed in MDPs. First, in common with the previous two models, there is a critical temperature $T_c = \varepsilon_0/k$ below which the bulk mobility vanishes. In this model containing both traps and barriers, the critical point appears to be determined by the presence of traps, which have a higher critical temperature than the barriers. In an infinite sample this corresponds to a transition to a transport regime, in which carriers can never equilibrate. Secondly, The Poole-Frenkel field dependence of the charge carrier mobility, and the associated temperature dependence observed in a trap-free sample, is predicted to be largely unaffected as the transition to dispersive transport is approached from the conducting side. The mobility monotonically (algebraically) decreases as a function of the fractional concentration c of exponentially distributed traps/barriers. This decrease became increasingly steep with increasing values of ε_0.

To test the features predicted by the 1D analytical calculations, a series of numerical calculations for 3D systems were carried out using computational methods.

Initial calculations on the 3D version of the model exhibited a strong mobility decrease with increasing values of $\beta\varepsilon_0$, but initial calculations seemed to suggest that the transition point was given not by the condition $\beta\varepsilon_0 = 1$, but by the condition $\beta\varepsilon_0 = 2$, appropriate to barriers. Further investigation revealed this to be an artifact of the finite sample size used in the initial numerical investigation. Additional investigations into the scaling behavior of the mobility with sample size confirmed that the mobility in a bulk system should vanish when $\beta\varepsilon_0 > 1$ as predicted by the 1D analytical model. On the non-dispersive side of the transition the PF behavior and the temperature dependence of mobility remained largely unchanged, as also predicted by the 1D model. Finally, numerical results on finite but large 3D systems show, as expected, that the mobility decreases monotonically with increasing trap concentration.

In summary,the results of extensive analytical and numerical studies, as presented in this dissertation, suggest that the two different classes of essential features commonly observed for photo-injected charges in molecularly-doped polymers (the field and temperature dependence of the mobility on the one hand, and the dispersive aspects of TOF transients on the other) could, in fact, arise from the coexistence of correlated Gaussian disorder arising from molecular charge distributions, and uncorrelated exponential disorder arising from chemical impurities and/or structural defects.

APPENDIX A

DERIVATION OF STATISTICAL PROPERTIES OF THE DISTRIBUTION

In this Appendix, details are provided for the evaluation of the distribution derived in section 2. Beginning with Eq.(22)

$$\begin{aligned}\rho(\varepsilon) &= \int_{-\infty}^{\infty} dv_n \rho_2(v_n) \int_{-\infty}^{\infty} du_n\ \rho_1(u_n)\delta[\varepsilon-(u_n+v_n)] \\ &= \int_{-\infty}^{\infty} dv_n \rho_2(v_n) \int_{-\infty}^{\infty} du_n\ \rho_1(u_n)\delta[u_n-(\varepsilon-v_n)]\end{aligned}$$

Substituting the two independent distributions from (15), (17), and (19)

$$\rho(\varepsilon) = \int_{-\infty}^{\infty} dv_n c\rho_e(v_n) + (1-c)\,\delta(v_n) \int_{-\infty}^{\infty} du_n \frac{\exp(-\frac{u_n^2}{2})}{\sqrt{2\pi\sigma_0^2}}\delta[u_n-(\varepsilon-v_n)]$$

$$\begin{aligned}\rho(\varepsilon) &= \frac{1}{\sqrt{2\pi\sigma_0^2}} \int_{-\infty}^{\infty} \left[c\frac{1}{2\varepsilon_0}\exp\left(-\frac{|v_n|}{\varepsilon_0}\right) + (1-c)\,\delta(v_n)\right] dv_n \times \exp(-\frac{(\varepsilon-v_n)^2}{2\sigma_0^2}) \\ &= \frac{1}{\sqrt{2\pi\sigma_0^2}} \left[\int_{-\infty}^{\infty} \frac{c}{2\varepsilon_0}\exp\left(-\frac{|v_n|}{\varepsilon_0}\right)\exp(-\frac{(\varepsilon-v_n)^2}{2\sigma_0^2})dv_n\right] \\ &\quad + \left[(1-c)\int_{-\infty}^{\infty}\delta(v_n)\exp(-\frac{(\varepsilon-v_n)^2}{2\sigma_0^2})dv_n\right] \\ &= \frac{1}{\sqrt{2\pi\sigma_0^2}} \left[\begin{array}{c}\int_{-\infty}^{0} \frac{c}{2\varepsilon_0}\exp\left(\frac{v_n}{\varepsilon_0}\right)\exp(\frac{-\varepsilon^2+2\varepsilon v_n-v_n^2}{2\sigma_0^2})dv_n \\ +\int_{0}^{\infty} \frac{c}{2\varepsilon_0}\exp\left(\frac{-v_n}{\varepsilon_0}\right)\exp(\frac{-\varepsilon^2+2\varepsilon v_n-v_n^2}{2\sigma_0^2})dv_n + (1-c)\exp(-\frac{\varepsilon^2}{2\sigma_0^2})\end{array}\right] \\ &= \frac{1}{\sqrt{2\pi\sigma_0^2}} \left[\begin{array}{c}\int_{-\infty}^{0} \frac{c}{2\varepsilon_0}\exp\left\{-\frac{\left[\varepsilon_0 v_n^2-2v_n\left(\varepsilon_0\varepsilon+\sigma_0^2\right)+\varepsilon_0\varepsilon^2\right]}{2\varepsilon_0\sigma_0^2}\right\}dv_n \\ +\int_{0}^{\infty} \frac{c}{2\varepsilon_0}\exp\left\{-\frac{\left[\varepsilon_0 v_n^2-2v_n\left(\varepsilon_0\varepsilon-\sigma_0^2\right)+\varepsilon_0\varepsilon^2\right]}{2\varepsilon_0\sigma_0^2}\right\}dv_n + (1-c)\exp(-\frac{\varepsilon^2}{2\sigma_0^2})\end{array}\right]\end{aligned}$$

For calculation simplicity and clarification let

$$\begin{aligned} I_1 &= \int_{-\infty}^{0} \exp\left\{-\frac{[\varepsilon_0 v_n^2 - 2v_n(\varepsilon_0\varepsilon + \sigma_0^2) + \varepsilon_0\varepsilon^2]}{2\varepsilon_0\sigma_0^2}\right\} dv_n \\ I_2 &= \int_{0}^{\infty} \exp\left\{-\frac{[\varepsilon_0 v_n^2 - 2v_n(\varepsilon_0\varepsilon - \sigma_0^2) + \varepsilon_0\varepsilon^2]}{2\varepsilon_0\sigma_0^2}\right\} dv_n \end{aligned}$$

The two integrals,I_1 and I_2 can be evaluated separately using the following general solution,with erfc(x) indicating the complementary error function ;

$$\int_0^{\infty} \exp -\left(ax^2 + bx + c\right) = \frac{1}{2}\sqrt{\frac{\pi}{a}} \exp \frac{(b^2 - 4ac)}{4a} \times \operatorname{erfc}\left(\frac{b}{2\sqrt{a}}\right)$$

$$\begin{aligned} I_1 &= \int_{-\infty}^{0} \exp\left\{-\frac{[\varepsilon_0 v_n^2 - 2v_n(\varepsilon_0\varepsilon + \sigma_0^2) + \varepsilon_0\varepsilon^2]}{2\varepsilon_0\sigma_0^2}\right\} dv_n \\ Let \quad v_n &= -V_n \\ dv_n &= -dV_n \\ I_1 &= \int_{0}^{\infty} \left\{-\frac{[\varepsilon_0 V_n^2 - 2V_n(\varepsilon_0\varepsilon + \sigma_0^2) + \varepsilon_0\varepsilon^2]}{2\varepsilon_0\sigma_0^2}\right\} dV_n \\ I_1 &= \sqrt{\frac{\pi\sigma_0^2}{2}} \exp\left(\frac{2\varepsilon_0\sigma_0^2\varepsilon + \sigma_0^4}{2\varepsilon_0^2\sigma_0^2}\right) \operatorname{erfc}\left(\frac{\varepsilon_0\varepsilon + \sigma_0^2}{\varepsilon_0\sigma_0^2\sqrt{2}}\right) \\ I_2 &= \int_{0}^{\infty} \exp\left\{-\frac{[\varepsilon_0 v_n^2 - 2v_n(\varepsilon_0\varepsilon - \sigma_0^2) + \varepsilon_0\varepsilon^2]}{2\varepsilon_0\sigma_0^2}\right\} dv_n \\ I_2 &= \sqrt{\frac{\pi\sigma_0^2}{2}} \exp\left(\frac{-2\varepsilon_0\sigma_0^2\varepsilon + \sigma_0^4}{2\varepsilon_0^2\sigma_0^2}\right) \operatorname{erfc}\left(\frac{-(\varepsilon_0\varepsilon - \sigma_0^2)}{\varepsilon_0\sigma_0^2\sqrt{2}}\right) \end{aligned}$$

$$\begin{aligned} I &= I_1 + I_2 \\ &= \sigma_0\sqrt{\frac{\pi}{2}} \left\{ \begin{array}{c} \exp\left(\frac{2\varepsilon_0\sigma_0^2\varepsilon + \sigma_0^4}{2\varepsilon_0^2\sigma_0^2}\right) \operatorname{erfc}\left(\frac{\varepsilon_0\varepsilon + \sigma_0^2}{\varepsilon_0\sigma_0\sqrt{2}}\right) \\ + \exp\left(\frac{-2\varepsilon_0\sigma_0^2\varepsilon + \sigma_0^4}{2\varepsilon_0^2\sigma_0^2}\right) \operatorname{erfc}\left(\frac{-(\varepsilon_0\varepsilon - \sigma_0^2)}{\varepsilon_0\sigma_0\sqrt{2}}\right) \end{array} \right\} \end{aligned}$$

This solution can be written as $I = \sigma_0\sqrt{\frac{\pi}{2}}I^{/}$ where

$$\begin{aligned} I^{/} &= \exp\left(\frac{2\varepsilon_0\sigma_0^2\varepsilon + \sigma_0^4}{2\varepsilon_0^2\sigma_0^2}\right)\operatorname{erfc}\left(\frac{\varepsilon_0\varepsilon + \sigma_0^2}{\varepsilon_0\sigma_0\sqrt{2}}\right) \\ &\quad + \exp\left(\frac{-2\varepsilon_0\sigma_0^2\varepsilon + \sigma_0^4}{2\varepsilon_0^2\sigma_0^2}\right)\operatorname{erfc}\left(\frac{-(\varepsilon_0\varepsilon - \sigma_0^2)}{\varepsilon_0\sigma_0\sqrt{2}}\right) \end{aligned}$$

and expanding the two exponential terms

$$\begin{aligned} I^{/} &= I_1^{/} + I_2^{/} \\ &= \{\exp\left(\frac{\sigma_0^2}{2\varepsilon_0^2}\right)\exp\left(\frac{\varepsilon}{\varepsilon_0}\right)\operatorname{erfc}\left(\frac{\varepsilon_0\varepsilon + \sigma_0^2}{\varepsilon_0\sigma_0\sqrt{2}}\right) \\ &\quad + \exp\left(\frac{\sigma_0^2}{2\varepsilon_0^2}\right)\exp\left(\frac{-\varepsilon}{\varepsilon_0}\right)\operatorname{erfc}\left(\frac{-(\varepsilon_0\varepsilon - \sigma_0^2)}{\varepsilon_0\sigma_0\sqrt{2}}\right)\} \end{aligned}$$

With these simplifications the total distribution is expressed as:

$$\begin{aligned} \rho(\varepsilon) &= \frac{1}{\sqrt{2\pi\sigma_0^2}}\left\{\frac{c\sigma_0}{2\varepsilon_0}\sqrt{\frac{\pi}{2}}I^{/} + (1-c)\exp(-\frac{\varepsilon^2}{2\sigma_0^2})\right\} \\ \rho(\varepsilon) &= \frac{c}{4\varepsilon_0}I^{/} + \frac{(1-c)}{\sigma_0\sqrt{2\pi}}\exp(-\frac{\varepsilon^2}{2\sigma_0^2}) \end{aligned}$$

$$\begin{aligned} I_1^{/} &= \left\{\exp\left(\frac{\sigma_0^2}{2\varepsilon_0^2}\right)\exp\left(\frac{\varepsilon}{\varepsilon_0}\right)\operatorname{erfc}\left(\frac{\varepsilon_0\varepsilon + \sigma_0^2}{\varepsilon_0\sigma_0\sqrt{2}}\right)\right\} \\ I_1^{/} &= \left\{\exp\left(\frac{\sigma_0^2}{2\varepsilon_0^2}\right)\exp\left(\frac{\varepsilon}{\varepsilon_0}\right)\left[1 - \operatorname{erf}\frac{\left(\varepsilon + \frac{\sigma_0^2}{\varepsilon_0}\right)}{\sqrt{2\sigma_0^2}}\right]\right\} \\ I_2^{/} &= \left\{\exp\left(\frac{\sigma_0^2}{2\varepsilon_0^2}\right)\exp\left(\frac{-\varepsilon}{\varepsilon_0}\right)\operatorname{erfc}\left(\frac{-(\varepsilon_0\varepsilon - \sigma_0^2)}{\varepsilon_0\sigma_0\sqrt{2}}\right)\right\} \\ I_2^{/} &= \left\{\exp\left(\frac{\sigma_0^2}{2\varepsilon_0^2}\right)\exp\left(\frac{-\varepsilon}{\varepsilon_0}\right)\left[1 + \operatorname{erf}\frac{\left(\varepsilon - \frac{\sigma_0^2}{\varepsilon_0}\right)}{\sqrt{2\sigma_0^2}}\right]\right\} \\ I^{/} &= \left(I_1^{/} + I_2^{/}\right) \\ I^{/} &= \exp\left(\frac{\sigma_0^2}{2\varepsilon_0^2}\right)f(\varepsilon) \end{aligned}$$

where

$$f(\varepsilon) = \exp\left(\frac{\varepsilon}{\varepsilon_0}\right)\left[1 - \mathrm{erf}\frac{\left(\varepsilon + \frac{\sigma_0^2}{\varepsilon_0}\right)}{\sqrt{2\sigma_0^2}}\right] + \exp\left(\frac{-\varepsilon}{\varepsilon_0}\right)\left[1 + \mathrm{erf}\frac{\left(\varepsilon - \frac{\sigma_0^2}{\varepsilon_0}\right)}{\sqrt{2\sigma_0^2}}\right]$$

$$\rho(\varepsilon) = c\left[\frac{1}{4\varepsilon_0}\exp\left(\frac{\sigma_0^2}{2\varepsilon_0^2}\right) f(\varepsilon)\right] + (1-c)\left[\frac{1}{\sqrt{2\pi\sigma_0^2}}\exp(-\frac{\varepsilon^2}{2\sigma_0^2})\right]$$

The final simplified full site energy distribution is expressed by the following equation:

$$\rho(\varepsilon) = c\widehat{\rho}(\varepsilon) + (1-c)\,\rho_1(\varepsilon) \tag{A.1}$$

with

$$\widehat{\rho}(\varepsilon) = \frac{1}{4\varepsilon_0}\exp\left(\frac{\sigma_0^2}{2\varepsilon_0^2}\right) f(\varepsilon) \tag{A.2}$$

$$\rho_1(\varepsilon) = \frac{1}{\sqrt{2\pi\sigma_0^2}}\exp(-\frac{\varepsilon^2}{2\sigma_0^2}) \tag{A.3}$$

and

Here, the following identities are used to perform the calculations :erfc$(x) = 1-$ erf(x),erf$(-x) = -$erf(x), and erf$(x) = 1-$erfc(x). Since an exponential function falls off more slowly than a Gaussian, the tails of the total distribution are dominated by the *exponential* energy dependence of the traps.Substituting the asymptotic expansion

$\mathrm{erf}\,(x) \sim 1 - x^{-1}\pi^{-1/2}e^{-x^2}$ of the error function into the $f(\varepsilon)$

$$\begin{aligned}
\mathrm{erf}\frac{\left(\varepsilon + \frac{\sigma_0^2}{\varepsilon_0}\right)}{\sqrt{2\sigma_0^2}} &= 1 - \sqrt{\frac{2\sigma_0^2}{\pi}}\frac{1}{\left(\varepsilon + \frac{\sigma_0^2}{\varepsilon_0}\right)}\exp\left\{-\frac{\left(\varepsilon + \frac{\sigma_0^2}{\varepsilon_0}\right)^2}{2\sigma_0^2}\right\} \\
\mathrm{erf}\frac{\left(\varepsilon - \frac{\sigma_0^2}{\varepsilon_0}\right)}{\sqrt{2\sigma_0^2}} &= 1 - \sqrt{\frac{2\sigma_0^2}{\pi}}\frac{1}{\left(\varepsilon - \frac{\sigma_0^2}{\varepsilon_0}\right)}\exp\left\{-\frac{\left(\varepsilon - \frac{\sigma_0^2}{\varepsilon_0}\right)^2}{2\sigma_0^2}\right\} \\
f(\varepsilon) &= \exp\left(\frac{\varepsilon}{\varepsilon_0}\right)\left[1 - 1 + \sqrt{\frac{2\sigma_0^2}{\pi}}\frac{1}{\left(\varepsilon + \frac{\sigma_0^2}{\varepsilon_0}\right)}\exp\left\{-\frac{\left(\varepsilon + \frac{\sigma_0^2}{\varepsilon_0}\right)^2}{2\sigma_0^2}\right\}\right] \\
&\quad + \exp\left(\frac{-\varepsilon}{\varepsilon_0}\right)\left[1 + 1 - \sqrt{\frac{2\sigma_0^2}{\pi}}\frac{1}{\left(\varepsilon - \frac{\sigma_0^2}{\varepsilon_0}\right)}\exp\left\{-\frac{\left(\varepsilon - \frac{\sigma_0^2}{\varepsilon_0}\right)^2}{2\sigma_0^2}\right\}\right]
\end{aligned}$$

$$\begin{aligned}
f(\varepsilon) &= \exp\left(\frac{\varepsilon}{\varepsilon_0}\right)\left[\sqrt{\frac{2\sigma_0^2}{\pi}}\frac{1}{\left(\varepsilon + \frac{\sigma_0^2}{\varepsilon_0}\right)}\exp\left\{-\frac{\left(\varepsilon + \frac{\sigma_0^2}{\varepsilon_0}\right)^2}{2\sigma_0^2}\right\}\right] \\
&\quad + \exp\left(\frac{-\varepsilon}{\varepsilon_0}\right)\left[2 - \sqrt{\frac{2\sigma_0^2}{\pi}}\frac{1}{\left(\varepsilon - \frac{\sigma_0^2}{\varepsilon_0}\right)}\exp\left\{-\frac{\left(\varepsilon - \frac{\sigma_0^2}{\varepsilon_0}\right)^2}{2\sigma_0^2}\right\}\right] \\
f(\varepsilon) &= \exp\left(\frac{\varepsilon}{\varepsilon_0}\right)\left[\sqrt{\frac{2\sigma_0^2}{\pi}}\frac{1}{\left(\varepsilon + \frac{\sigma_0^2}{\varepsilon_0}\right)}\exp\left\{-\frac{\left(\varepsilon + \frac{\sigma_0^2}{\varepsilon_0}\right)^2}{2\sigma_0^2}\right\}\right] + 2\exp\left(\frac{-\varepsilon}{\varepsilon_0}\right) \\
&\quad - \exp\left(\frac{-\varepsilon}{\varepsilon_0}\right)\left[\sqrt{\frac{2\sigma_0^2}{\pi}}\frac{1}{\left(\varepsilon - \frac{\sigma_0^2}{\varepsilon_0}\right)}\exp\left\{-\frac{\left(\varepsilon - \frac{\sigma_0^2}{\varepsilon_0}\right)^2}{2\sigma_0^2}\right\}\right]
\end{aligned}$$

if $|\varepsilon| >> \frac{\sigma_0^2}{\varepsilon_0}$

$$f(\varepsilon) \sim 2\exp\left(\frac{-\varepsilon}{\varepsilon_0}\right)$$

making the combined distribution for high concentrations $c \sim 1$,

$$\begin{aligned}
\rho(\varepsilon) &\simeq c\widehat{\rho}(\varepsilon) \\
\rho(\varepsilon) &\simeq \frac{c}{4\varepsilon_0} \exp\left(\frac{\sigma_0^2}{2\varepsilon_0^2}\right) f(\varepsilon) \\
\rho(\varepsilon) &\simeq \frac{c}{4\varepsilon_0} \exp\left(\frac{\sigma_0^2}{2\varepsilon_0^2}\right) 2\exp\left(\frac{-|\varepsilon|}{\varepsilon_0}\right) \\
\rho(\varepsilon) &\simeq \frac{c}{2\varepsilon_0} \exp\left(\frac{\sigma_0^2}{2\varepsilon_0^2}\right) \exp\left(\frac{-|\varepsilon|}{\varepsilon_0}\right)
\end{aligned}$$

APPENDIX B

HOPPING TRANSPORT IN ORDERED LATTICES

The probability distribution $P_n(t)$ for finding the particle in each of the different localized states $\{n\}$ in which it might find itself. Equations which describe the evolution of such probabilities,arising from an underlying stochastic process, are usually referred to as Master Equations.Markovian Master Equation (ME) for an ordered chain with an external electric field can be written as:

$$\frac{dP_n}{dt} = W_- P_{n+1} - W_+ P_n - W_- P_n + W_+ P_{n-1} \tag{B.1}$$

where the W_+ and W_- are transition rates in the forward direction and backward direction, i.e., they describe the transition probability per unit time between the different states of the system.

B.1. SYSTEM WITHOUT AN APPLIED ELECTRIC FIELD

If the external field is zero $W_- = W_+ = W$ and the master equation is simplified as:

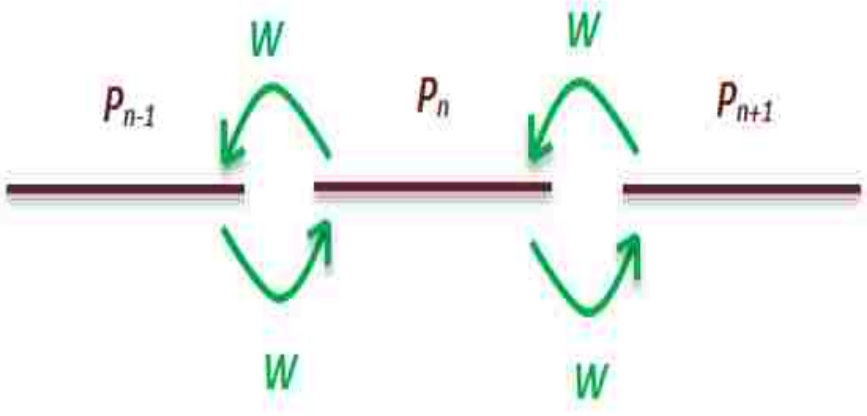

Figure B.1. Hopping between three neighboring states without electric field.

$$\frac{dP_n}{dt} = -2WP_n + WP_{n+1} + WP_{n-1} \tag{B.2}$$

Define discrete Fourier transform pairs

$$P_k(t) = \sum_{n=-\infty}^{\infty} P_n(t)\, e^{ikn} \tag{B.3}$$

and

$$P_n(t) = \frac{1}{2\pi} \int_0^{2\pi} dk\ P_k(t)\, e^{-ikn} \tag{B.4}$$

Here $P_k(t) = P_{k+2\pi}(t)$ is periodic in the variable k,with period 2π,and thus is expressible as a discrete Fourier expansion, as indicated, where the Fourier expansion coefficients are given by the usual formula on the right hand side. Using this, master equation can be expressed in terms of the quantities $P_k(t)$;

$$\frac{dP_k}{dt} = \sum_n \frac{dP_n}{dt} e^{ikn}$$

Substituting to the master equation and simplifying

$$\begin{aligned}
\frac{dP_k}{dt} &= -2W \sum_n P_n e^{ikn} + W \sum_n P_{n+1} e^{ikn} + W \sum_n P_{n-1} e^{ikn} \\
&= -2WP_k + W \sum_n P_n e^{ikn} e^{ik} + W \sum_n P_n e^{ikn} e^{-ik} \\
&= -2WP_k + 2WP_k \left(\frac{e^{ik} + e^{-ik}}{2} \right) \\
\frac{dP_k}{dt} &= -2WP_k \left[1 - Cos(k) \right]
\end{aligned}$$

Defining $W_k = 2W\,[1 - Cos(k)]$ and substituting to the above equation will provide an uncoupled equation of motion for the P_k.

$$\frac{dP_k}{dt} = -2W_k P_k$$

Which gives

$$P_k(t) = P_k(0)e^{-W_k t}$$

For the initial condition we can consider that the particle starts at the origin, i.e., $P_n(0) = \delta_{n,0}$. From $P_k(0) = \sum_{n=-\infty}^{\infty} P_n(0)e^{ikn}$ we get $P_k(0) = 1$, $P_k(t) = e^{-W_k t}$ Then,

$$P_n(t) = \int_0^{2\pi} \frac{dk}{2\pi} P_k(t)e^{-ikn}$$
$$P_n(t) = \int_0^{2\pi} \frac{dk}{2\pi} e^{-W_k t}e^{-ikn}$$
$$P_n(t) = \frac{1}{2\pi}\int_{-\pi}^{\pi} dk\ e^{-2Wt}\ e^{2WtCosk}\ e^{-ikn}$$
$$P_n(t) = \frac{1}{2\pi}e^{-2Ft}\int_{-\pi}^{\pi} dk\ e^{2WtCosk}\ e^{-ikn}$$

Bessel function is defined as $J_n(z) = \int_{-\pi}^{\pi} \frac{dk}{2\pi} e^{izCosk}e^{-ikn}$ Then

$$P_n(t) = e^{-2Wt}J_n(2iWt)$$

Modified Bessel function is defined as $I_n(z) = J_n(iz)$ Therefore,

$$P_n(t) = e^{-2Wt}I_n(2Wt) \tag{B.5}$$

From this $P_n(t)$ one can compute the first two moments of the distribution: The first moment

$$\langle n(t) \rangle = \sum_n P_n(t) n$$

or

$$\langle n(t) \rangle = \sum_n n e^{-2Wt} I_n(2Wt)$$

At the same time one can express $\langle n(t) \rangle$ in terms of derivatives of $P_k(t)$, evaluated at $k = 0$.

$$\begin{aligned} P_k(t) &= \sum_n P_n(t) e^{ikn} \\ \frac{dP_k(t)}{dk} &= i \sum_n n P_n(t) e^{ikn} \\ \left[\frac{dP_k(t)}{dk} \right]_{k=0} &= i \sum_n n P_n(t) = i \langle n(t) \rangle \end{aligned}$$

Also $P_k(t) = e^{-W_k t} = e^{-2W(1-Cos(k))t}$

$$\begin{aligned} \frac{dP_k(t)}{dk} &= e^{-2Wt} e^{-2WtCosk} (-\sin nk) \\ \frac{dP_k(t)}{dk} &= -P_k(t) (\sin k) 2Wt \\ \left[\frac{dP_k(t)}{dk} \right]_{k=0} &= 0 \end{aligned}$$

Therefore

$$\langle n(t) \rangle = 0$$

For a particle starting at the origin

$$\langle x(t)\rangle = \langle n(t)\rangle\, a = 0$$

The second moment

$$\begin{aligned}
\left\langle n^2(t)\right\rangle &= \sum_n P_n(t) n^2 \\
\frac{dP_k(t)}{dk} &= i \sum_n n P_n(t) e^{ikn} \\
\frac{d^2P_k(t)}{dk^2} &= -\sum_n n^2 P_n(t) e^{ikn} \\
\left[\frac{d^2P_k(t)}{dk^2}\right]_{k=0} &= -\sum_n n^2 P_n(t) = -\left\langle n^2(t)\right\rangle
\end{aligned} \tag{B.6}$$

Also;

$$\begin{aligned}
\frac{dP_k(t)}{dk} &= -P_k(t)(\sin k) 2Wt \\
\frac{d^2P_k(t)}{dk^2} &= -2Wt\left\{(\sin k)\frac{dP_k(t)}{dk} + P_k(t)\cos k\right\} \\
&= -2Wt\left\{-(\sin^2 k) 2WtP_k(t) + P_k(t)\cos k\right\} \\
&= \left(2Wt(\sin^2 k)\right)^2 P_k(t) - 2WtP_k(t)\cos k \\
\left[\frac{d^2P_k(t)}{dk^2}\right]_{k=0} &= -2Wt \\
\left\langle n^2(t)\right\rangle &= 2Wt
\end{aligned}$$

When multiplied by the square of the lattice spacing a ,

$$\left\langle n^2(t)\right\rangle a^2 = \left\langle x^2(t)\right\rangle = 2a^2Wt$$

Defining the diffusion constant $D = a^2W$,

$$\left\langle x^2(t) \right\rangle = 2Dt \tag{B.7}$$

B.2. SYSTEM WITH AN APPLIED ELECTRIC FIELD

Now consider an ordered chain with an electric field E and the Eq.(B.1)

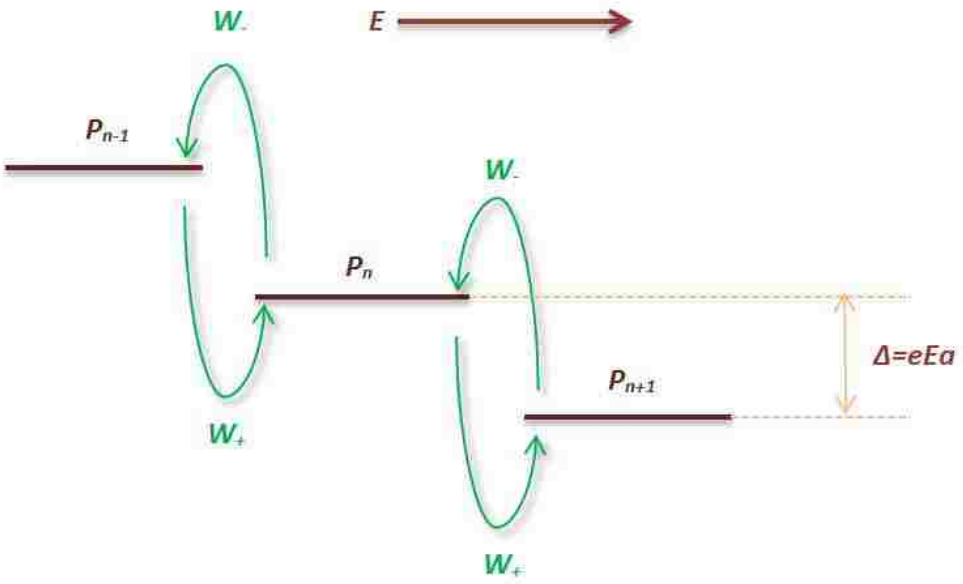

Figure B.2. Hopping between three neighboring states with electric field.

$$\frac{dP_n}{dt} = W_- P_{n+1} - W_+ P_n - W_- P_n + W_+ P_{n-1} \tag{B.8}$$

Using Fourier transform

$$P_k(t) = \sum_{n=-\infty}^{\infty} P_n(t)\, e^{ikn}$$
$$\frac{dP_k}{dt} = \sum_n \frac{dP_n}{dt} e^{ikn}$$

Substituting for the $\frac{dP_n}{dt}$ term;

$$\begin{aligned}
\frac{dP_k}{dt} &= -W_+ \sum_n P_n e^{ikn} - W_- \sum_n P_n e^{ikn} + W_- \sum_n P_{n+1} e^{ikn} + W_+ \sum_n P_{n-1} e^{ikn} \\
\frac{dP_k}{dt} &= -W_+ \sum_n P_n e^{ikn} - W_- \sum_n P_n e^{ikn} + W_- \sum_n P_n e^{ikn} e^{-ik} + W_+ \sum_n P_n e^{ikn} e^{ik} \\
\frac{dP_k}{dt} &= -W_+ P_k - W_- P_k + W_- P_k e^{-ik} + W_+ P_k e^{ik} \qquad \text{(B.9)}
\end{aligned}$$

Now letting the rates W_+ and W_- as Miller-Abrahams like rates- $W_+ = W$, $W_- = We^{-\beta\Delta}$ the above equation can be expressed as

$$\frac{dP_k}{dt} = -W\left(1 + e^{-\beta\Delta}\right) P_k + We^{-ik} e^{-\beta\Delta} P_k + We^{ik} P_k$$

Defining $W_k = W\left[1 + e^{-\beta\Delta} - e^{-ik} e^{-\beta\Delta} - e^{ik}\right]$ the expression can be simplified to:

$$\frac{dP_k}{dt} = -W_k P_k$$

which has a solution

$$P_k(t) = P_k(0) e^{-W_k t} \qquad \text{(B.10)}$$

Using the same boundary conditions and the equation for the first moment as the non electric field case

$$P_k(t) = e^{-W_k t}$$

$$\begin{aligned}
\langle n(t) \rangle &= -i \left[\frac{dP_k(t)}{dk} \right]_{k=0} \\
&= -i \, \frac{d \left\{ \exp \left[-W \left(1 + e^{-\beta\Delta} - e^{-ik} e^{-\beta\Delta} - e^{ik} \right) t \right] \right\}}{dk} \, |_{k=0} \\
&= -i \left[iWt \left(1 - e^{-\beta\Delta} \right) \right] \\
\langle n(t) \rangle &= Wt \left(1 - e^{-\beta\Delta} \right)
\end{aligned}$$

Using this relation one can calculate the mobility

$$\mu = \frac{V_d}{E} = \frac{\langle x(t) \rangle}{tE}$$

where $\langle x(t) \rangle = a \langle n(t) \rangle$

$$\mu = \frac{Wa \left(1 - e^{-\beta\Delta} \right)}{E} \tag{B.11}$$

To generalize the above derivation one can specifically not assign values for the two rates ($W_+ = W$, $W_- = We^{-\beta\Delta}$). Keeping the two rates as it is and using Eq.B.9

$$\begin{aligned}
\frac{dP_k}{dt} &= -W_+ P_k - W_- P_k + W_- P_k e^{-ik} + W_+ P_k e^{ik} \\
&= \left[W_+ \left(e^{ik} - 1 \right) + W_- \left(e^{-ik} - 1 \right) \right] P_k \\
\int \frac{dP_k}{P_k} &= \left[W_+ \left(e^{ik} - 1 \right) + W_- \left(e^{-ik} - 1 \right) \right] \int dt \\
P_k(t) &= P_k(0) \exp \left[W_+ \left(e^{ik} - 1 \right) + W_- \left(e^{-ik} - 1 \right) \right] t
\end{aligned}$$

Using the fact that $P_k(0) = 1$

$$
\begin{aligned}
P_k(t) &= \exp\left[W_+\left(e^{ik}-1\right)+W_-\left(e^{-ik}-1\right)\right]t \\
\langle n(t)\rangle &= -i\left[\frac{dP_k(t)}{dk}\right]_{k=0} \\
&= -i\frac{d}{dk}\left\{\exp\left[W_+\left(e^{ik}-1\right)+W_-\left(e^{-ik}-1\right)\right]t\right\}_{k=0} \\
&= -it\left[W_+e^{ik}(i)+W_-e^{-ik}(-i)\right]_{k=0} \\
\langle n(t)\rangle &= \left[W_+ - W_-\right]t
\end{aligned}
$$

using the mobility equation

$$\mu = \frac{a\langle n(t)\rangle}{tE} \tag{B.12}$$

$$\mu = \frac{a\left[W_+ - W_-\right]}{E} \tag{B.13}$$

BIBLIOGRAPHY

[1] L.B. Schein, A. Rosenberg, and S.L. Rice. *J. Appl. Phys.*, 60:4287, 1986.

[2] J. X. Mack, L.B. Schein, and A. Peled. Hole mobilities in hydrazone-polycarbonate dispersions. *Phys. Rev. B*, 39:7500, 1989.

[3] G. Pfister. *Phys. Rev. B*, 16:3676, 1977.

[4] D. H. Dunlap, L. B. Schein, A. Tyutnev, V. Saenko, E. D. Pozhidaev, P. E. Parris, and D. S. Weiss. *J. Phys. Chem. C*, 114:9076, 2010.

[5] U. Scherf D. Hertel, H. Bssler and H. H. Hrhold. *J. Chem. Phys.*, 110:9214, 1999.

[6] D. M. Pai. *J. Chem. Phys.*, 52:2285, 1970.

[7] W. D. Gill. *J. Appl. Phys.*, 43:2285, 1972.

[8] J. Hirsch. *J. Phys. C*, 12:321, 1979.

[9] H. Baessler, G. Schonherr, M. Abkwitz, and D. M. Pai. *Phys. Rev. B*, 26:3105, 1982.

[10] M. Stolka, J. F. Yanus, and D. M. Pai. *J. Phys. Chem.*, 88:4704, 1984.

[11] M. Abkowitz and M. Stolka. *Phil. Mag. Lett.*, 58:239, 1988.

[12] L. B. Schein, A. Peled, and D. Glatz. *J. Appl. Phys.*, 66:686, 1989.

[13] L. B. Schein. *Mol. Cryst. Liq. Cryst.*, 183:41, 1990.

[14] M. Abkowitz, H. Baessler, and M. Stolka. *Phil. Mag. B*, 63:201, 1991.

[15] G. Pfister and H. Scher. *Adv. Phys.*, 27:747, 1978.

[16] H. Baessler. *Phys. Stat. Sol. (b)*, 107:9, 1981.

[17] H. Baessler. *J. Mod. Phys. B*, 8:847, 1994.

[18] P. M. Borsenberger and H. Baessler. *J. Chem. Phys.*, 95:5327, 1991.

[19] L. B. Schein. *Phil. Mag. B*, 65:795, 1992.

[20] L. B. Schein, D. Glatz, and J. C. Scott. *Phys. Rev. Lett.*, 65:472, 1990.

[21] L. T. Pautmeier, J. C. Scott, and L. B. Schein. *Chem. Phys. Lett.*, 197:568, 1992.

[22] Z. G. Soos, S. Bao, J. M. Sin, and G. W. Hayden. *Chem. Phys. Lett.*, 319:631, 2000.

[23] D. M. Pai. *J. Non-Cryst. Solids*, 59 & 60:1255, 1983.

[24] D. M. Pai and A. R. Melnyk. *Proc. SPIE*, 617:82, 1986.

[25] A. R. Melnyk and D. M. Pai. *Proc. SPIE*, 1253:141, 1990.

[26] M. Stolka and J. Mort. *Kirk-Othmer Encylopedia of Chemical Technology*. John Wiley and Sons, New York, 1994.

[27] D. M. Pai and B. E. Springett. *Rev. Mod. Phys.*, 65:163, 1993.

[28] K. Y. Law. *Chem. Rev.*, 93:449, 1993.

[29] D. M. Pai. *Frontiers of Polymer Research*. Plenum Press, New York, 1991.

[30] P. M. Borsenberger and S. Weiss. *Organic Photoreceptors for Xerograph*. CRC Press, 1998.

[31] C.W. Tang. *Appl. Phys. Lett.*, 48:183, 1986.

[32] P. W. M Blom, V. D. Mihailetchi, L. J. A. Koster, and D. E. Markov. *Adv. Mater.*, 19:1551, 2007.

[33] E. Bundgaard and F. C. Krebs. *Solar Energy Materials & Solar Cells*, 91:954, 2007.

[34] J.H. Burroughes, C.A. Jones, and R.H. Friend. *Nature*, 335:137, 1988.

[35] H. Inada, Y. Yonemoto, T. Wakimoto, K. Imai, and Y. Shirota. *Mol. Cryst. Liq. Cryst.*, 280:331, 1996.

[36] R. H. Jordan, L. J. Rothberg, A. Dodabalapur, and R. E. Slusher. *Appl. Phys. Lett.*, 280:1997, 1996.

[37] A. B. Walker, A. Kambili, and S. J. Martin. *J. Phys.: Condens. Matter*, 14:9825, 2000.

[38] D. P. West, M. D. Rahn, C. Im, and H. Baessler. *Chem. Phys. Lett.*, 326:407, 2000.

[39] J. Kalinowski, P. DiMarco, M. Cocchi, V. Fattori, N. Camaioni, and J. Duff. *Appl. Phys. Lett.*, 68:2317, 1996.

[40] J. Kido, G. Harada, and K. Nagai. *Chem. Lett.*, 44:161, 1996.

[41] C. Tanase, E. J Meijer, P. W. Blom, and D. M. de Leeuw. *Phys. Rev.Lett.*, 91:216601, 2003.

[42] J. H. Burroughes, C. A. Jones, and R. H Friend. *Nature*, 335:137, 1988.

[43] A. Tsumura, H. Koezuka, and T. Ando. *Synth. Met.*, 25:11, 1988.

[44] A. R. Brown, D. M. Deleeuw, E. J Lous, and E. E. Havinga. *Synth. Met.*, 66:257, 1994.

[45] Y. Y. Lin, D. J. Gundlach, S. F Nelson, and T. N. Jackson. *IEEE Trans. Electron Devices*, 44:1325, 1997.

[46] M. Pope and C.E. Swenberg. *Electronic Processes in Organic Crystals and Polymers*. Oxford University Press,USA, 1999.

[47] P. Drude. *Annalen der Physik*, 306:566, 1900.

[48] J. Ziman. *Electrons and phonons: The theory of transport phenomena in solids*. Oxford University Press,USA, 1960.

[49] A. Miller and E. Abrahams. *Phys. Rev.*, 120:745, 1960.

[50] N.E. Gruhn, D.A. da Silva, T.G. Bill, M. Malagoli, V. Coropceanu, A. Kahn, and J.L. Bredas. *J. Am. Chem. Soc.*, 124:7918, 2002.

[51] J. H. Schon, C. Kloc, R. A. Laudise, and B. Batlogg. *Phys. Rev. B*, 58:12952, 1998.

[52] J. H. Schon, C. Kloc, and B. Batlogg. *Phys. Rev.Lett.*, 86:3843, 2001.

[53] J. H. Schon, S . Berg, C. Kloc, and B. Batlogg. *Science*, 287:1022, 2000.

[54] J. H. Schon, C. Kloc, and B. Batlogg. *Sci*, 288:2338, 2000.

[55] T. Holstein. *Phil. Mag. B*, 37, 1977.

[56] David Emin. *Advances in Physics*, 24:305, 1975.

[57] R. A. Marcus. *J. Chem. Phys.*, 24:966, 1956.

[58] N.G. VanKampen. *Stochastic Processes in Physics and Chemistry*. North Holland, 2007.

[59] N.F. Mott. *Phil. Mag.*, 19:835, 1969.

[60] S. C. Tse, S. W. Tsang, and S. K. So. *J. Appl. Phys.*, 100:063708, 2006.

[61] M. A. Lampert and P. Mark. *Current Injection in Solids*. Academic Press, New York, 1970.

[62] J.R. Haynes and W. Shockley. *Phys. Rev.*, 81:835, 1951.

[63] J. Frenkel. *Phys. Rev.*, 54:647, 1938.

[64] D.H. Dunlap, V.M. Kenkre, and P.E. Parris. *J. Imaging Sci. Technol.*, 43:437, 1999.

[65] S.V. Novikov and A.P. Tyutnev. *J. Chem. Phys.*, 138:104120, 2013.

[66] P. E. Parris, V. M. Kenkre, and D. H. Dunlap. *Phys. Rev. Lett.*, 87:126601, 2001.

[67] H. Scher and E.W. Montroll. *Phys. Rev. B*, 12:2455, 1975.

[68] H. Baessler. *phys. stat. sol. (b)*, 175:15, 1993.

[69] A. Dieckmann, H. Baessler, and P. M. Borsenberger. *J. Chem. Phys.*, 99:8136, 1993.

[70] A. Chowdhury and P.E. Parris. Unpublished. 2013.

[71] L.B. Schein and P.M. Borsenberger. *Chem. Phys.*, 177:773, 1993.

[72] Y. Gartstein and E. Conwell. *Chem. Phys. Lett.*, 245:351, 1995.

[73] V. Novikov and A.V. Vannikov. *J. Phys. Chem.*, 99:14573, 1995.

[74] S.V. Novikov, D. H. Dunlap, V. M. Kenkre, P. E. Parris, and A. V. Vannikov. *Phys. Rev. Lett.*, 20:4472, 1998.

[75] D.H. Dunlap, P.E. Parris, and V.M. Kenkre. *Phys. Rev.Lett.*, 77:542, 1996.

[76] P.E Parris, V.M. Kenkre, and D.H. Dunlap. *Phys. Rev. Lett.*, 87:126601, 2001.

[77] B. Derrida. *J. Stat. Phys.*, 31:433, 1983.

[78] D. Stauffer and A. Aharony. *Introduction to Percolation Theory.* Taylor and Francis, Philadelphia, 1991.

[79] P.E. Parris and B.D. Bookout. *Physical Review B*, 53:629, 1996.

VITA

Nilanka Praveena Gurusinghe obtained his B.Sc. degree from University of Peradeniya in Sri Lanka in 2004. He was a Physics student with chemistry and computer science as subsidiary subjects.

Nilanka was selected from the Department of Physics and Astronomy at Bowling Green State University (BGSU) to do his graduate studies. During his time in Kottan-Labs at BGSU, completing the Masters in Physics, under the supervision of Dr. Bruno Ullrich and Dr. Mikhail Zamikov, he worked extensively in material science mainly focusing on semiconductor hetero-structures (ZnS/Si) as the thesis project and semiconductor nano structures (QDs) as an extra project. His thesis project was presented as "Investigation of optoelectronic properties of thin film n-type ZnS on p-type Si". Findings from the second project were published in two papers in The Journal of Physical Chemistry:

"Composition-Tunable Properties of CdSxTe1-x Alloy Nanocrystals", along with Nishshanka N. Hewa-Kasakarage, and Mikhail Zamkov;

"Blue-Shifted Emission in CdTe/ZnSe Heterostructured Nanocrystals", along with Nishshanka N. Hewa-Kasakarage, and Mikhail Zamkov.

Because of his academic excellence, he was invited to be a member of the oldest all-discipline honor society-The Honor Society of Phi Kappa Phi of the BGSU chapter.

He started his studies towards a Ph.D. in Physics in 2008 at Missouri University of Science and Technology. In 2010, he joined the group of Dr. Paul Parris to work on his research project, which focuses on the transport properties of charges in molecularly doped polymers.